

FOREWORD

This report was prepared by Solar, a Division of International Harvester Company, San Diego, California on Air Force Contract No. AF 33(616)-8497, under Task No. 136804 of Project No. 1368, "Development of Frontal Section for Super-Orbital, Lifting, Re-entry Vehicle." The work was administered under the direction of the Flight Dynamics Laboratory, Research and Technology Division. S M/Sgt. Jesse Ingram, Jr. was project engineer for the Laboratory.

The studies presented began in July 1961, were concluded in May 1964. Solar was the prime contractor and Lockheed Missiles and Space Company (LMSC) was subcontractor in the field of trajectory analyses and vehicle design.

Solar, as prime contractor, retained overall program management and orientation, and performed the majority of the materials development, producibility studies, composite system development, materials property measurements, and materials and structures test programs. The program was managed by the Aerospace Activity of Solar with Mr. M. R. Licciardello as Program Manager. All materials development, testing, and structural fabrication was performed by the Solar Research Laboratories. Acknowledgement is given to Dr. A. G. Metcalfe and Mr. A. R. Stetson, whose advice and guidance throughout the contract period was instrumental in maintaining a technically sound program. Major contributors to the contract work, and to the body of this are Messrs. L. Fredlund, now deceased, B. Ohnysty, V. S. Moore, and F. K. Rose. Particular acknowledgement is given to Mr. R. Polvitz, who shouldered the demanding task of fabricating test specimens and final structural forms with eminent success.

Trajectory and vehicle analyses, nose cone structural and thermal analyses, and early oxidation tests on tungsten and tantalum were performed by Lockheed Missiles and Space Company under subcontract to Solar.

The program at LMSC was concentrated within, but not confined to, the Mechanical and Mathematical Sciences Laboratory of the research organization.

Mr. W.E. Jacobsen of Solid Mechanics served as project leader and directed the structural analyses; Messrs. A.C. Buckingham and R.G. Wilson of Fluid Mechanics provided the thermodynamics analyses; Messrs. D.A. Price and L.A. Manning of Flight Mechanics provided vehicle aerodynamic characteristics, trajectories, and environments. In the earlier phases of the study, Mr. R.A. Perkins of the Materials Sciences Laboratory, Metallurgy and Ceramics, supplied pertinent data concerning high-temperature mechanical and thermo-physical properties of refractory materials (especially their oxidation characteristics) and comparative properties of protective coatings. Able assistance was also contributed toward performing the structural studies by Messrs. C.E. Stuhlman and P. Stern. Mr. F.L. Guard assisted in the area of transient temperature distribution. Final designs were prepared by Messrs. R.V. Beck and A.D. Daniel of Experimental Engineering.

The ASSET nose cap work was conducted by Solar, with analysis performed by LMSC. Acknowledgement is given to Messrs. C.C. LaMaster, P. Beardsley, and W. Giddings of McDonnell Aircraft Company, ASSET Project, who kept their sense of humor under trying circumstances, and to Mr. C.J. Cosenza, ASSET Program Manager for the Air Force, for his cooperation and guidance.

This report is the final report and it concludes the work on Contract No. AF 33(616)-8497, Task No. 136804, Project No. 1368. Solar's report number is ER 1115-30.

ABSTRACT

A tungsten-thoria composite structure was selected for use on the nose cap of the ASSET glide re-entry vehicle. The design, fabrication, and qualification ground tests for that nose cap are presented.

The maximum stagnation point hot wall flux was $206 \text{ Btu/ft}^2 \text{ sec}$, resulting in a maximum thoria surface temperature of 4150 F and a maximum temperature of the tungsten structure of 3300 F. Based on measured thermal properties of thoria, a composite design was developed, weighing a total of 12.8 pounds.

A test nose cap survived a static pressure load test to 320 pounds; acoustic vibration to 155 db; and a combined temperature/vibration test of 10 g at 2000 F and 3 g at 4100 F. Other nose caps were tested successfully in a plasma arc tunnel at surface temperatures to 5000 F.

This technical documentary report has been reviewed and is approved.



W. A. Sloan, Jr.
Colonel USAF
Chief, Structures Division

Contrails

TABLE OF CONTENTS

Section		Page
I.	INTRODUCTION	1
	1.1 Mechanical Load Environment	1
	1.2 Thermal Environment	4
II.	DESIGN AND FABRICATION OF ASSET NOSE CAP	5
	2.1 Design Details	5
	2.2 Weight Statement	17
	2.3 Fabrication and Assembly	17
III.	MATERIALS PROPERTY DATA	27
	3.1 Properties of Tungsten	27
	3.2 Properties of Molybdenum	27
	3.3 Properties of Thoria Overlay	28
IV.	SUMMARY OF ANALYSES ON ASSET NOSE CAP	43
	4.1 Thermal Analysis	43
	4.2 Strength Analysis	49
V.	TEST PROGRAMS FOR ASSET NOSE CAP	51
	5.1 Test Facilities and Conditions	52
	5.2 Subscale Test Program	60
	5.3 Full-Scale Test Program	69
VI.	CONCLUSIONS	89
APPENDICES		
I	THERMO-STRUCTURAL ANALYSIS	
II	ACCELERATION TEST REPORT	
III	VIBRATION TEST REPORT	
IV	ACOUSTIC TEST REPORT	
V	VIBRATION AND ACOUSTIC NOISE TEST REPORT	

Contrails

LIST OF ILLUSTRATIONS

Figure		Page
1.	ASSET Hypersonic Glider	2
2.	ASV-4 Design Trajectory	4
3.	Nose Cap for ASV-4	7
4.	Tungsten Substructure	13
5.	Special Molybdenum Alloy Attachment Bolt	16
6.	Fabricating Outline for ASSET Nose Caps	19
7.	Process Outline for Coating ASSET Shapes with SO-86 and SO-84	20
8.	Tungsten Forging for ASSET Nose Cap Showing Holes for Instrumentation Plugs and Tungsten Pins for Reinforcement Mesh	21
9.	Tungsten Reinforcement Coils Being Applied to Mesh Fastened to Tungsten Forging	22
10.	Tungsten Forging with Reinforcements and Instrumentation Parts in Place; Ready for Thoria Overlay	22
11.	Application of Thoria Overlay Showing Rake Used to Obtain Approximate Coating Thickness and Aluminum Edge Mold to Obtain Proper Angle at Edge of Cap	23
12.	Machining Coating to Thickness and Shape; Machining Performed After 600 F Cure	23
13.	Appearance of Coating SO-86 After Machining	24
14.	Appearance of Coating SO-86 After Curing to 2200 F for Two Hours in Air-Argon Atmosphere	24
15.	Cap Mounted in Tooling Fixture Showing Assembly of Instrumentation, Half of Molybdenum Base Plate, and Half of Graphite Insert	25
16.	Completed Flight Cap Showing All Instrumentation Cemented in Place with Coating SO-84; Cap Shipped in Tooling Fixture	25
17.	Completed ASSET Flight Cap Showing Coating; Cover Coat SO-86 Cured to 600 F	26
18.	Thermal Expansion of Wrought Tungsten	28
19.	Modulus of Elasticity of Wrought Tungsten; 0.060-Inch Sheet	29
20.	Mechanical Properties of Tungsten at Room Temperature and 1000 F	30

LIST OF ILLUSTRATIONS (Cont)

Figure		Page
21.	Mechanical Properties of Tungsten at Elevated Temperatures	31
22.	Isothermal Shrinkage vs Time of Coating SO-86	33
23.	Thermal Expansion of Thoria, Tungsten, and Coating SO-86	34
24.	Thermal Conductivity Apparatus; Cross-Sectional Drawing	36
25.	Thermal Conductivity of Chemically Bonded Thoria Coatings	38
26.	Emittance of Thoria	40
27.	Emittance of Stabilized Zirconia	41
28.	Emittance of Stabilized Hafnia	42
29.	Stagnation Point Laminar Convective Heat Transfer Coefficient Factor; ASV-4 Trajectory	43
30.	Analytical Results for Hot Wall Convective Heat Flux at Stagnation Point; ASV-4	44
31.	Temperature History of Various Points on the Nose and Skirt Sections; ASV-4	46
32.	Comparison of Test Inputs with Design Requirements; Hot-Wall Convective Heat Flux at Stagnation Point; ASV-4	56
33.	Radial Model Stagnation Pressure Survey, 5/8-Inch Nozzle	59
34.	Stagnation Point Temperature; Test No. 5	64
35.	ASSET Nose Shape After Plasma-Arc Testing	65
36.	Reinforced SO-71 Coating After Plasma-Arc Testing to 3500 F for 3 Minutes	65
37.	Model Surface Temperature; Test No. 6	66
38.	SO-86 Coated Subscale ASSET Shape After Plasma-Arc Testing	66
39.	Model Surface Temperature; Test No. 7	68
40.	SO-71 + SO-84 Coated Subscale ASSET Shape; After Plasma-Arc Testing	69
41.	Model Surface Temperature; Test No. 8	70
42.	SO-86 Coated ASSET Cap Mounted in Molybdenum Skirt; After Plasma-Arc Testing	70
43.	ASSET Nose Cap in Molybdenum Skirt Showing Instrumentation Tubes	74
44.	ASSET Nose Cap and Load Bearing Test Fixture	74
45.	Model Surface Temperature	76

LIST OF ILLUSTRATIONS (Cont)

Figure		Page
46.	ASSET Nose Cap After Thermal Test; Coating SO-86 with Half of Cap Covered with Wash Coat of SO-84	77
47.	Comparison of Surface Temperatures; Full-Scale Tests	78
48.	Specimen After Test; Test No. 10	79
49.	Combined Temperature/Vibration Test Facility	81
50.	ASSET Cap After Temperature/Vibration Test	82
51.	Temperature History; ASSET Nose Cap	83
52.	Thermal Shock Tests on Thoria Plugs	84
53.	Coated ASSET Cap for Temperature/Vibration Test	86
54.	ASSET Cap During Test at Maximum Temperature	87
55.	ASSET Cap Prior to Cool Down	87
56.	ASSET Cap After Temperature/Vibration Test	88

Contrails

LIST OF TABLES

Table		Page
1.	ASSET Nose Cap Weight Analysis	18
2.	Thoria Overlay Compositions	32
3.	Maximum Test Conditions for Plasma-Arc Tests	54
4.	Plasma-Arc Tunnel Tests; Calibration Data	55
5.	Calorimeter Data - Model Calibration Test	58
6.	Subscale Calorimeter Data	60
7.	Test Conditions; Plasma-Arc Tests	64
8.	Summary of Test on Thoria Instrumentation Plugs	85

Contrails

I. INTRODUCTION

The ASSET program includes a series of flight tests of small unmanned hypersonic gliders, shown in Figure 1. The glider, designed by McDonnell Aircraft Corporation, is fully instrumented to record appropriate temperatures, pressures, and loads, and to telemeter all data during flight. In addition, water recovery of the glider is planned to allow direct examination of the vehicle after re-entry.

Two basic ASSET vehicle types will be flown; Aerothermodynamic and Structural Vehicle (ASV) and Aerothermoelastic Vehicle (AEV). The ASV vehicles will be subjected to the most severe thermal environments, and will assess the basic capability of materials and composite structures under re-entry conditions. The AEV vehicles, to be flown in a less severe trajectory than the ASV's, are aimed at evaluating aeroelastic phenomena.

The basic objective of this portion of the program was to design a composite tungsten-thoria nose structure for ASV-4 and AEV-1 (ASV-4 was subsequently changed to ASV-3). The Solar ASSET nose cap to meet this objective is a radiation-cooled structure with an external envelope shape consisting of a portion of a sphere with a radius of 3.110 inches. The cap is retained in an afterbody skirt of forged molybdenum. The cap is installed in the skirt such that its axis of symmetry is inclined 20 degrees to the centerline of the vehicle. This inclination compensates for the 20-degree angle of attack of the vehicle during the early stages of glide, and positions the stagnation point at the center of symmetry.

Design environmental conditions were based on McDonnell Aircraft Company Specification Control Drawing (MAC SCD) 51-30012 for ASSET nose cap.

1.1 MECHANICAL LOAD ENVIRONMENT

The load and vibration environments used to qualify the Solar nose cap, taken from MAC SCD 51-30012, were:

Manuscript released by the author May 1964 for publication as an FDL Technical Documentary Report.

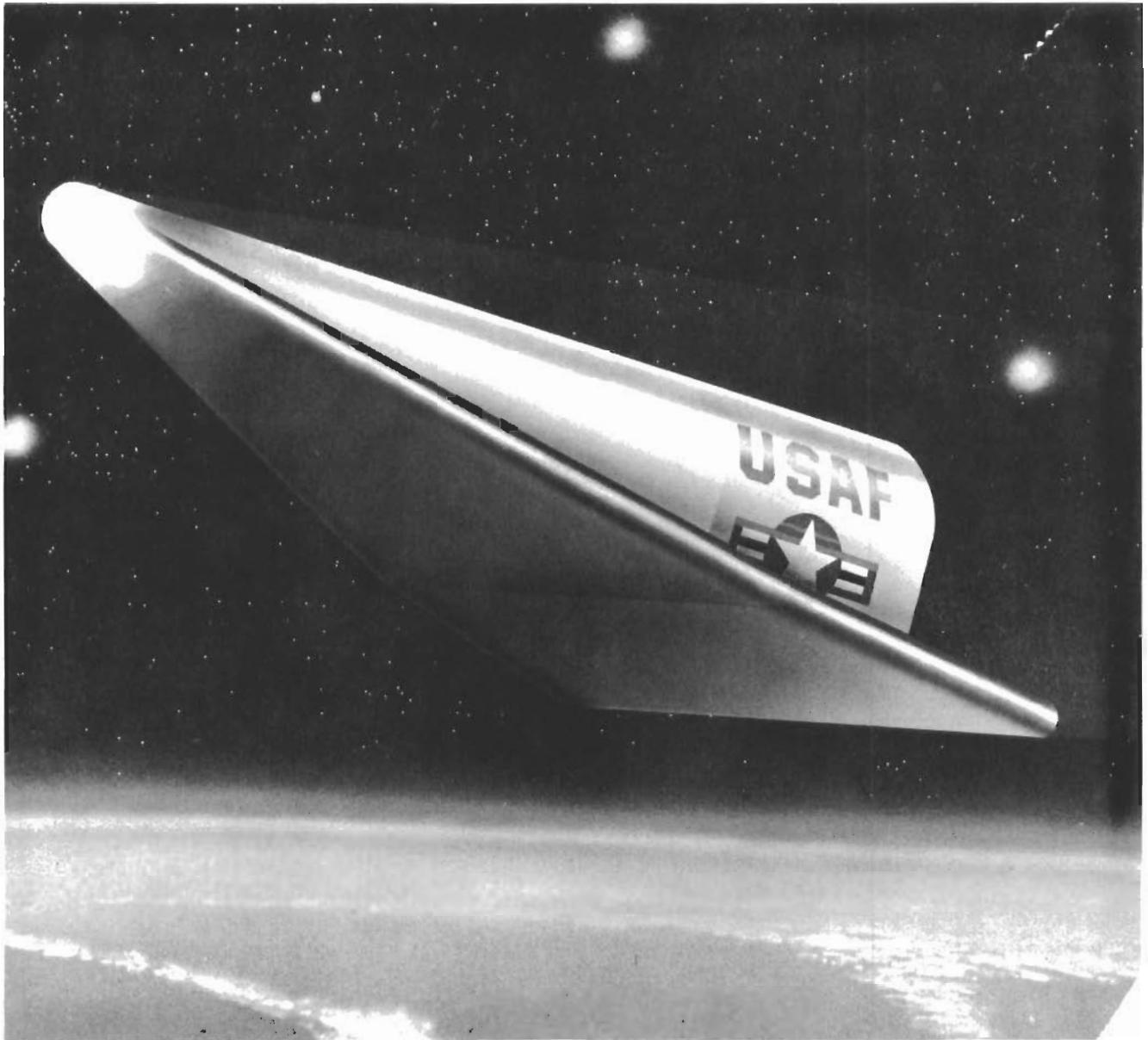


FIGURE 1. ASSET HYPERSONIC GLIDER

Contrails

Load A static load uniformly distributed, applied at room temperature, simulating maximum dynamic pressure during boost. Maximum stagnation point dynamic pressure is 22.2 psi, occurring at 67 seconds after launch. A variation of pressure over the nose was taken as

$$P = P_{\text{stag}} \cos^2 \theta$$

The component of pressure parallel to the centerline of symmetry of the nose cap is therefore

$$P_N = P_{\text{stag}} \cos^3 \theta$$

And the total force is

$$F_N = 2\pi r^2 P_{\text{stag}} \int_0^{\pi/3} \sin \theta \cos^3 \theta \, d\theta$$

$$F_N = 317 \text{ pounds}$$

for $r = 3.11$ inches

$$P_{\text{stag}} = 22.2 \text{ pounds/square inch}$$

Since the design trajectories already include a factor of safety, the design ultimate load was set at 320 pounds.

Acoustic 155 db above $0.0002 \text{ dynes/cm}^2$ at 37.5 cps to 9600 cps for 5 minutes.

Vibration The following vibration spectra held for 7.5 minutes each, simulating flight conditions:

Boost		Glide	
5-15 cps	0.3 inch D.A.	5-5 cps	0.3 inch D.A.
15-100	3.0g	15-100	± 3.0g
100-500	5.0g	100-500	± 1.0g
500-200	10.0g	1500-2000	± 2.0g

1.2 THERMAL ENVIRONMENT

The design trajectory for ASV-4 was defined in Figures 4 and 5 of MAC SCD 51-30012. As these trajectories included a factor of safety on altitude and velocity, additional factors were not required during the design. The design trajectory is shown in Figure 2.

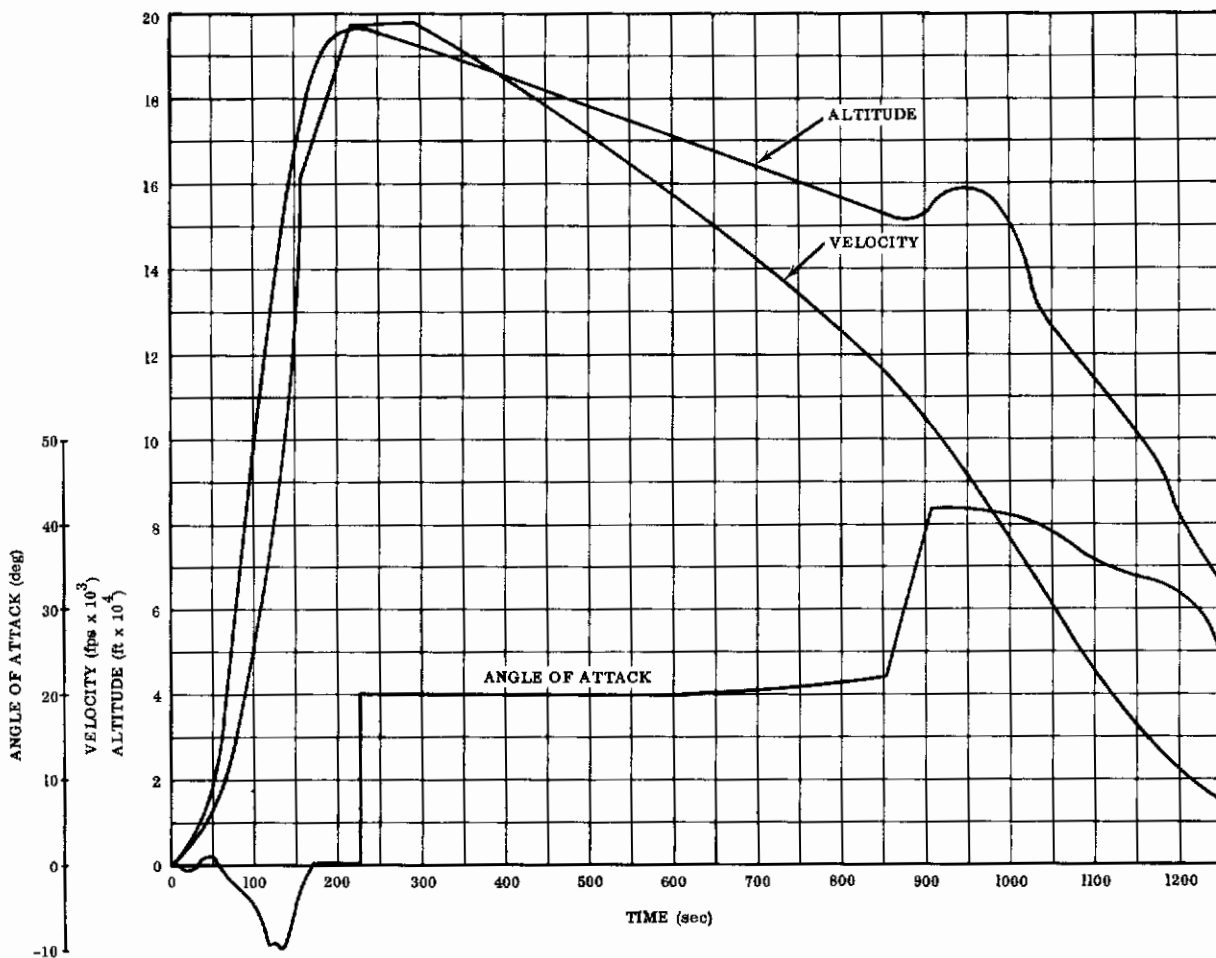


FIGURE 2. ASV-4 DESIGN TRAJECTORY

II. DESIGN AND FABRICATION OF ASSET NOSE CAP

Detail design and analysis of the nose cap for ASV-4 vehicle was conducted. The cap for AEV-1 was not analyzed, since the conditions resulting from the decreased velocity are much less severe.

Design of the ASSET nose cap was performed in accordance with MAC SCD 51-30012. No deviations were requested, however, by mutual consent of MAC, RTD, and Solar, it was decided not to minimize the nose cap weight. All interface and attachment dimensions and tolerances were in conformance with the MAC specification control drawing. Detailed design drawings are presented as Figure 3 (Solar drawing 36722).

The basic design of the nose cap incorporated a forged unalloyed tungsten substructure to which was attached a tungsten wire mesh. This wire mesh formed a mechanical reinforcement for the thoria overlay, which acted as a thermal protection system. Pressure and temperature instrumentation was provided by six pressure ports and one thermocouple on or near the surface of the cap. Location of the instrumentation points was to the dimensions and tolerances specified in Figure 1 of MAC SCD 51-30012. A split molybdenum support plate with graphite block inserts provided a clamping device for the instrumentation lines as they emerged from the aft end of the cap.

Mounting provisions and attachment points were provided in accordance with Figure 1 of MAC SCD 51-30012.

2.1 DESIGN DETAILS

A detailed description of the various cap elements is presented in the following paragraphs.

2.1.1 Tungsten Substructure

The tungsten substructure is detailed in Figure 4 (Solar drawing 36288). This structure was machined from an unalloyed tungsten forging procured from Arc-turus Manufacturing Company under Solar Specifications ES 1105 and ES 1106. Counter-bored holes were Eloxed into the tungsten cap to receive thoria plugs which serve as termination points for the pressure instrumentation tubing. Thirty 1/8-inch diameter holes were Eloxed into the forging to receive slotted pins which provide support for the tungsten wire mesh reinforcement.

Design dimensions and tolerances of the outside diameter of the cap provided a minimum gap of 0.001 inch between the cap and the molybdenum nose skirt based on the dimensions and tolerances of MAC SCD 51-30012.

2.1.2 Reinforcement System

The reinforcement system for the thoria-overlay coating consisted of a 5-by 5-inch tungsten screw mesh of 0.030-inch diameter wire, hot-formed to the same contour as the tungsten substructure. The screen was supported 0.105 ± 0.005 inch above the surface of the substructure by 1/8-inch diameter slotted tungsten pins which were crimped over the wire screen. Tungsten wire coils, formed from 0.010-inch diameter wire to an 0.090-inch internal diameter, were twisted around each of the wires of the screen for additional reinforcing. Details of the reinforcing system are shown in Figure 3.

2.1.3 Thoria Overlay System

The thoria overlay system of SO-86 (Table 2) was troweled onto the reinforcement using a rake to obtain the approximate coating thickness. After being cured at 600 F, it was machined to a thickness of 0.200 inch. The coating was then high fired to 2200 F. A washcoat of SO-84 (Table 2) was then applied to the surface to provide a smoother finish. A detailed description of the properties of this system is presented in Section 3.3.

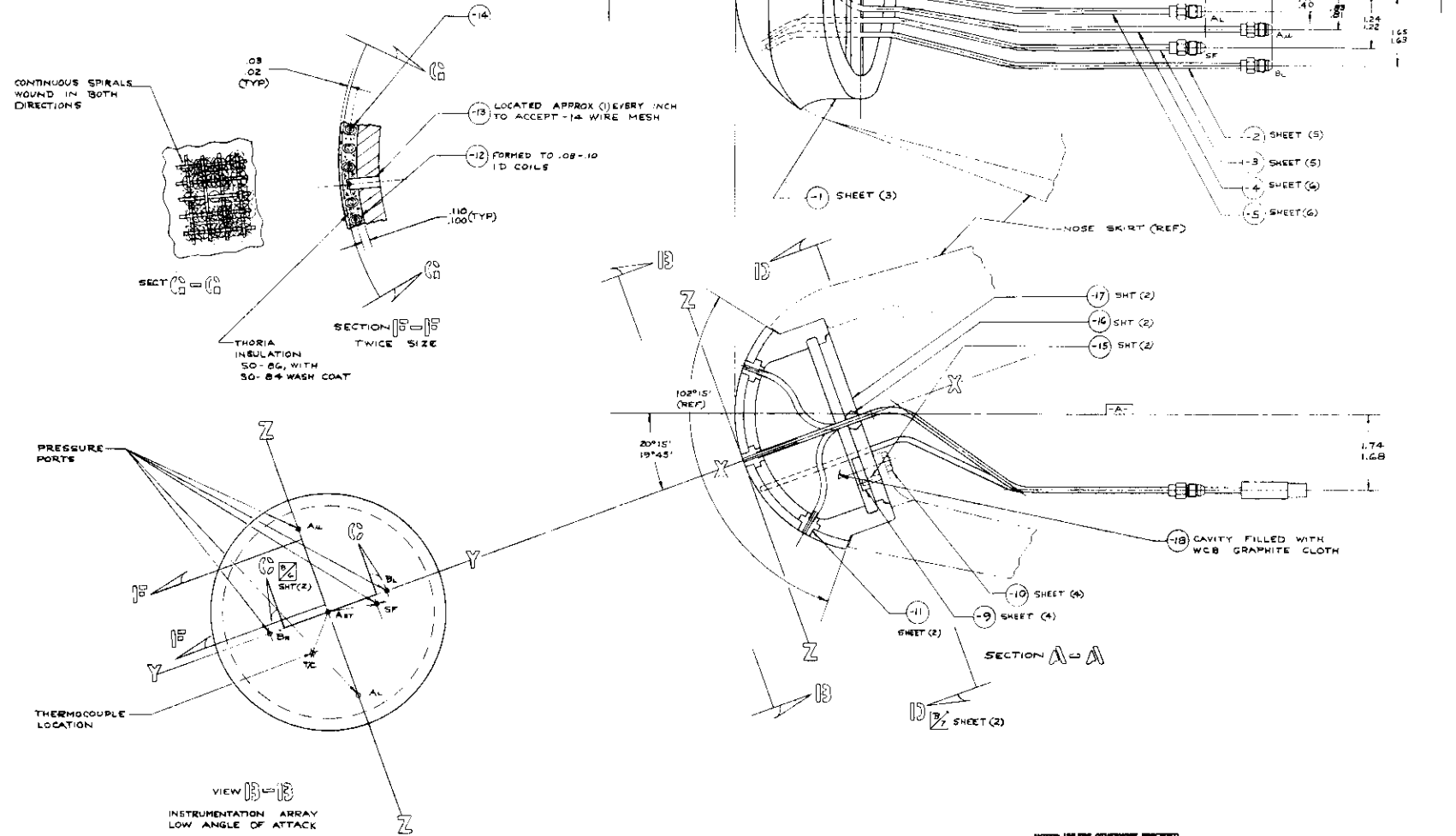
2.1.4 Instrumentation

Six pressure instrumentation ports, positioned in accordance with the dimensions and tolerances of MAC SCD 51-30012 were provided by sintered 80-percent density thoria plugs inserted into the counterbored holes in the tungsten substructure.

REVISIONS			
NO.	DATE	DESCRIPTION	BY

ITEM	LOW ANGLE OF ATTACK		
	X	Y	Z
AP	.753	0	2.004
AL	0	0	0
BL	.733	0	2.004
BR	.343	1.419	0
SF	.203	1.088	.209
TC	.190	.650	.75

TABLE OF COORDINATES FOR DIMENSIONS ON OUTER SURFACE OF NOSE CAP
SEE DET-1 SHEET (3) FOR ACTUAL DIMENSIONS ON FORGING



- NOTES: UNLESS OTHERWISE SPECIFIED
- 1 DIMENSIONS LOCATING THE TRUE POSITION ARE IN INCH
 - 2 DO NOT SCALE DRAWINGS. WORK TO DIMENSIONS GIVEN
 - 3 DRAWING INTERPRETATION PER MIL-D-3875 AND SOLAR SPEC 3-A, SECT 50
 - 4 PER SOLAR SPEC ES 1105
 - 5 PURCHASE FROM MCDONNELL PART NO.
 - 6 THREAD FORM PER MIL-S-8879 AND VOI-SHAN MFG CO SPEC VS-T-O-7 SHEET (4)
 - 7 100% RADIOGRAPHIC INSPECTION PER MIL-I-6865 SHEET (4)
 - 8 100% DYE PENETRANT INSPECTION PER MIL-I-6866 SHEET (4)
 - 9 PURCHASE FROM: VOI-SHAN MFG CO. PART NO. VR47
 - 10 PARTS TO BE COATED WITH DURAK-B* .001 MAX SOURCE CHROMIZING CORP, HAWTHORN CALIF

QTY	DESCRIPTION	UNIT	REMARKS
6	3G418-1 FITTING-PRESS TUBING		
2	19 PINS .06 DIA PURE TUNGSTEN ROD (REDHAR)		
1	10 WCB GRAPHITE CLOTH		
1	17 PLATE PURE MOLYBDENUM (GG)		
1	16 SPACER BLOCK 1/4" GRAPHITE		
2	15 PINS .125 DIA PURE TUNGSTEN ROD (REDHAR)		
1	14 WIRE MESH .03 DIA 60/IN PURE TUNGSTEN		
1	13 PINS .128 DIA PURE TUNGSTEN ROD (REDHAR)		
1	12 WIRE .01 DIA PURE TUNGSTEN		
1	11 TUBES .30% DENSITY THORA 99% PURITY		
2	10 BOLT SPECIAL ITEM		
2	9 CAM LOCK EB MELTED PURE MOLYBDENUM		
1	8 THERMOCOUPLE		
1	7 PRESS TUBE .0918X.1250X.14.0 LG MOLYBDENUM		
1	6		
1	5		
1	4		
1	3		
1	2 PRESS TUBE .0918X.1250X.14.0 LG MOLYBDENUM		
1	1 NOSE CAP UNALLOYED TUNGSTEN FORMING		

APPROVED BY	DATE	DESIGNED BY	DATE
<i>[Signature]</i>		<i>[Signature]</i>	
NOSE CAP ASSY		ASSET	
SOLAR		3G722	
REV 1		DATE 11/72	

FIGURE 3. NOSE CAP FOR ASV-4 (Sheet 1 of 6) 7

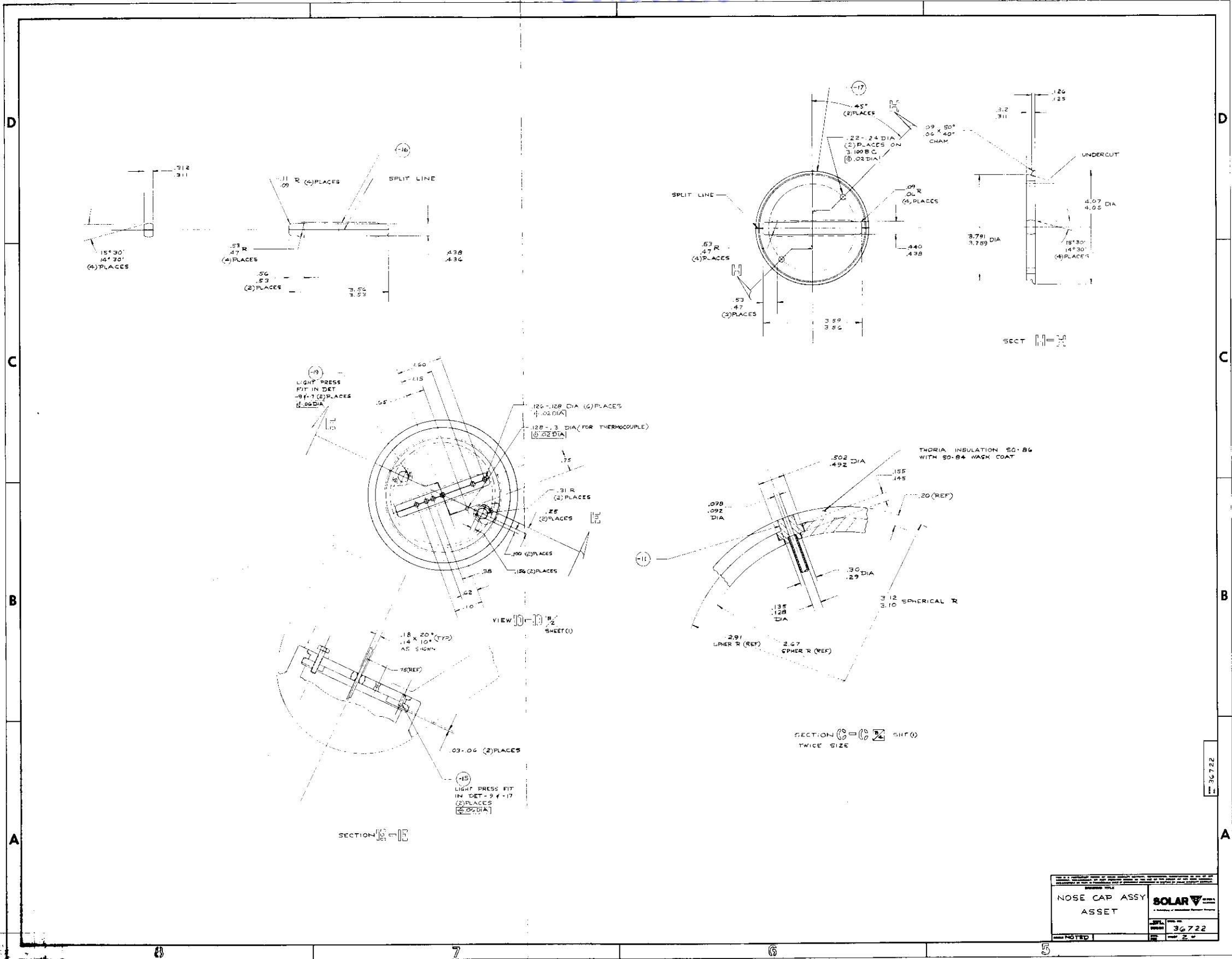


FIGURE 3. NOSE CAP FOR ASV-4 (Sheet 2 of 6)

DRAWING TITLE		SOLAR V
NOSE CAP ASSY ASSET		
DATE	36722	NOTED
REV	2	

Contracts

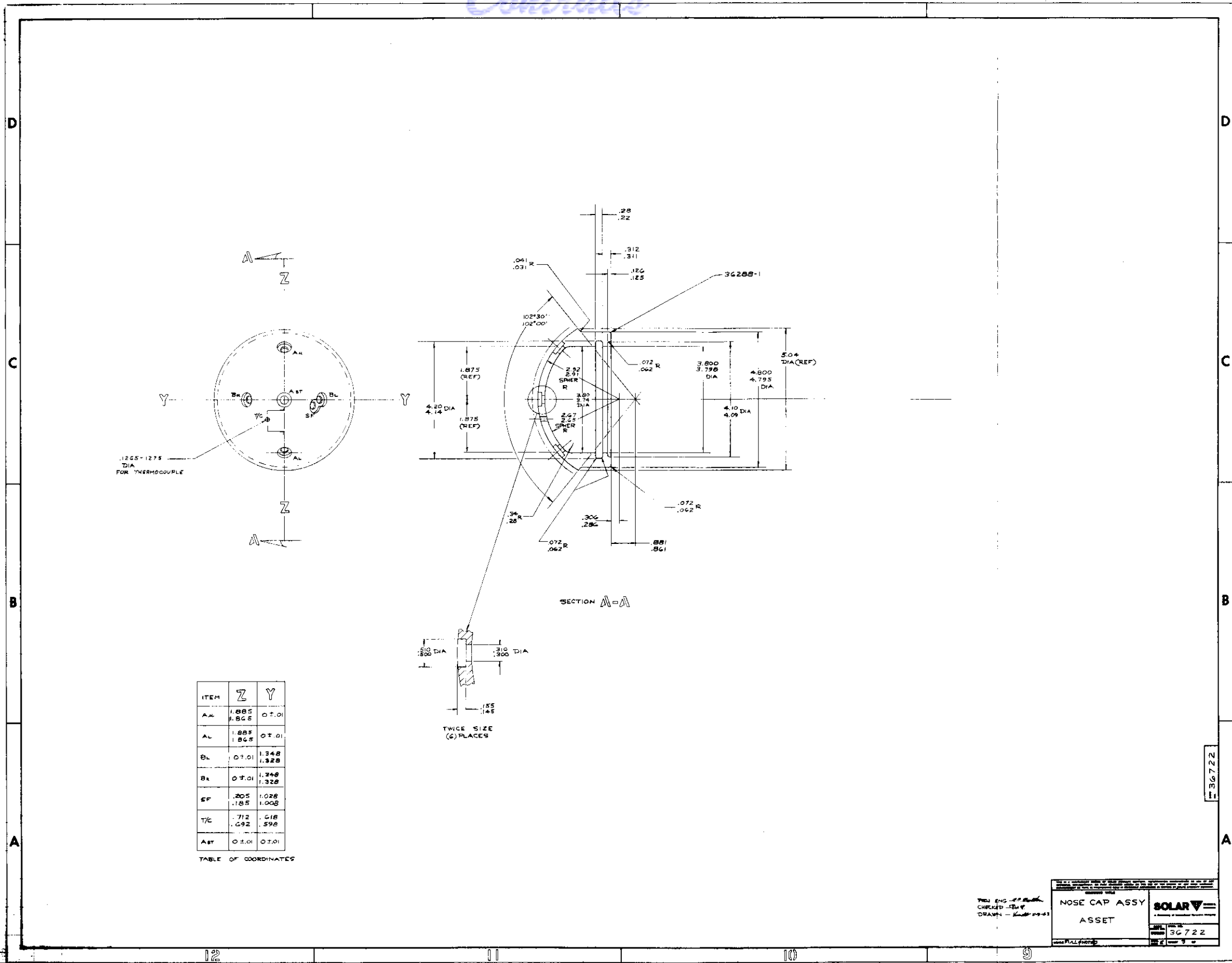
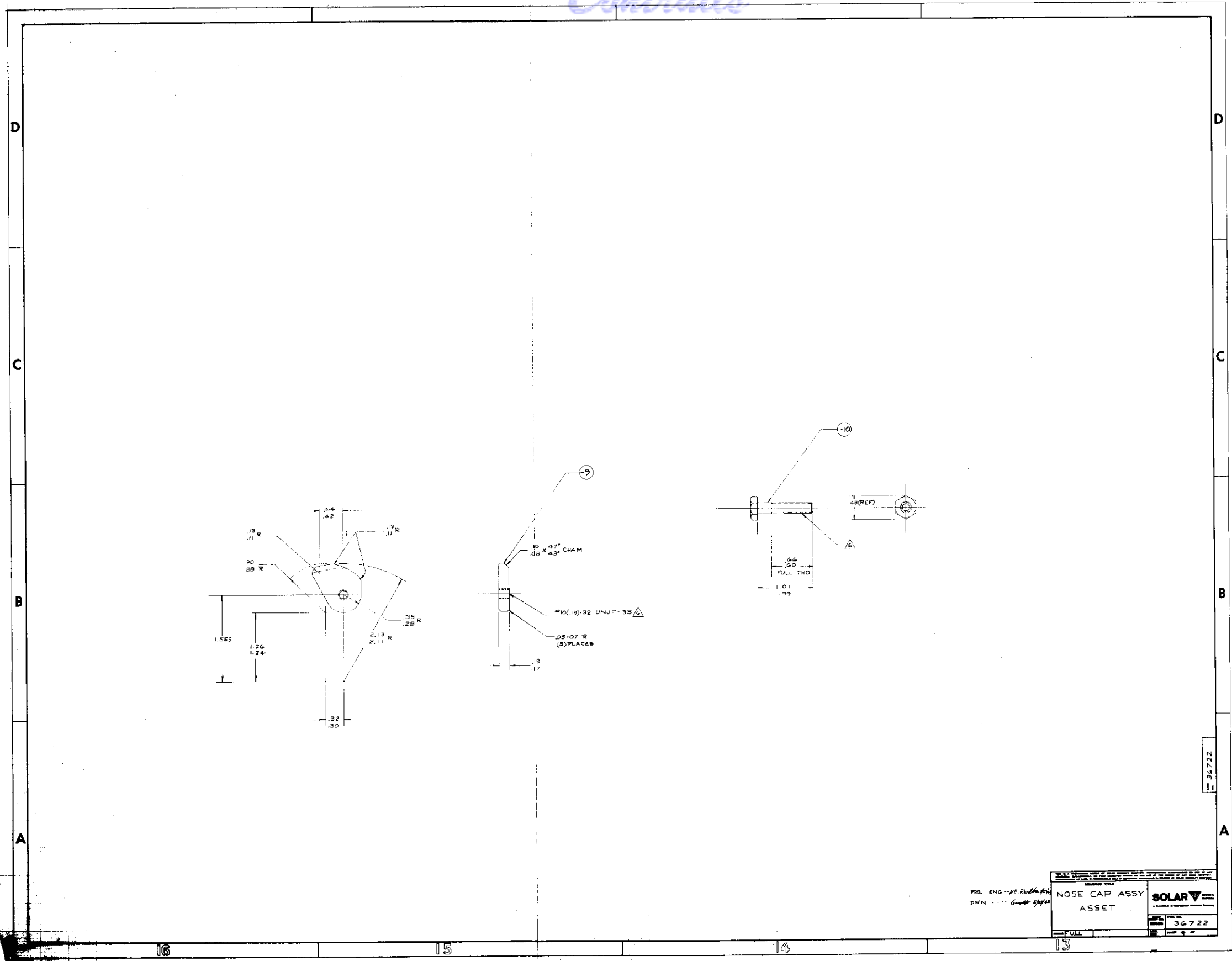


FIGURE 3. NOSE CAP FOR ASV-4 (Sheet 3 of 6)



PROJ ENG - P.C. R...
DWN - ...

NOSE CAP ASSY	
ASSET	
DATE	36722
REV	

SOLAR V

FIGURE 3. NOSE CAP FOR ASV-4 (Sheet 4 of 6)

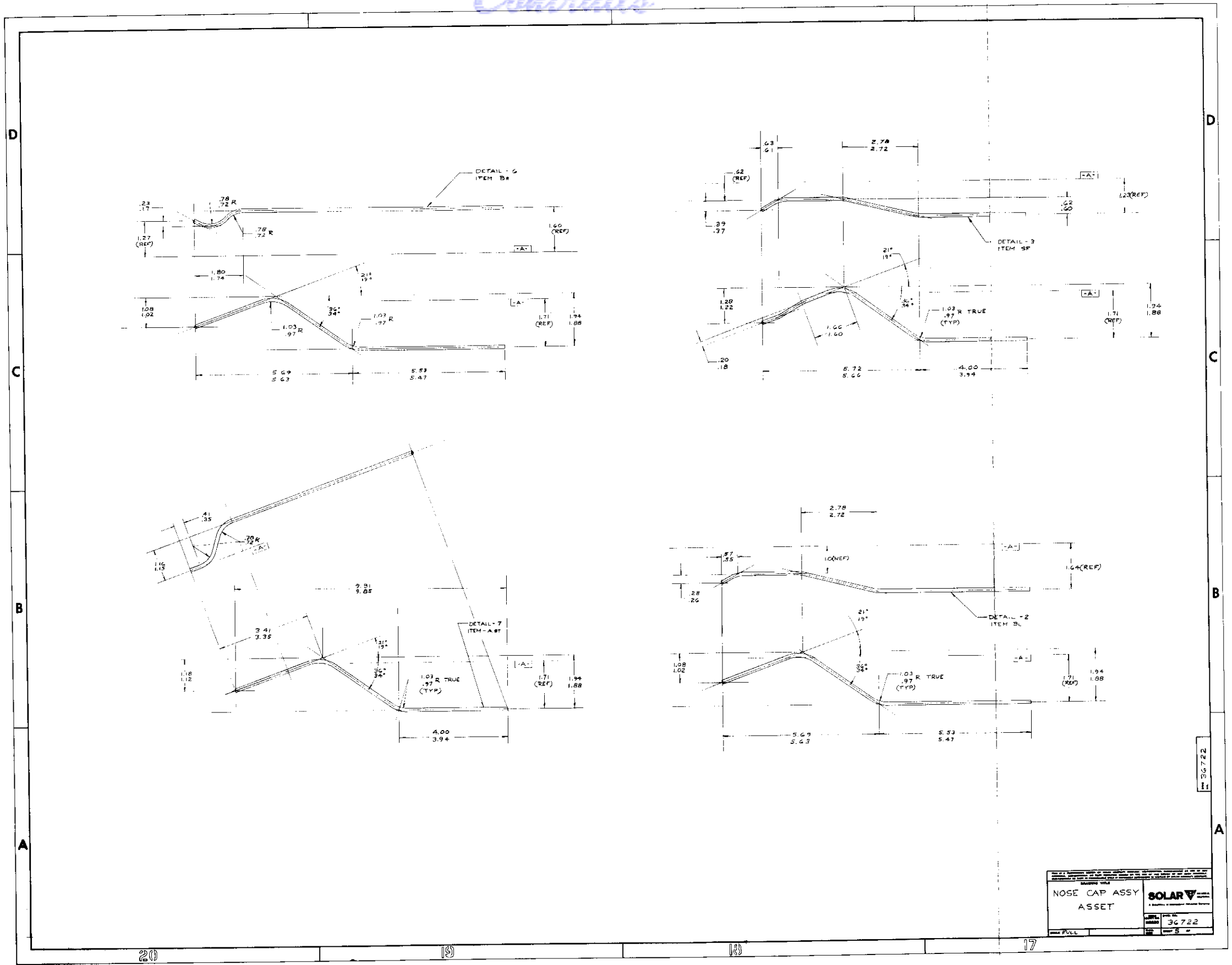
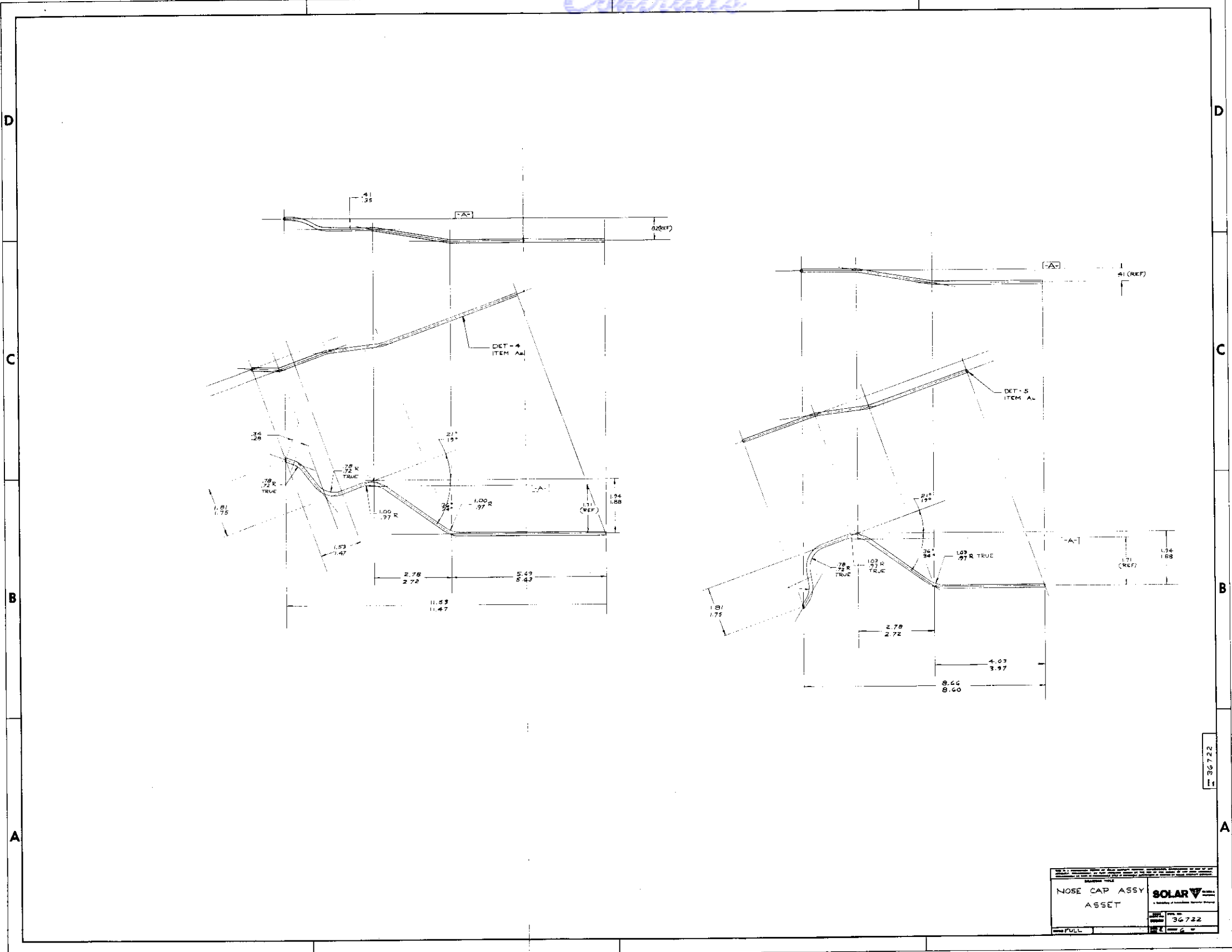


FIGURE 3. NOSE CAP FOR ASV-4 (Sheet 5 of 6)

Continued



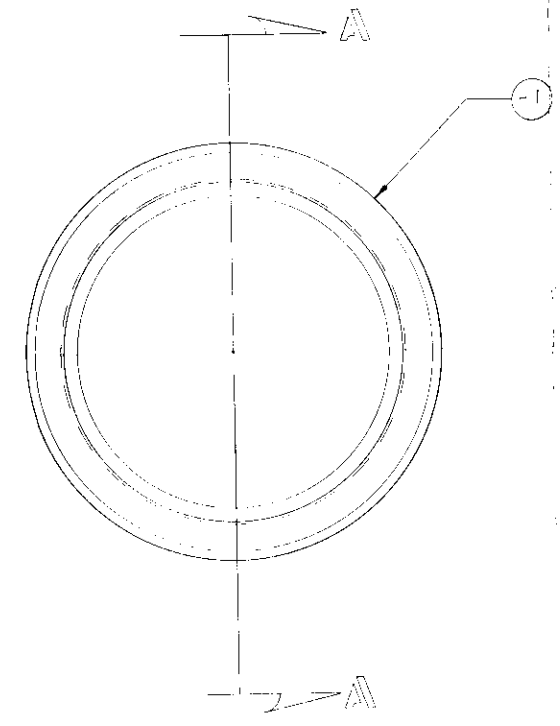
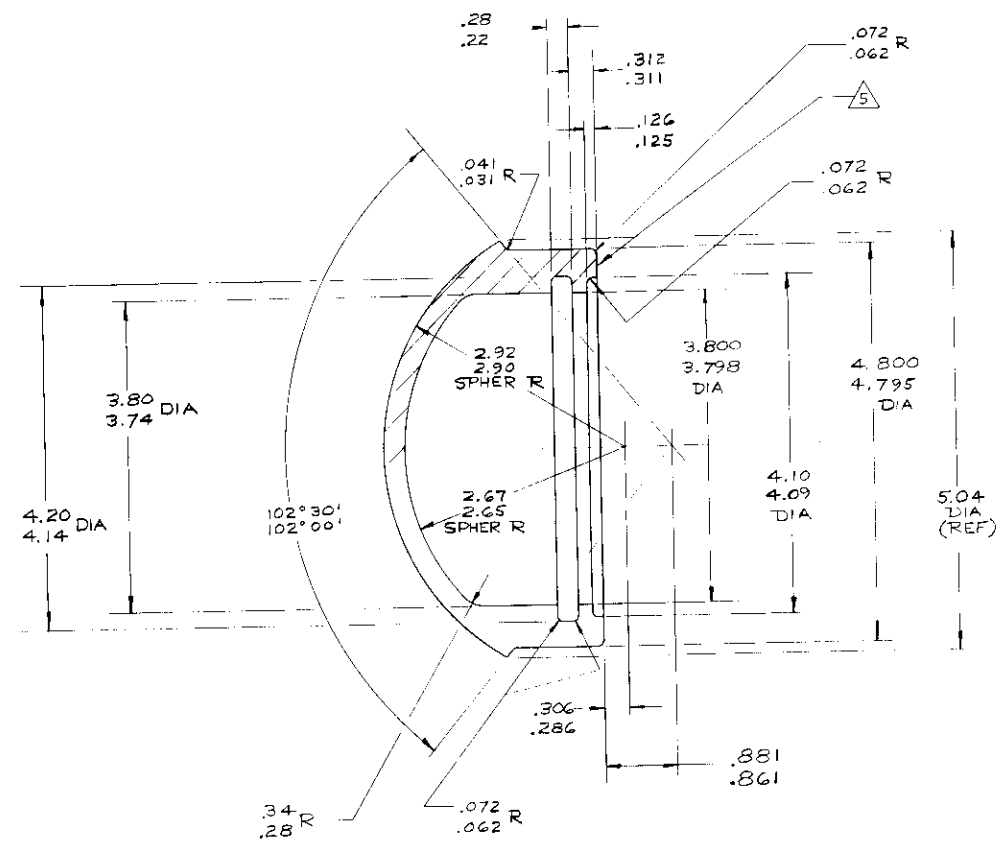
36722

NOSE CAP ASSY		SOLAR A Division of Lockheed Martin Space Research Corp.
ASSET		
36722	36722	
FULL		

FIGURE 3. NOSE CAP FOR ASV-4 (Sheet 6 of 6)

Controls

REVISIONS			
ZONE	LETTER	DESCRIPTION & E.O. NO.	DATE



SECTION A-A

- NOTES: UNLESS OTHERWISE SPECIFIED
- 1 DIMENSIONS LOCATING THE TRUE POSITION ARE BASIC
 - 2 DO NOT SCALE DRAWING. WORK TO DIMENSIONS GIVEN
 - 3 DRAWING INTERPRETATION PER MIL-D-70327 AND SOLAR SPEC 9-4, SECT 6.0
 - 4 MAT'L : UNALLOYED TUNGSTEN FORGING PER SOLAR SPEC ES 1105
 - 5 RUBBER STAMP PART NO. 12-139 HIGH NUMERALS WITH NON PERMANENT INK PER SOLAR SPEC 9-6 CLASS "E"
 - 6 ALL FINISH MACH DIMS 63

REQD	REQD	REQD	PART NO.	DESCRIPTION	MATL.	MATL. SPEC.	ASMT. WT.	UNIT WT.
			-1	NOSE CAP				

<table border="1"> <thead> <tr> <th>ISSUE NO.</th> <th>DATE</th> <th>APPROVED BY</th> </tr> </thead> <tbody> <tr> <td>1</td> <td> </td> <td> </td> </tr> <tr> <td>2</td> <td> </td> <td> </td> </tr> <tr> <td>3</td> <td> </td> <td> </td> </tr> <tr> <td>4</td> <td> </td> <td> </td> </tr> <tr> <td>5</td> <td> </td> <td> </td> </tr> <tr> <td>6</td> <td> </td> <td> </td> </tr> </tbody> </table>	ISSUE NO.	DATE	APPROVED BY	1			2			3			4			5			6			<p>UNITS PER ASMT</p> <p>THIS IS A PROPRIETARY DESIGN OF SOLAR AIRCRAFT COMPANY. REPRODUCTION, MANUFACTURE OR USE OF ANY ASSEMBLY, SUB-ASSEMBLY, OR PART INDICATED HEREIN OR THE USE OF THE DESIGN OF ANY SUCH ASSEMBLY, SUB-ASSEMBLY OR PART, IS PROHIBITED UNLESS EXPRESSLY AUTHORIZED IN WRITING BY SOLAR AIRCRAFT COMPANY.</p>	<p>DRAWING TITLE</p> <p>ASSET NOSE CAP</p>	<p>SOLAR AIRCRAFT COMPANY A Subsidiary of International Harvester Company</p> <p>CODE IDENT NO. 00820</p> <p>DWG. NO. 36288</p> <p>DWG. SIZE D SHEET 1 OF 1</p>
ISSUE NO.	DATE	APPROVED BY																						
1																								
2																								
3																								
4																								
5																								
6																								

DWS No. 36288

DIETERICH-POST CLEARPRINT 100H

4

2

ISO 150 REV. 1-82

1 INITIAL RELEASE LAYOUT NNA 36027 MOD

FIGURE 4. TUNGSTEN SUBSTRUCTURE

A close-tolerance hole was ultrasonically counterbored through each plug, prior to insertion, to accommodate the pressure tubes. The pressure tubing, formed from 0.095-inch ID pure molybdenum, was coated with an oxidation-resistant coating (Durak B) before assembly. The pressure tubes were inserted in the thoria plugs and formed a tight mechanical joint. This joint was then cemented with SO-86 coating. The tubing connections aft of the cap were standard 1/8-inch tube fittings brazed to the molybdenum tubing. These fittings terminated in accordance with the dimension and tolerance requirements of Figure 1 of MAC SCD 51-30012.

Temperature instrumentation was provided by a thermocouple located as shown in Figure 3. The thermocouple, purchased from MAC, was W5Re/W26Re wire with BeO insulation. The thermocouple was covered by a molybdenum sheath with (W-3) oxidation protection coating. The thermocouple tip was positioned 0.025 inch below the surface of the thoria overlay.

The pressure tubes were clamped between ZTA graphite blocks as they pass through the aft support plate. The clamping prevented lateral movement of the tubes while permitting them axial movement to allow for thermal expansion.

2.1.5 Support Plate

A split molybdenum plate with ZTA graphite insert blocks served as a clamping device for the pressure tubing and thermocouple. The instrumentation passed through holes drilled into the graphite blocks. These holes were designed in a manner to provide lateral support of the tubing yet allow axial movement for thermal expansion of the tubes.

The molybdenum plate served also to enclose the cavity of the cap which was filled with graphite cloth. The graphite cloth prevented radiation from the forging to the pressure tubes, and provided a reducing atmosphere inside the cap.

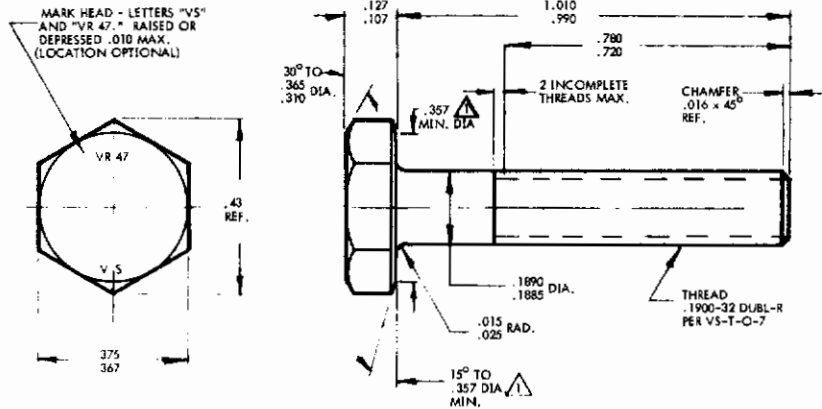
Plate thickness was held to a close tolerance in order to serve as a spacer block between the attachment lugs on the molybdenum nose skirt and the locking cams which rest in an internal groove in the tungsten forging. Details of the support plate assembly are shown in Figure 3.

VOI-SHAN MANUFACTURING COMPANY
A DIVISION OF VOI-SHAN INDUSTRIES, INC.



Distribution in whole or in part of this document should be limited to those persons who must necessarily review the same for the purpose, above set forth. No right to reproduce this document is hereby granted, in whole or in part, to any person other than those specifically named in the permission of Voi-Shan Industries, Inc. Nothing contained herein is intended to restrict the use by customers of Voi-Shan Industries, Inc. of any parts or products purchased from Voi-Shan Industries, Inc.

This document contains technical information proprietary to Voi-Shan Industries, Inc. and is only conditionally issued. Neither receipt nor possession thereof confers or conveys any right to reproduce, copy, disseminate, or otherwise use this document, its design or technical information shown thereon, nor any right to reproduce this document, nor any part thereof, except for manufacturing by vendors for Voi-Shan Industries, Inc. and for manufacturing under any written license granted by Voi-Shan Industries, Inc.



GENERAL NOTES:



1. BEARING FACE DIA. SHALL NOT EXCEED ACTUAL ACROSS FLATS DIMENSION.
2. SHANK (.1890 DIA. SHALL BE CONCENTRIC TO THREAD PITCH DIA. WITHIN .0045 TIR.
3. SHANK SHALL BE STRAIGHT WITHIN .004 TIR PER INCH OF LENGTH.
4. BEARING SURFACE OF HEAD SHALL BE SQUARE TO SHANK WITHIN .003 TIR.
5. SURFACE ROUGHNESS PER MIL-STD-10, MAX. RIR; BEARING SURFACE OF HEAD, HEAD TO SHANK FILLET, SHANK AND ALL THREAD ELEMENTS -32. ALL OTHER SURFACES -63.
6. BREAK ALL SHARP EDGES .005 / .015 RAD.
7. ALL DIMENSIONS AND GENERAL NOTES TO BE MET BEFORE COATING APPLICATION.
8. DIMENSIONS IN INCHES.

MATERIAL:

TZM MOLYBDENUM ALLOY.

FINISH:

TO BE APPLIED BY CUSTOMER.

TOLERANCES:

UNLESS OTHERWISE SPECIFIED: ANGLES ±3°

**COORDINATION
COPY ONLY**

SENT TO.....DATE.....
APPROVED.....DATE.....

RECOMMENDED NUT CONTACT VOI-SHAN		CODE IDENT. NO. 92215
APPROVED DATE 31 MAY 1963	TITLE BOLT, HEX HEAD REFRACTORY ALLOY (SOLAR SPECIAL)	STANDARD
LATEST REVISION DATE		VR 47 SHEET 1 OF 1

FIGURE 5. SPECIAL MOLYBDENUM ALLOY ATTACHMENT BOLT

2.1.6 Attachments

The nose cap attachment was in accordance with the dimensional requirements of Figure 1 of MAC SCD 51-30012. Attachment of the cap to the nose skirt was accomplished by two TZM .1900-32 special bolts which pass through two lugs in the nose skirt. The two bolts pass through the support plate and screw into locking cams which rotate and seat in an internal groove in the tungsten forging. During assembly, the cams were rotated into place in the groove and then pinned to the support plate with one 1/8-inch and one 1/16-inch tungsten pin, thus preventing rotation of the cam after assembly. The pins are in a blind hole and cannot be removed after the attachment bolts are in place.

The attachment bolts were manufactured from TZM alloy by Voi-Shan Manufacturing Company in accordance with Voi-Shan specification VS-T-0-7 for "Dubl-R" screw threads. The screw threads were tapped in the locking cam using a special tap made to the above thread specification.

All attachment parts made from molybdenum were coated with Durak B.

Complete details of the attachment design are shown in Figures 3 and 5.

2.2 WEIGHT STATEMENT

In designing the structure, consideration was given to the requirements for extra weight in the nose section of ASSET vehicles to shift the center of gravity forward. On this basis, the thickness of the tungsten substructure was much greater than actually required to withstand design loads. The tungsten forging was machined to a thickness of 0.25 inch, however, a thickness of 0.40 inch would have been ample.

The total weight of the cap, including attachment bolts, was 12.839 pounds. A breakdown of the various component weights is presented in Table 1.

2.3 FABRICATION AND ASSEMBLY

A typical assembly sequence for the Solar ASSET nose cap is presented in Figure 6. A process outline for coating the ASSET nose caps with SO-86 and SO-84 is presented in Figure 7.

TABLE 1
ASSET NOSE CAP WEIGHT ANALYSIS

Part Number	Number Required	Description	Weight (grams)
36722-1	1	Tungsten Forging	4375.0
-2	1	Pressure Tube, B _L	10.0
-3	1	Pressure Tube, SF	8.8
-4	1	Pressure Tube, AM	10.5
-5	1	Pressure Tube, A _L	9.1
-6	1	Pressure Tube, B _R	9.8
-7	1	Pressure Tube A _{st}	9.1
-8	1	Thermocouple	31.3
-9	2	Cam, Locking	33.1
-10	2	Bolt, Special (Voi-Shan)	12.2
-11	6	Plug, Thoria	36.9
-12	As req'd	Tungsten Wire, Coil	22.0
-13	30	Tungsten Pin, Support	57.0
-14	As req'd	Tungsten Wire, Mesh	58.0
-15	2	Tungsten Pin, Locking (0.125-in. dia)	3.5
-16	1	Spacer Block, Graphite	15.2
-17	1	Plate, Molybdenum	510.7
-18	As req'd	Graphite Cloth	26.5
-19	2	Tungsten Pin, Locking (0.062-in. dia)	0.8
36418-1	6	Fitting, Pressure Tubing	34.2
	As req'd	SO-86 Coating	550.0
		Total Weight	5823.7 grams or 12.8389 pounds

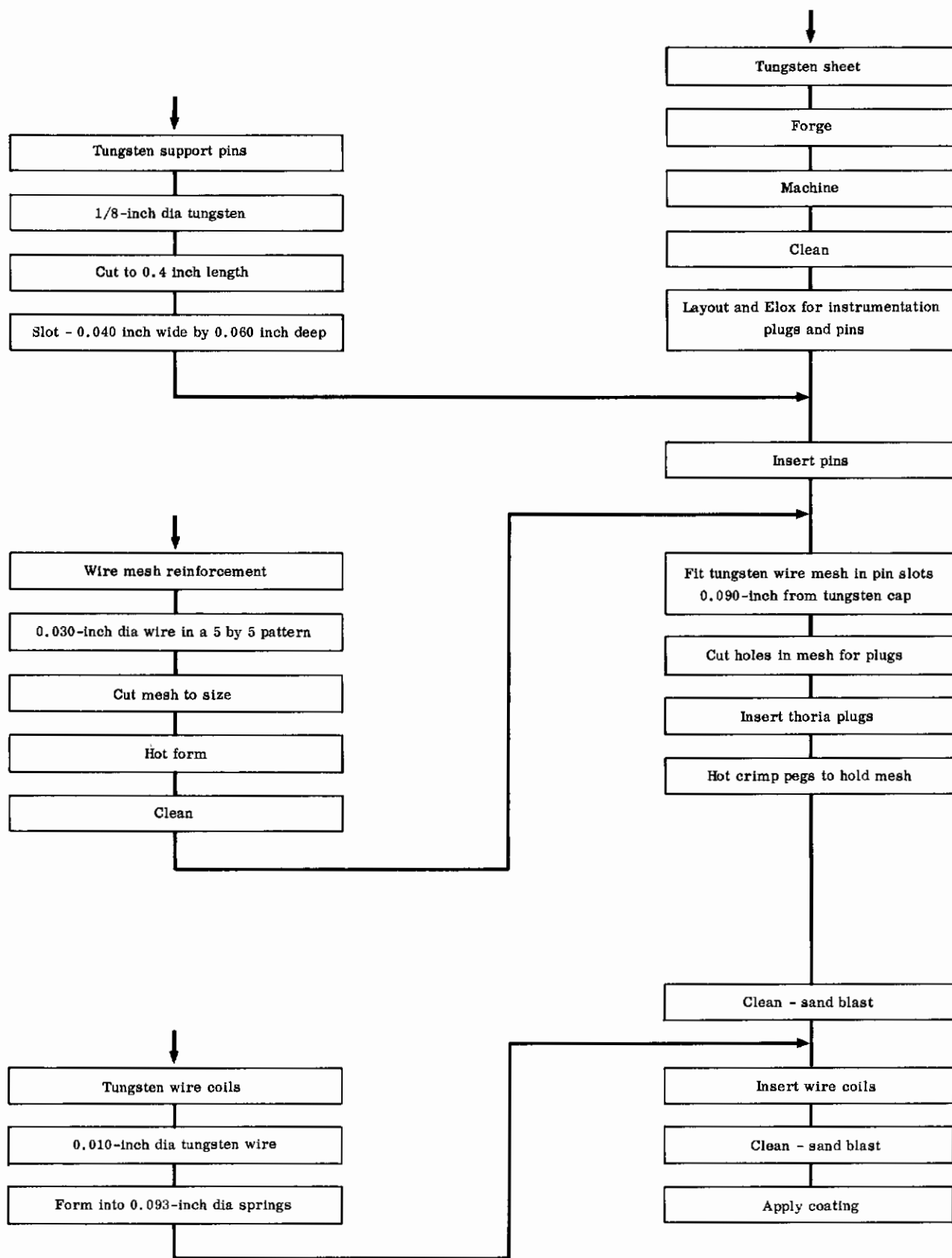


FIGURE 6. FABRICATING OUTLINE FOR ASSET NOSE CAPS

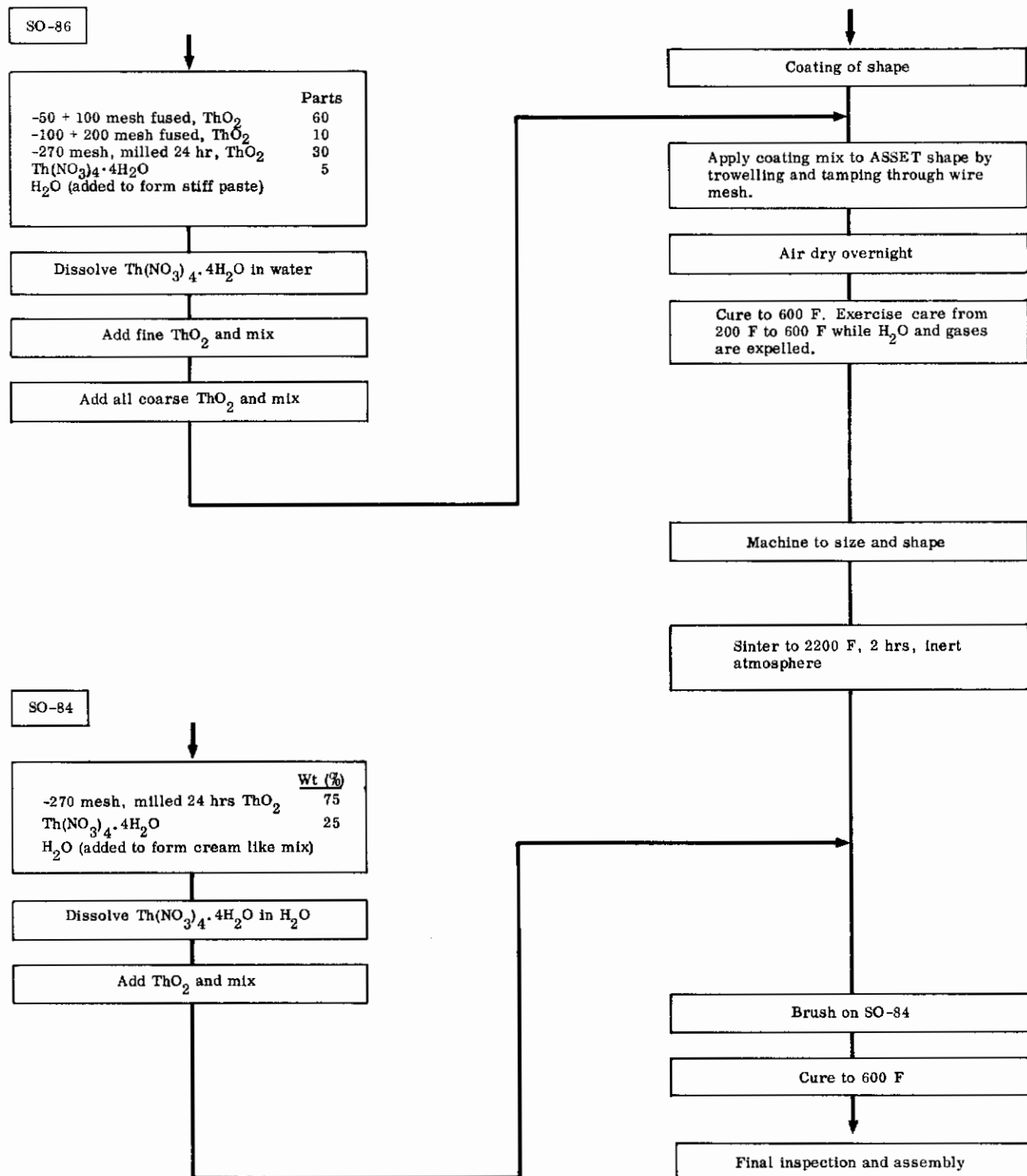


FIGURE 7. PROCESS OUTLINE FOR COATING ASSET SHAPES WITH SO-86 AND SO-84

The basic structure included the tungsten forging, reinforcement system, thoria instrumentation plugs, and thoria overlay coating. Following the fabrication of this structure, the cap was positioned in an assembly layup fixture for the forming and layup of the molybdenum pressure tubing and thermocouple. Special U-shaped dies were used to form the desired shapes in the molybdenum pressure tubes. Tubing was centerless ground prior to forming. All forming was conducted at temperatures between 400 and 800 F. Each tube was pressure checked for leaks prior to coating.

All molybdenum parts used on the nose cap assembly were coated by Chromizing Corporation with Durak B. The parts include the split support plate, pressure tubes, locking cams, and attachment bolts. The sheathed thermocouple, purchased from MAC, was coated with W-3 coating.

During assembly, all instrumentation components were sealed into place using SO-86 coating.

A pictorial account of the various stages of assembly is presented in Figures 8 through 17.

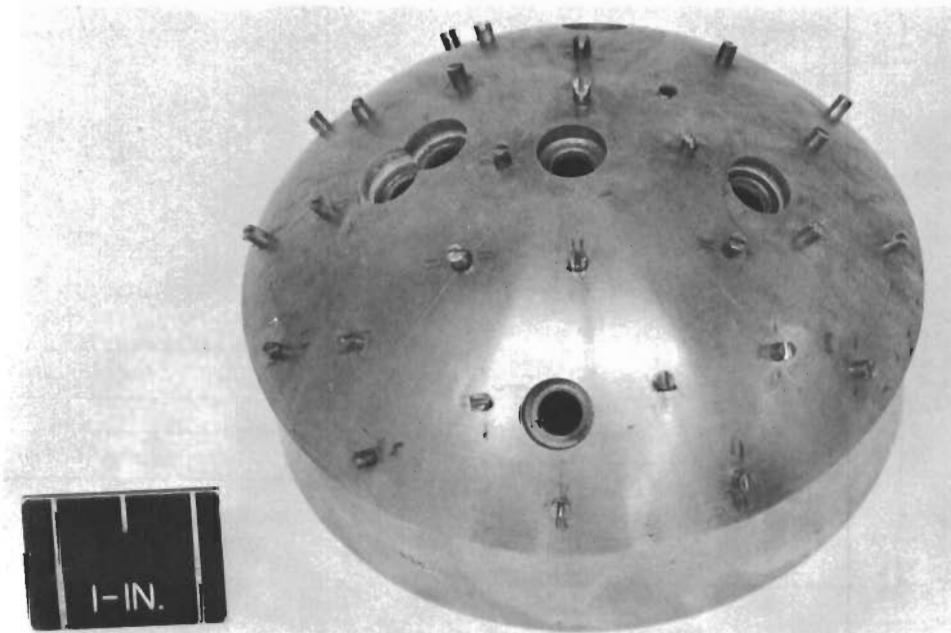


FIGURE 8. TUNGSTEN FORGING FOR ASSET NOSE CAP SHOWING HOLES FOR INSTRUMENTATION PLUGS AND TUNGSTEN PINS FOR REINFORCEMENT MESH



FIGURE 9. TUNGSTEN REINFORCEMENT COILS BEING APPLIED TO MESH FASTENED TO TUNGSTEN FORGING

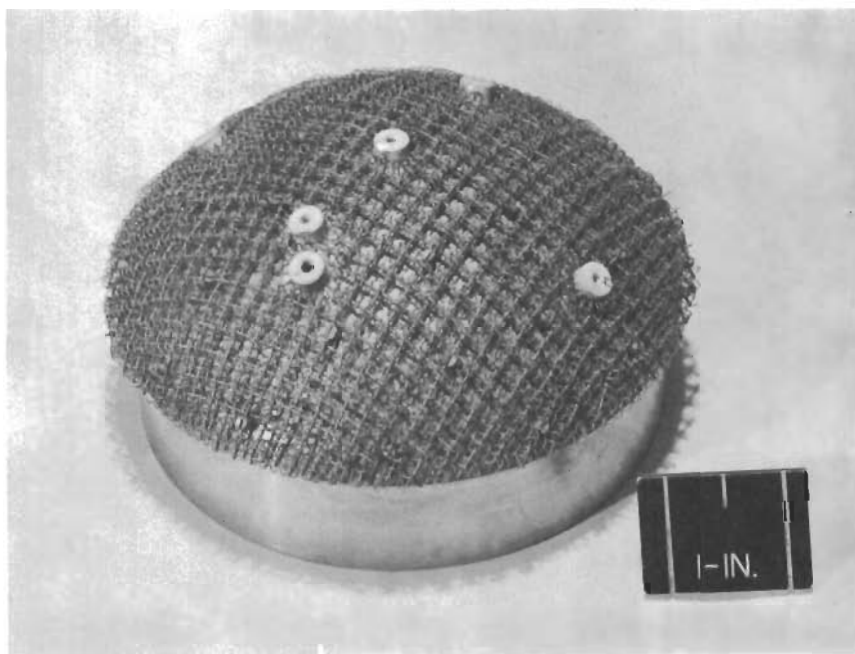


FIGURE 10. TUNGSTEN FORGING WITH REINFORCEMENTS AND INSTRUMENTATION PARTS IN PLACE; Ready for Thoria Overlay

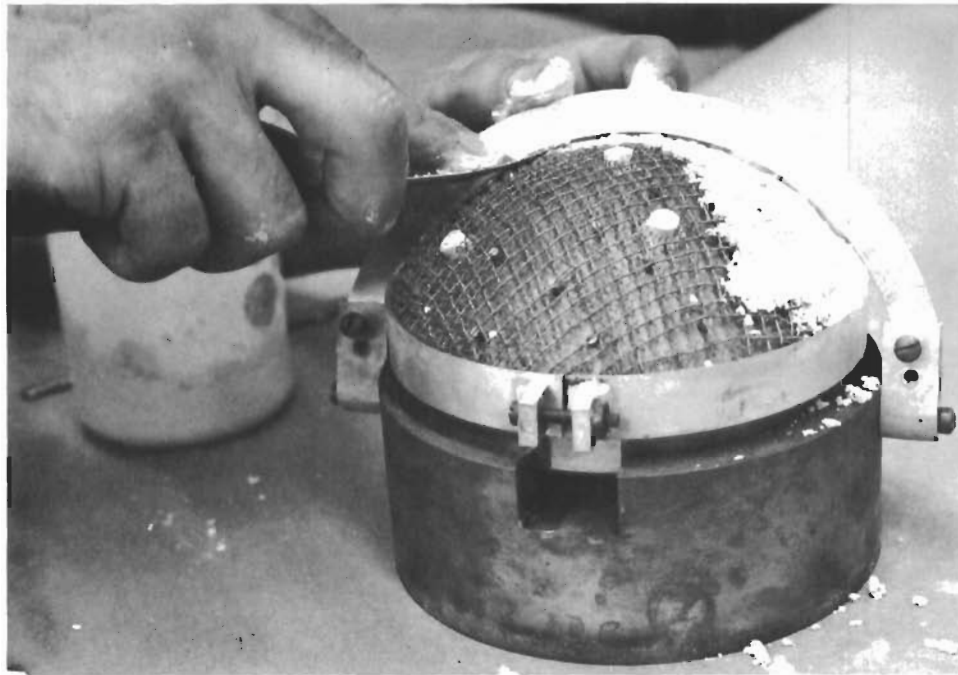


FIGURE 11. APPLICATION OF THORIA OVERLAY SHOWING RAKE USED TO OBTAIN APPROXIMATE COATING THICKNESS AND ALUMINUM EDGE MOLD TO OBTAIN PROPER ANGLE AT EDGE OF CAP

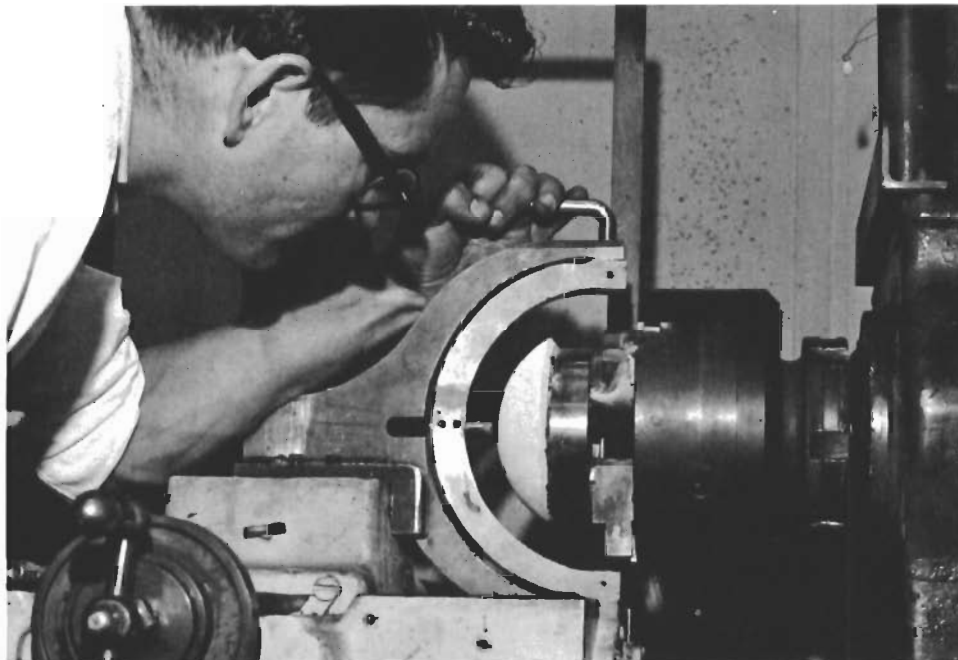


FIGURE 12. MACHINING COATING TO THICKNESS AND SHAPE; Machining Performed After 600 F Cure

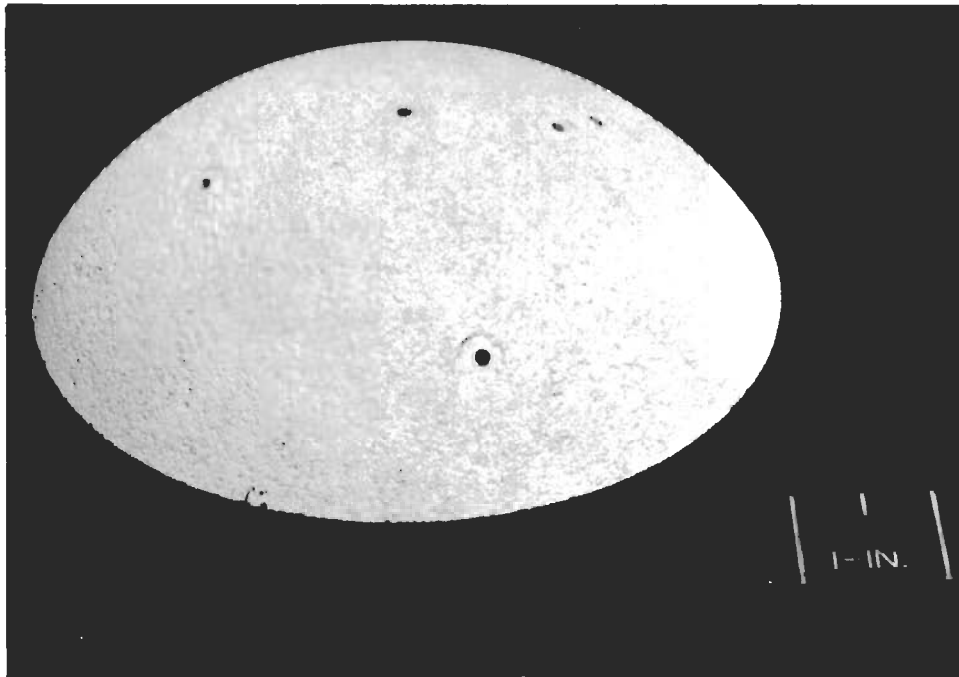


FIGURE 13. APPEARANCE OF COATING SO-86 AFTER MACHINING

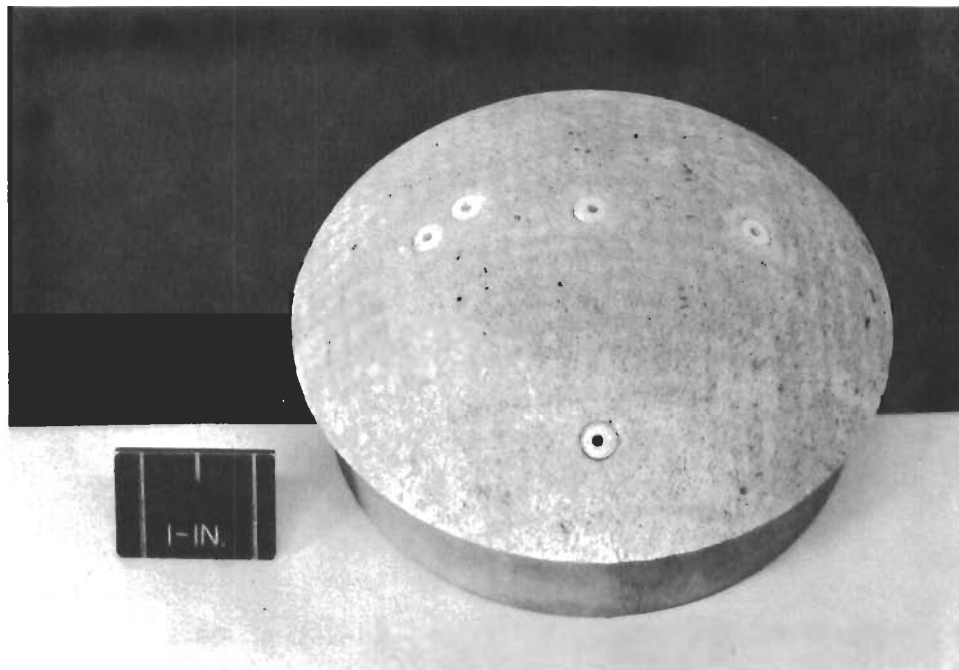


FIGURE 14. APPEARANCE OF COATING SO-86 AFTER CURING TO 2200 F FOR TWO HOURS IN AIR-ARGON ATMOSPHERE

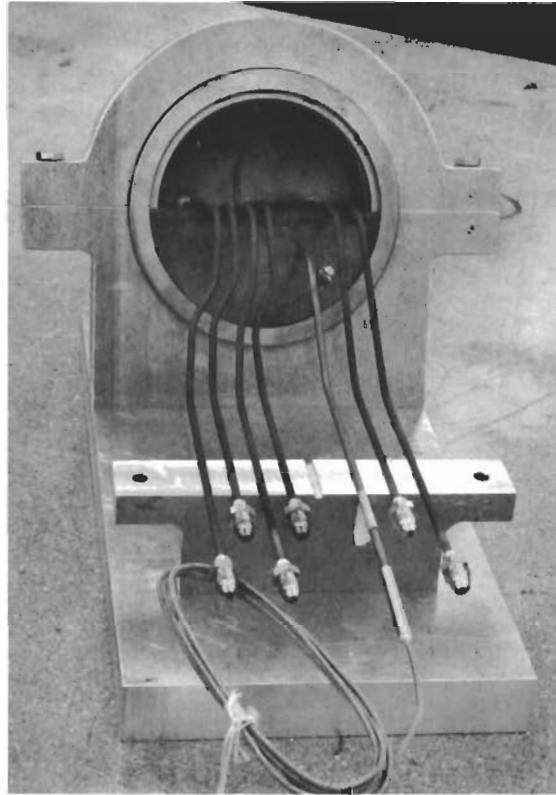


FIGURE 15. CAP MOUNTED IN TOOLING FIXTURE SHOWING ASSEMBLY OF INSTRUMENTATION, HALF OF MOLYBDENUM BASE PLATE, AND HALF OF GRAPHITE INSERT

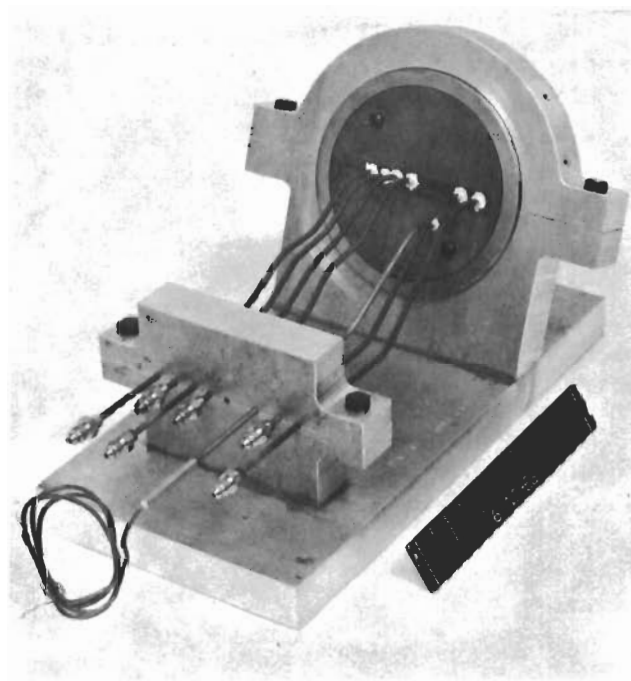
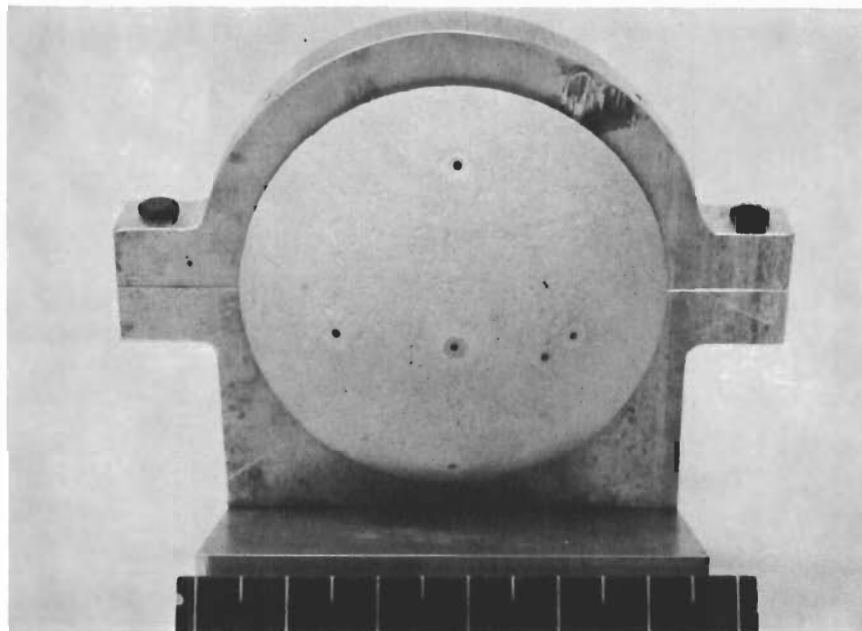


FIGURE 16. COMPLETED FLIGHT CAP SHOWING ALL INSTRUMENTATION CEMENTED IN PLACE WITH COATING SO-84; Cap Shipped in Tooling Fixture



**FIGURE 17. COMPLETED ASSET FLIGHT CAP SHOWING COATING; Cover
Coat SO-86 Cured to 600 F**

III. MATERIALS PROPERTY DATA

The properties of each material used in the ASV cap are presented in this section. Some literature data were available, and were used when possible. The remaining data were generated by Solar. Details of the test methods used and discussions of material development work are presented in Volume II, Materials and Composite Structure Development, of this report.

3.1 PROPERTIES OF TUNGSTEN

Tungsten properties used were taken from published literature. These data are shown in Figures 18 through 21, and are the data used in the thermal stress analysis of the tungsten forging. An extremely conservative design was used for this forging as proved by the analysis. Refinement of the properties used for tungsten to make them uniquely correct for this particular part was therefore considered unnecessary.

3.2 PROPERTIES OF MOLYBDENUM

The Solar ASSET nose cap contained three molybdenum detail parts: the closure plate, the attach lugs, and the attach bolts.

The closure plate carries no load during flight, so properties of the material were not considered critical.

The attachment lugs and bolts react the 10-g deceleration force acting on the nose cap during re-entry. Design calculations indicated maximum loads of 48.5 pounds on each bolt and lug combination. According to MAC analyses, maximum bolt and lug temperatures would not exceed 2900 F. Rather than attempt to predict fastener strength based on material properties, a load test of a bolt-plus-lug was conducted. The combination of bolt and lug was heated to 3000 F and a tensile load of 120 pounds was applied to the bolt. No failure occurred after 5 minutes of test. Bolt and lug design was considered satisfactory, based on these results.

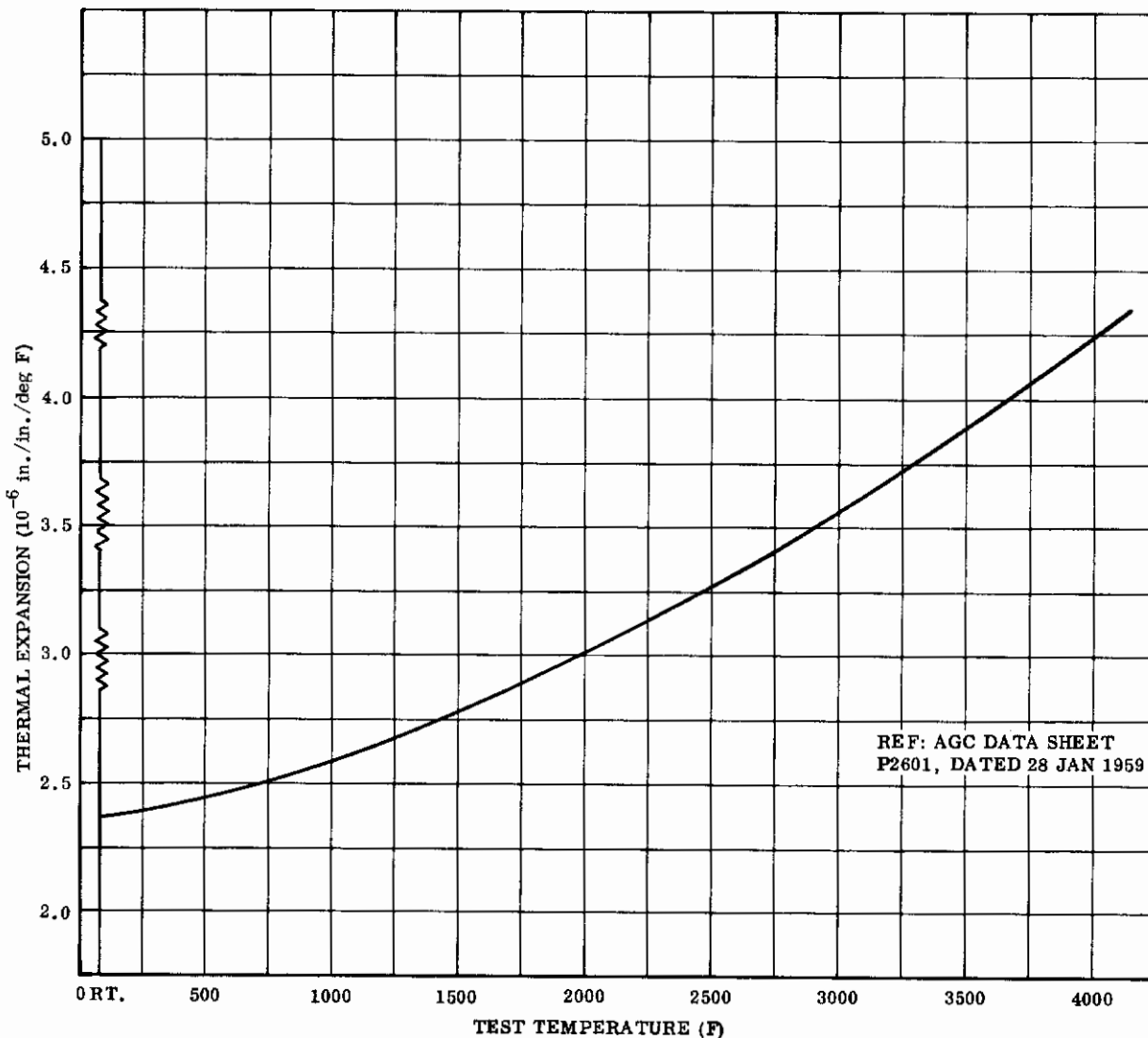


FIGURE 18. THERMAL EXPANSION OF WROUGHT TUNGSTEN

3.3 PROPERTIES OF THORIA OVERLAY

The thoria overlay used on the Solar ASSET nose cap was a composite, consisting of thoria particles and tungsten reinforcing filaments. The weight of the composite used was 0.0489 lb/in.^2 of nose cap surface, made up of 0.0397 lb/in.^2 of thoria and 0.0092 lb/in.^2 of tungsten pins, mesh, and wire. Since the dispersion of tungsten in thoria is in a pattern that repeats itself only at large intervals (the spacing of the pins, for instance), it was not feasible to make thermophysical property measurements on actual samples of reinforced thoria. Instead, unreinforced thoria coating samples were used

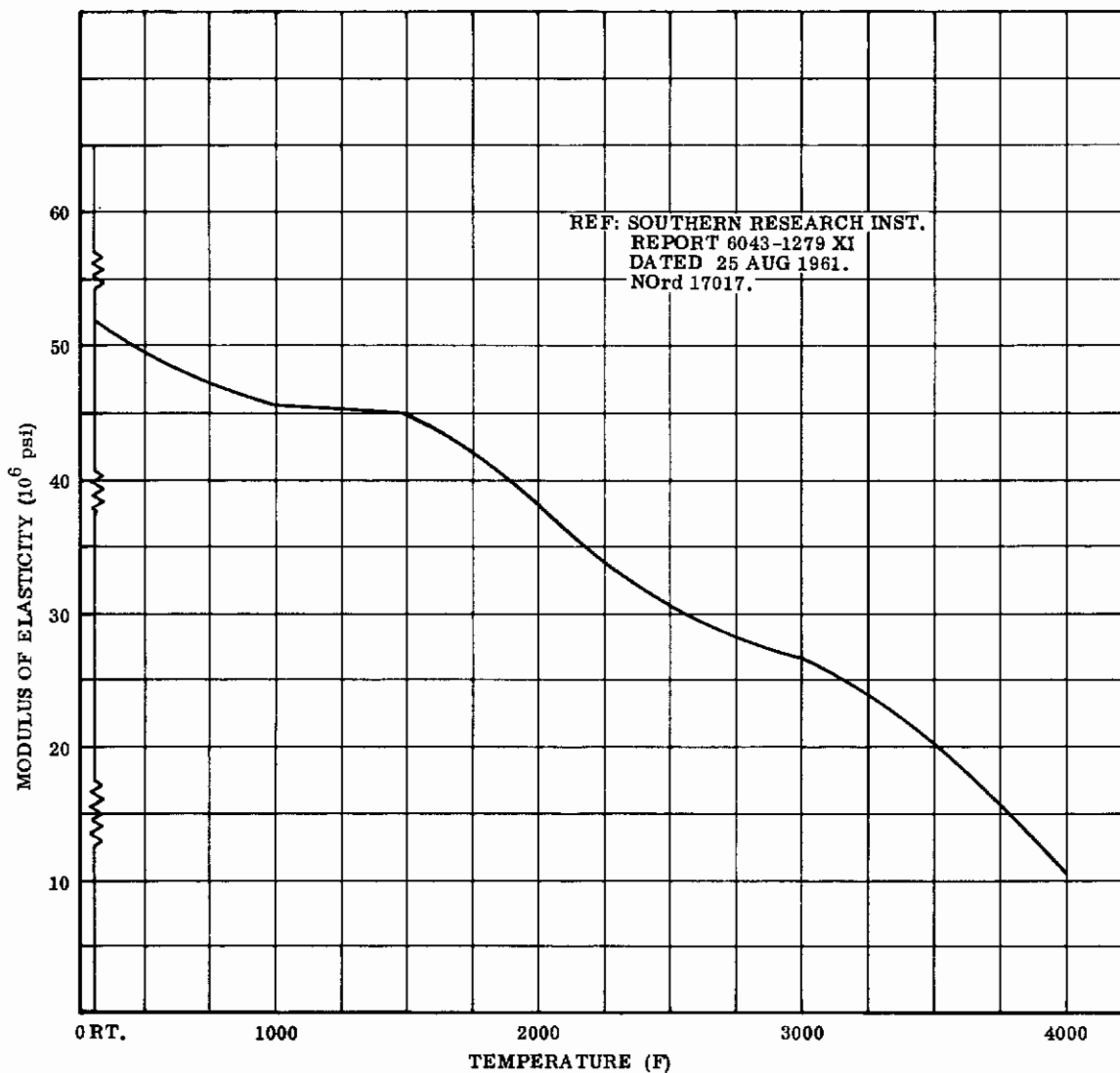


FIGURE 19. MODULUS OF ELASTICITY OF WROUGHT TUNGSTEN;
0.060-Inch Sheet

in tests. Values of thermal conductivity used in design were then adjusted on a relative volume basis to obtain a composite material property where required.

Material properties of significance in the design of the nose cap were:

- Density
- Modulus of rupture
- Specific heat
- Thermal conductivity
- Emittance

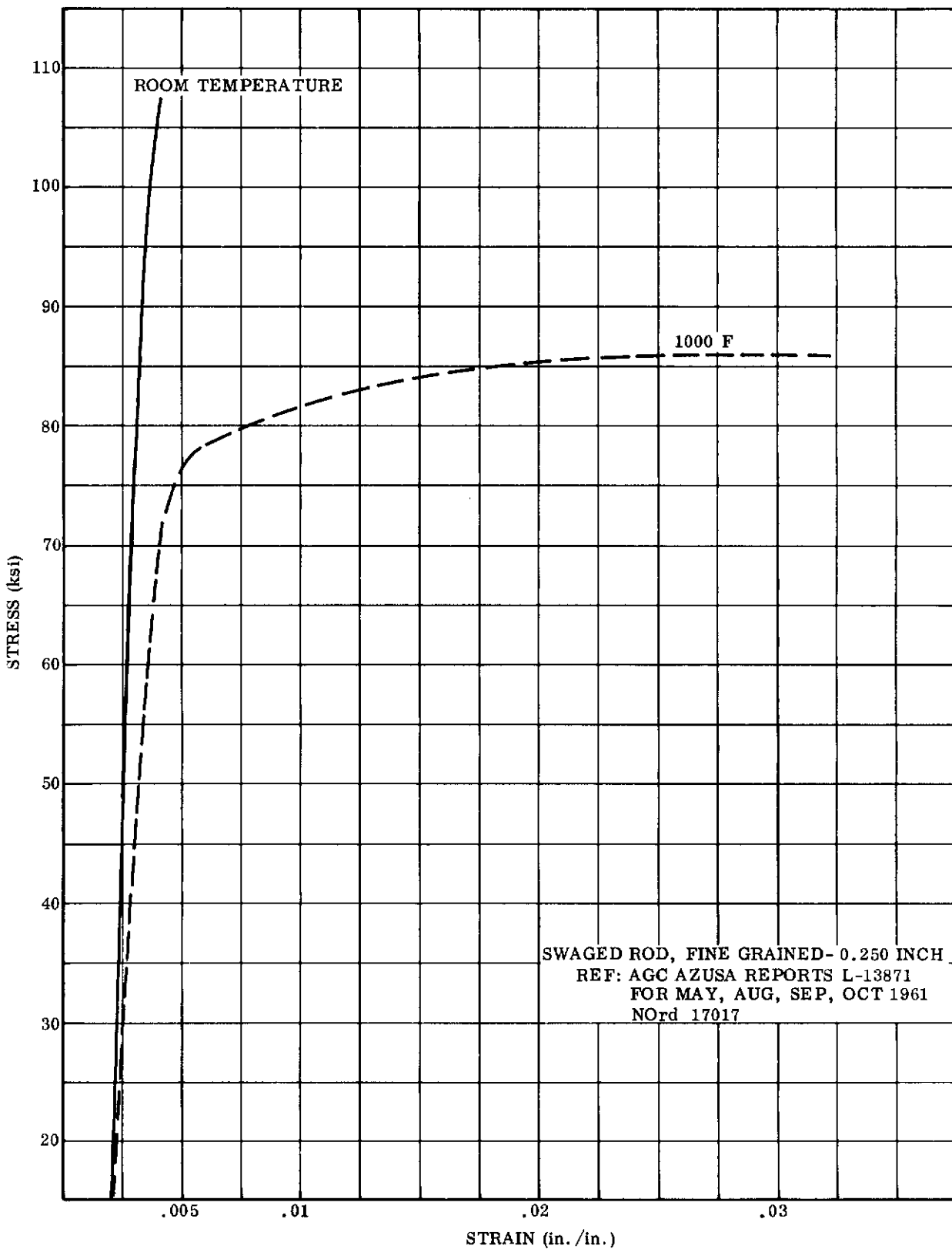


FIGURE 20. MECHANICAL PROPERTIES OF TUNGSTEN AT ROOM TEMPERATURE AND 1000 F

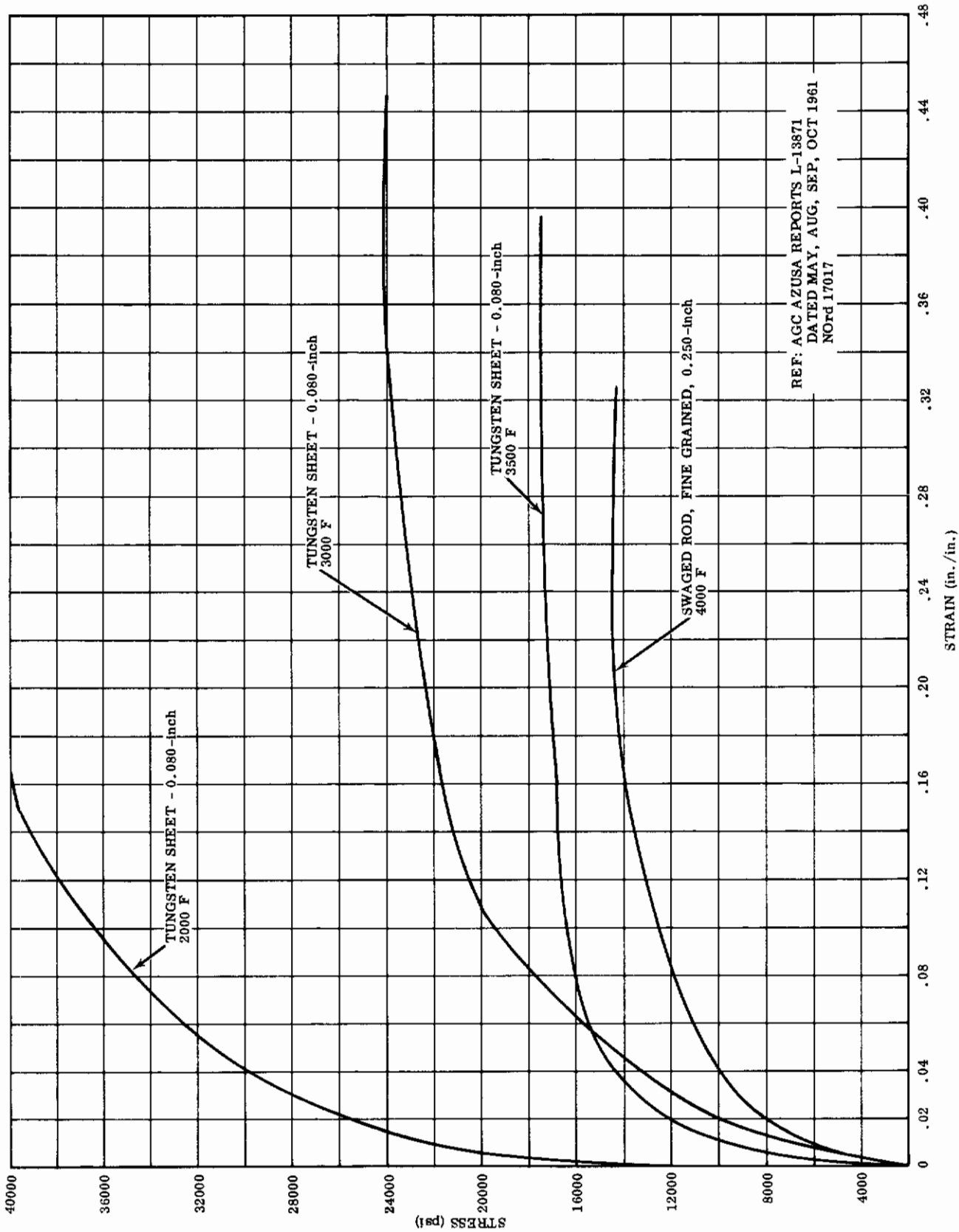


FIGURE 21. MECHANICAL PROPERTIES OF TUNGSTEN AT ELEVATED TEMPERATURES

Due to the extremely short development time available, coating development and property measurement were done concurrently in most cases. Therefore, certain properties of the coating were not measured on SO-86 (the final coating system) but rather on earlier, slightly different formulations. If these properties were not expected to change significantly, they were not remeasured. The coating compositions are shown in Table 2, indicating their similarity.

TABLE 2
THORIA OVERLAY COMPOSITIONS

<u>Material</u>	Coating Number				
	SO-16	SO-71	SO-84	SO-86	SO-100
	(Parts by Weight)				
ThO ₂ , -50 +200 mesh Lindsay Code 116	70	--	--	--	--
ThO ₂ , -270 mesh Rio Tinto	25	--	--	--	--
ThO ₂ , -50 +100 mesh Norton	--	60	--	60	--
ThO ₂ , -100 +200 mesh Norton	--	10	--	10	--
ThO ₂ , Y 890 Zircoa	--	--	--	--	93
Th(NO ₃) ₄ · 4H ₂ O Lindsay Code 103	5	10	25	5	--
Y710 binder, Zircoa	--	--	--	--	7
ThO ₂ , -270 mesh, milled 24 hours Rio Tinto	--	30	75	30	--
Water	(1)	(1)	(1)	(1)	--

1. Sufficient water added to dissolve Th(NO₃)₄ · 4H₂O and to form a paste-like mix

3.3.1 Density and Shrinkage

Both the original as-cured density and the final density after thermal exposure are of interest. Coating SO-86 densities were the highest of any of the coating formulations tried for ASSET. Whereas, the early SO-16 coating densities were 5.3 gm/cm^3 , the density of SO-71+SO-84 increased to 6.0 gm/cm^3 . This steady increase in density resulted from a change to fused thoria powders and the use of less binder (therefore, less water present during trowelling).

Densities ranging from 6.9 gm/cm^3 to 7.1 gm/cm^3 have been recorded for trowelled SO-86 bars. The trowelling technique was expected to result in materials with less reproducibility than those made by certain production techniques. This variation in SO-86 as-cured density was therefore not surprising.

Density variation with temperature was determined by measuring expansion and isothermal shrinkage. All measurements were made in Solar's thermal expansivity apparatus. The SO-86 coating was prepared by trowelling into 1-1/2-inch by 1-1/2-inch by 1/4-inch metal molds and curing to 2200 F. Samples 1/4 inch by 1/4 inch by 1-1/2 inch were then cut from these plates.

Results of isothermal shrinkage at 4360 F are shown in Figure 22. Shrinkage (0.43 percent) occurred during the first few minutes of testing. Maximum temperature for the isothermal test was achieved in 3 to 5 minutes.

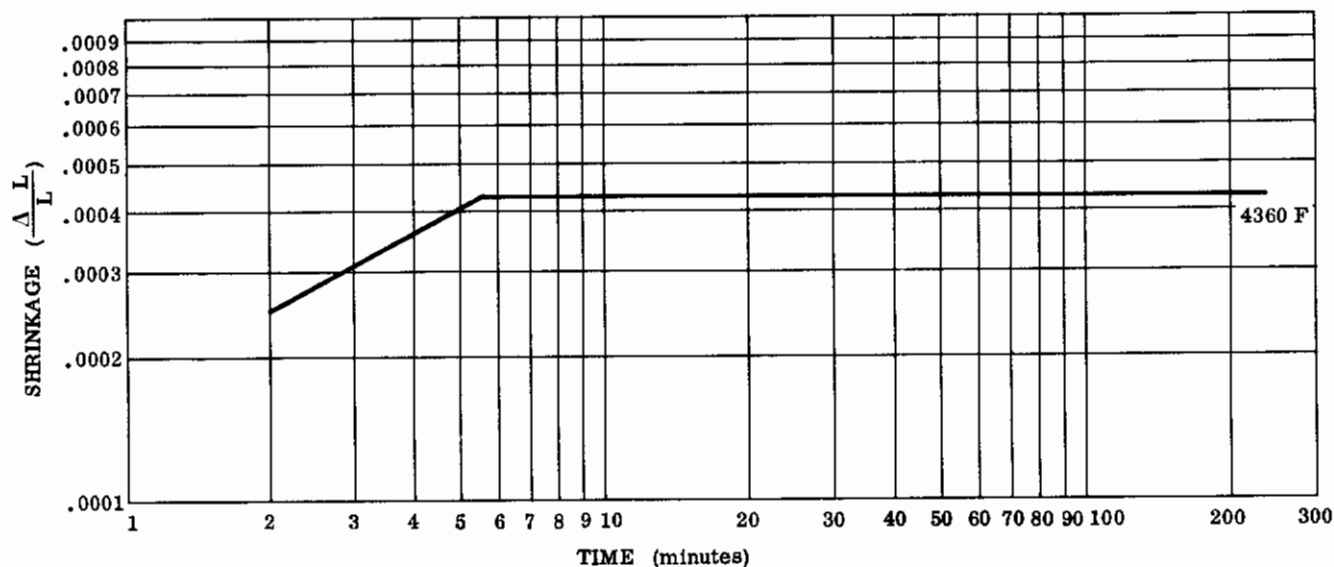


FIGURE 22. ISOTHERMAL SHRINKAGE VS TIME OF COATING SO-86

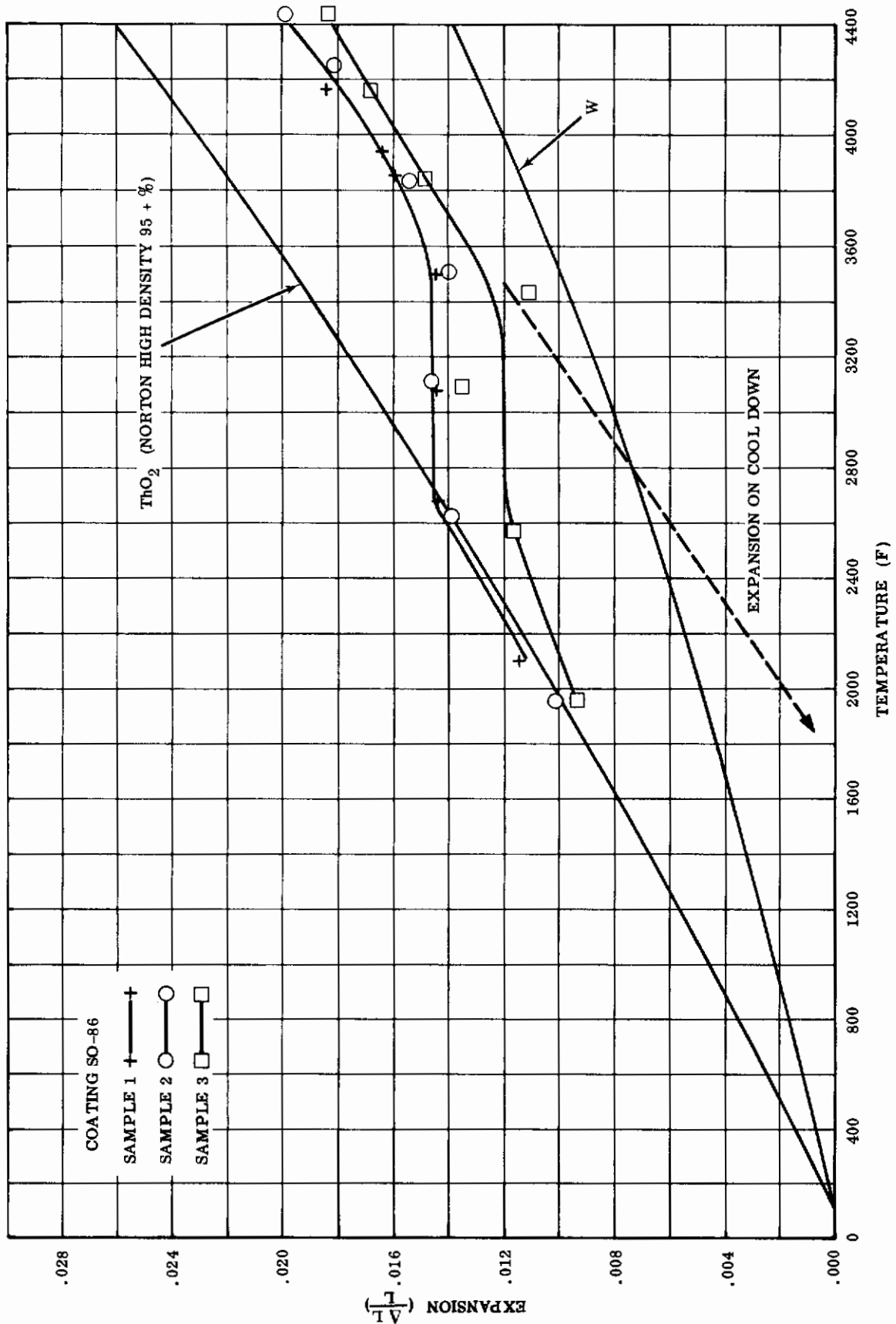


FIGURE 23. THERMAL EXPANSION OF THORIA, TUNGSTEN, AND COATING SO-86

Expansion of the coating is shown in Figure 23. Here, shrinkage began at 2200 F and compensated for the expansion difference between thoria and tungsten.

The density of the coating at any time is related to the length, L, at any time by the equation:

$$P = \left(\frac{L_f}{L}\right)^3 P_f$$

$$P = \left(1 - \frac{\Delta L}{L}\right)^3 P_f$$

Where P_f is the final density, ΔL is the change in length at any time, and L_f the final length.

Actual average linear shrinkage measured on six SO-86 samples was 0.66 percent. This slight change would have only a small effect on density. Gross changes in thermal conductivity resulting from an increase in density (decrease in porosity) can be considered improbable.

3.3.2 Modulus of Rupture

Values of modulus of rupture were measured at room temperature on the unreinforced coating only. This parameter was used as an evaluation tool, comparing the strength of one coating candidate with another.

Modulus of rupture of overlays was obtained from samples prepared during the shrinkage study. A center-point load was applied to 1/4-inch by 1/4-inch by 1-1/4-inch samples using a one-inch span, at a rate of 0.925 in./min. Loads were applied with a Riehle testing machine, and recorded on a Moseley X-Y recorder.

Coating SO-86 achieved as high a strength as any coating tested. Two different batches of SO-86 were evaluated. Results of the modulus of rupture (MR) test were:

Batch	Cure Temperature (F) and Time (hr)	Samples Tested	Modulus of Rupture		
			High (psi)	Low (psi)	Average (psi)
1	2200 - 2	5	1440	723	950
2	2200 - 2	5	1290	1020	1150

The strength of coating SO-86 was very satisfactory for a chemically bonded ceramic cured at such a low temperature (2200 F). Early vibration tests indicated that a coating with modulus of rupture of 200 psi would be adequate for the ASSET program.

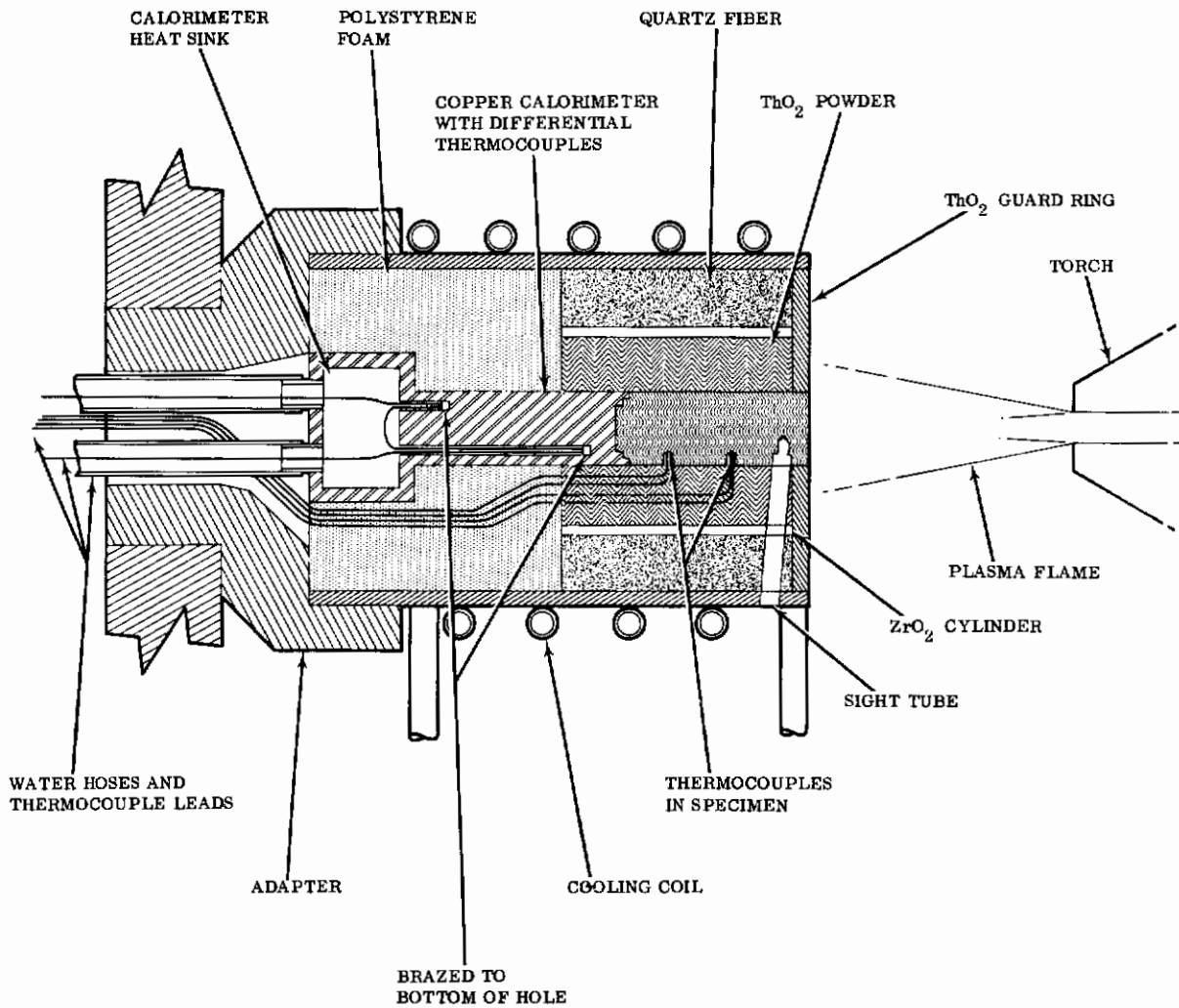


FIGURE 24. THERMAL CONDUCTIVITY APPARATUS; Cross-Sectional Drawing

3.3.3 Specific Heat

The specific heat of overlays was not determined as part of the program. The values reported were obtained from a literature survey. The data should not show any differences due to phase changes since thoria retains its cubic structure to its melting temperature. Specific heat of 0.065 Btu/lb used for this program was taken from Stull and Sinke⁽¹⁾.

3.3.4 Thermal Conductivity

The thermal conductivity of typical thoria coatings was determined to 3800 F. The technique used a 1/2-inch diameter by 1-inch long specimen attached at one end to a copper calorimeter and heated at the other end with a plasma torch. A schematic of the apparatus is shown in Figure 24. With suitable insulation to minimize radial heat flow, a thermal gradient was established along the specimen. The gradients for this experiment were measured with chromel-alumel, Pt/Pt13Rh thermocouples attached to the specimen and by a pyromicro optical pyrometer for the sight tube and front-face temperatures. A W/W25Re thermocouple was substituted for the sight tube on the zirconia sol bonded specimen, but failed at 2500 F. This failure showed a requirement to use optical front-face temperatures for the high-temperature data points.

The specimens were heated in the plasma-arc test chamber at an absolute pressure of 40 Torr. Temperatures were recorded after stabilization of the calorimeter temperature.

When steady state was reached, the thermal conductivity was determined from the heat flow measured by the copper calorimeter and the temperature difference between various points on the specimens.

Values of thermal conductivity measured in the fashion described are presented in Figure 25. The curve of design data used in all nose cap heat transfer calculations is also shown on that figure. The lower band of values is representative of specimens tested in the as-cured condition. The thermal conductivity of the as-cured coatings was lower than the corrected value of slip-cast thoria because the cure temperatures produced only small amounts of sintering at the particle contacts. Conductive heat

1. Stull, D.R. and Sinke, G.C., "Thermodynamic Properties of the Elements," American Chemical Society (1956).

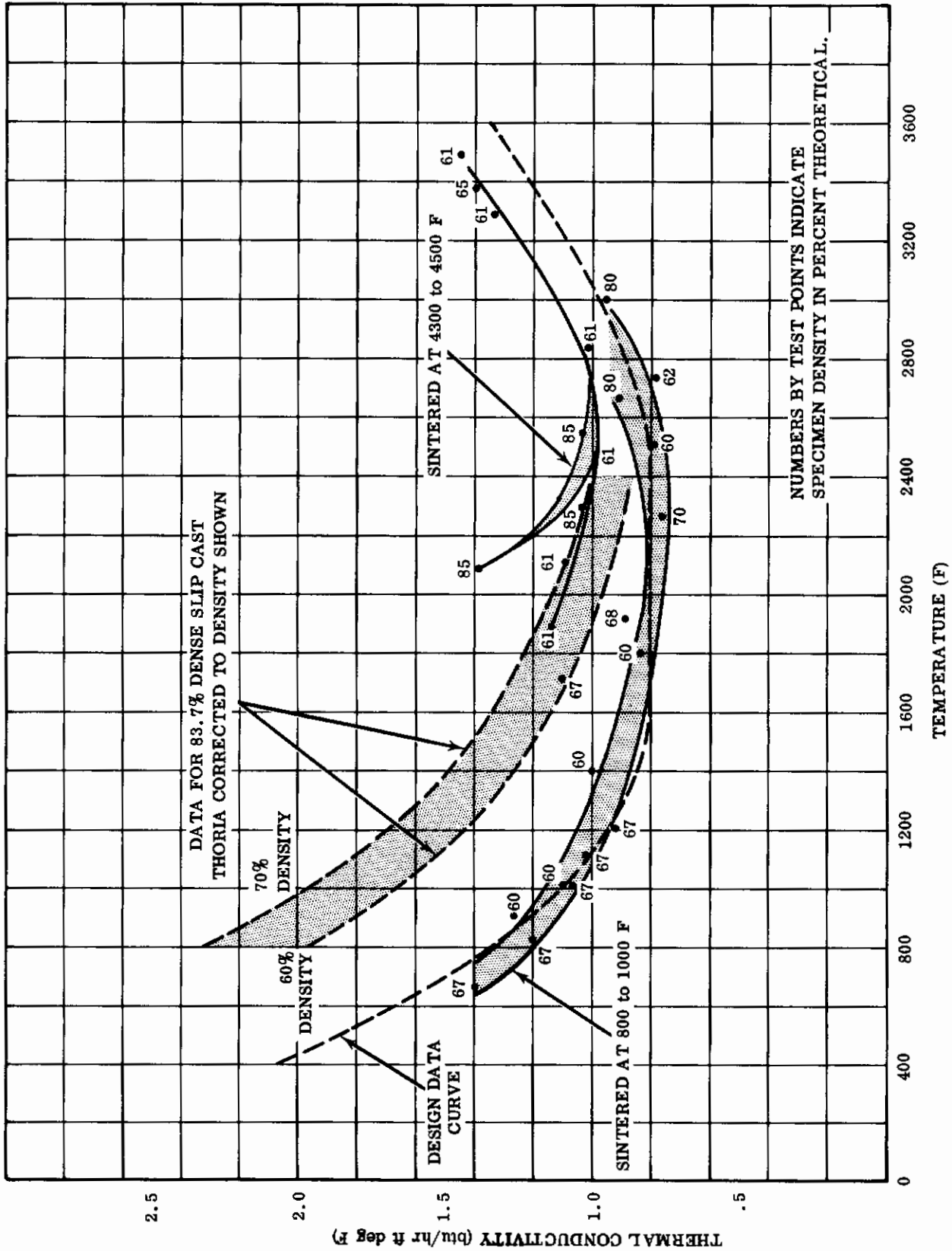


FIGURE 25. THERMAL CONDUCTIVITY OF CHEMICALLY BONDED THORIA COATINGS

transfer, the prime contribution to net heat transfer at low temperatures, is therefore lower than for a high-fired specimen of the same density. When specimens were tested after exposure at 4300 to 4500 F however, the band of thermal conductivity values appeared to follow the values for slip cast thoria very closely.

The coating SO-86 used on the Solar ASSET nose caps is cured at 2200 F and has a nominal density of 7 gm/cm^3 , corresponding to a density of 70 percent. During heat-up of the nose cap, the thermal conductivity will follow the lower curve of Figure 25 typical of as-cured coatings. As the temperature increases above 2500 F, sintering of the coating will begin, and will accelerate as the temperature is increased further. The thermal conductivity will approach the values typical of high-fired thoria. As the temperature of the nose cap decreases, the thermal conductivity will vary as that of high-fired thoria, or along the higher band of values in Figure 25.

The design curve for thermal conductivity was chosen to reflect the values for as-cured thoria coatings, since rate of coating temperature rise during boost is a significant design factor.

3.3.5 Emittance

Emittance values for thoria were measured by Solar, SRI, and Norton over a range of temperatures and environmental conditions. Unfortunately, there is little agreement in these data. Errors in measurements resulted from the inability to measure surface temperatures accurately, and the inability to operate test equipment to high temperatures with air environments.

Solar measured the emittance of hafnia and thoria to 4000 F. Two basic methods of measurement were used--reference black body, and hot filament. The procedures are described in considerable detail in Volume II of this report.

The reference black-body method was developed to measure emittance at 4000 F using a black-body cavity and ATJ graphite as a calibration standard. The heating of the test specimens in an atmosphere with carbon present produced an oxygen-deficient oxide with higher emittance than the stoichiometric oxide. Therefore, the results were not suitable for design. The data do form an upper limit to the true emittance value, however. Data measured on hafnia indicated that true emittance tended to approach that measured in the reference black-body apparatus at high temperatures.

The hot-filament method involved resistance heating of coated tungsten rods in a vacuum, and the emittance was calculated from the Stephan Boltzman radiation equation by the process described in Volume II of this report.

This method should give very good data on ceramic materials in vacuum and was used with much success on hafnia. However, the method depends on the ability of the ceramic to adhere to the tungsten rod without separation or surface cracking. Hafnia was satisfactory, but thoria separated from the tungsten in certain areas. Erroneously high values of emittance therefore resulted. These data are shown on Figure 26, labeled "resistometric." Surface optical temperatures were measured during the hot-filament test, and the emittance was also calculated from this temperature, using gray-body assumptions. These data are also shown in Figure 26, labeled

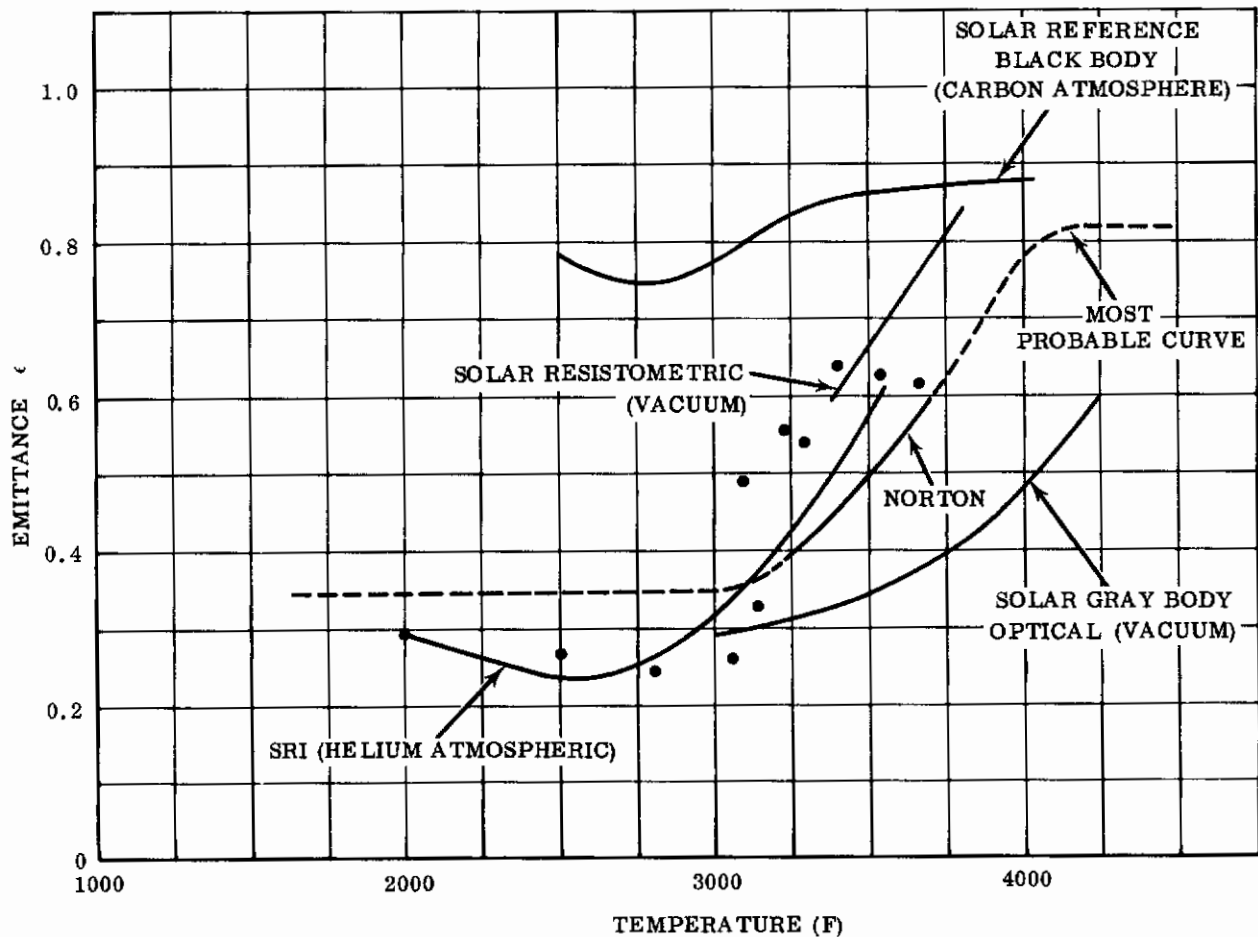


FIGURE 26. EMITTANCE OF THORIA

"gray-body optical." Errors in optical surface temperature measurement, due to tungsten radiation through the surface cracks in the thoria coating, tend to make these data low.

The only data available on which to base a choice of a design curve for the emittance of thoria are those shown in Figure 26. A comparison of the properties of zirconia, hafnia, and thoria suggests a similarity of emittance values is to be expected on all these oxides.

The Vought data on zirconia in air are shown in Figure 27, and the Solar resistometric data on hafnia are shown in Figure 28. The peak value of thoria emittance

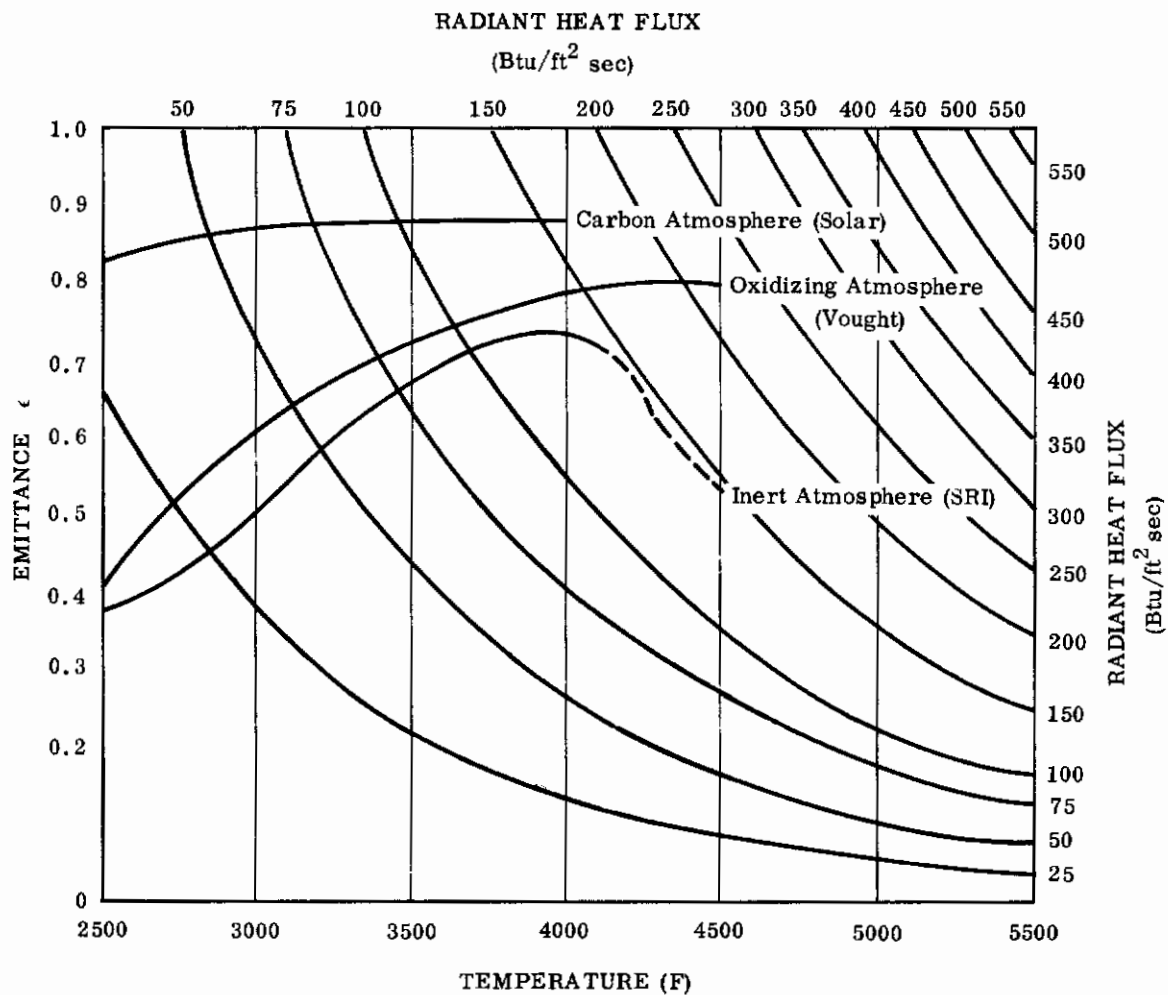


FIGURE 27. EMITTANCE OF STABILIZED ZIRCONIA

should also fall into 0.80 to 0.85 category at 4000 F and above. The most probable emittance curve for thoria is therefore in the vicinity of the Norton and SRI data, increasing to something slightly over 0.80 at 4000 F. The curve labeled "most probable curve" in Figure 26 was chosen on this basis for design.

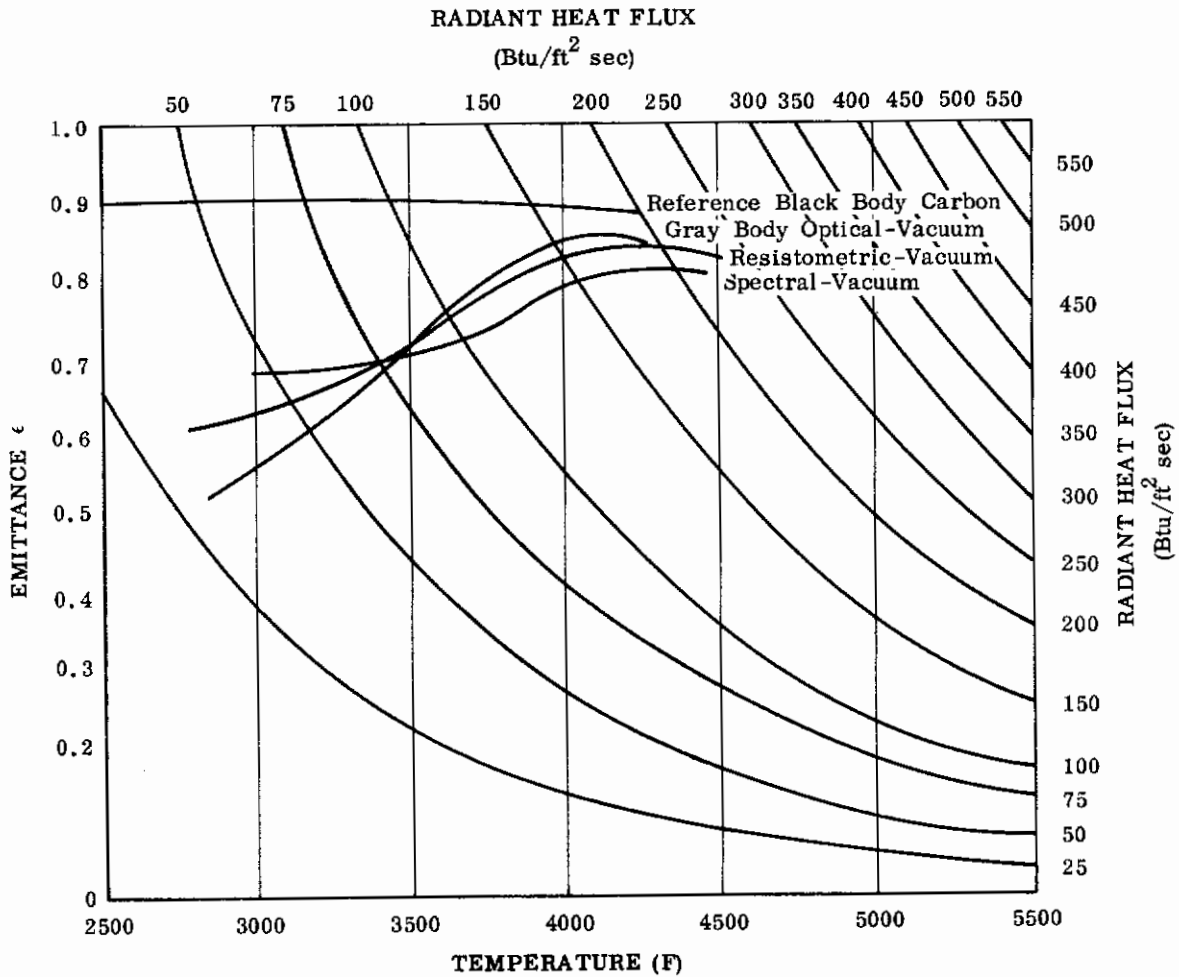


FIGURE 28. EMITTANCE OF STABILIZED HAFNIA

IV. SUMMARY OF ANALYSES ON ASSET NOSE CAP

A thermal and structural analysis of the Solar nose cap for ASV-4 was conducted, using the materials property data presented in Section III. This analysis was performed by Lockheed Missiles and Space Company under subcontract to Solar. A detailed discussion of the complete analysis is presented in Appendix I. Conclusions and pertinent comments are presented in the following paragraphs.

4.1 THERMAL ANALYSIS

LMSC thermal analysis of the nose cap was conducted using Fay & Riddell equations for stagnation point convective heating rates. Stagnation point heat transfer coefficients during glide are shown in Figure 29, presented as the ratio of convective heat transfer coefficient and specific heat, h/c_p . Distribution of heat flux along the cap

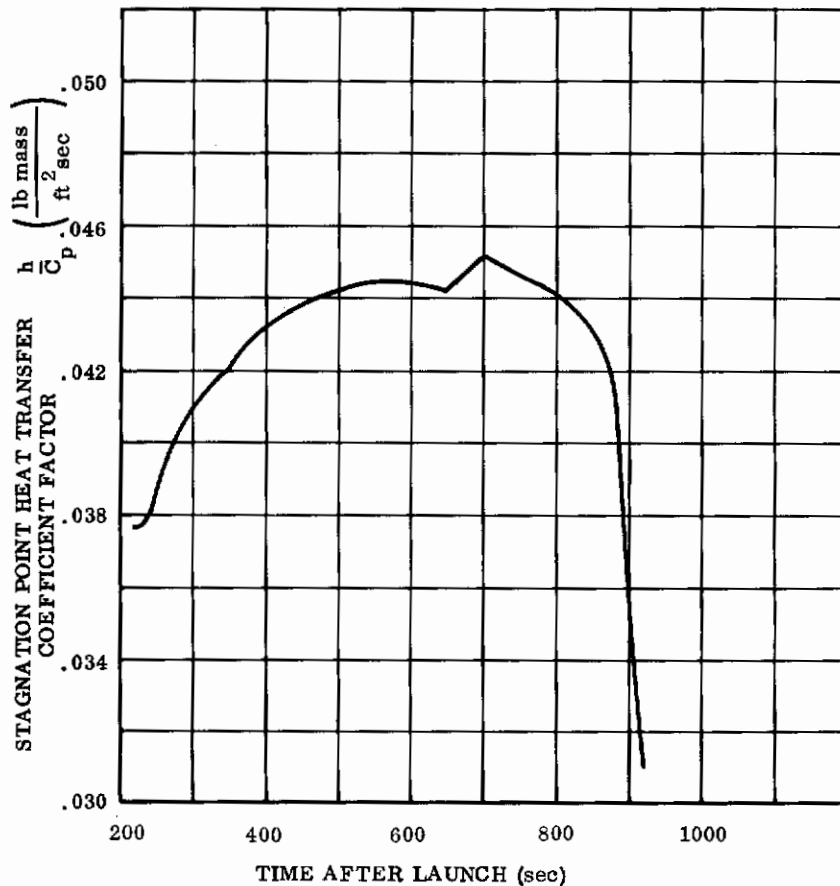


FIGURE 29. STAGNATION POINT LAMINAR CONVECTIVE HEAT TRANSFER COEFFICIENT FACTOR; ASV-4 Trajectory

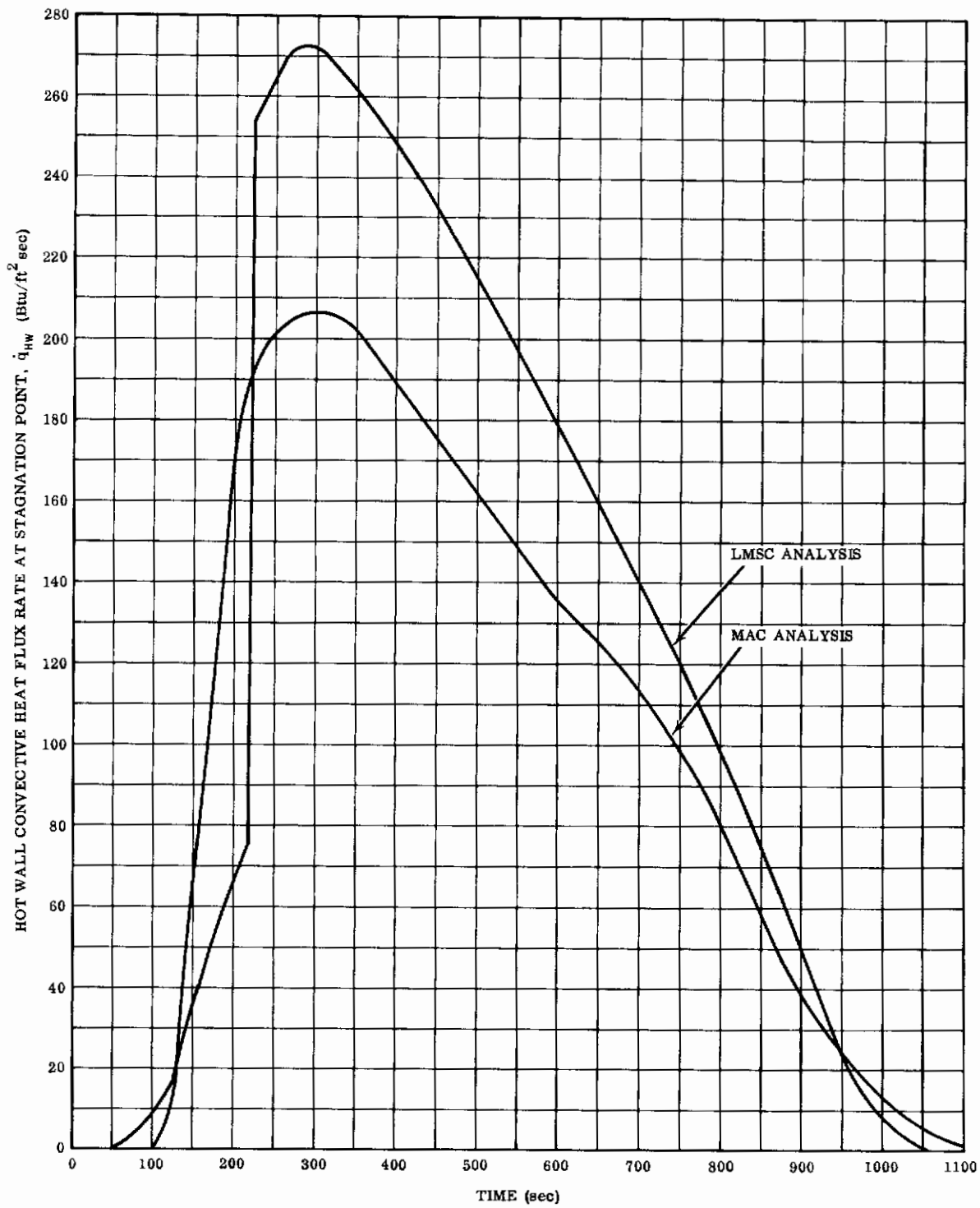


FIGURE 30. ANALYTICAL RESULTS FOR HOT WALL CONVECTIVE HEAT FLUX AT STAGNATION POINT; ASV-4

was determined from Lee's analysis. The results of the LMSC analysis are presented in Appendix C. Hot wall convective heating rates at the stagnation point reach a maximum value of 271 Btu/ft² sec at 290 seconds after launch. The stagnation point reaches a maximum temperature of 4540 F at the same time.

McDonnell Aircraft Corporation also conducted a thermal analysis of the Solar nose cap in conjunction with the thermocouple response calculations for which they were responsible. The MAC analysis utilizes Lee's approximate equation for stagnation point heating. Distribution around the cap was based on $q = q_s \cos^{3/2} s/r$ where s is the surface distance from the stagnation point, and r is 3.11 inches. Based on wind tunnel and shock tube data available to MAC, the Lee's theoretical stagnation point maximum heat flux rates were reduced by 18 percent for this analysis. This same analysis was used by MAC on the MAC nose cap and molybdenum afterbody to which the nose cap is attached. A comparison of hot-wall convective heat flux rates calculated by LMSC and MAC for the Solar nose cap is shown in Figure 30.

The basic differences in analytical approach resulted in widely divergent results. Temperature-time profiles for the nose cap and molybdenum forging varied considerably, both in shape and in maximum value. The resulting temperatures for both LMSC and MAC analyses are compared, for selected points, in Figure 31. LMSC analysis is more critical in all respects. A tabulated comparison of the analysis is:

	<u>LMSC</u>	<u>MAC</u>
Maximum hot-wall flux (Btu/ft ² sec)	271	206
Maximum surface temperature (F)	4540	4120
Maximum tungsten temperature (F)	4040	3320
Maximum bolt temperature (F)	3410	2910
Maximum molybdenum forging temperature (F)	3500	3100

Differences in the analytical results can be explained in the following ways.

1. Differences in maximum value of temperature at the stagnation point results primarily from difference in convective heat flux calculations to the surface. LMSC actual temperature lags equilibrium surface temperature by approximately 100 F at maximum temperature. MAC indicates a lag of 220 F.

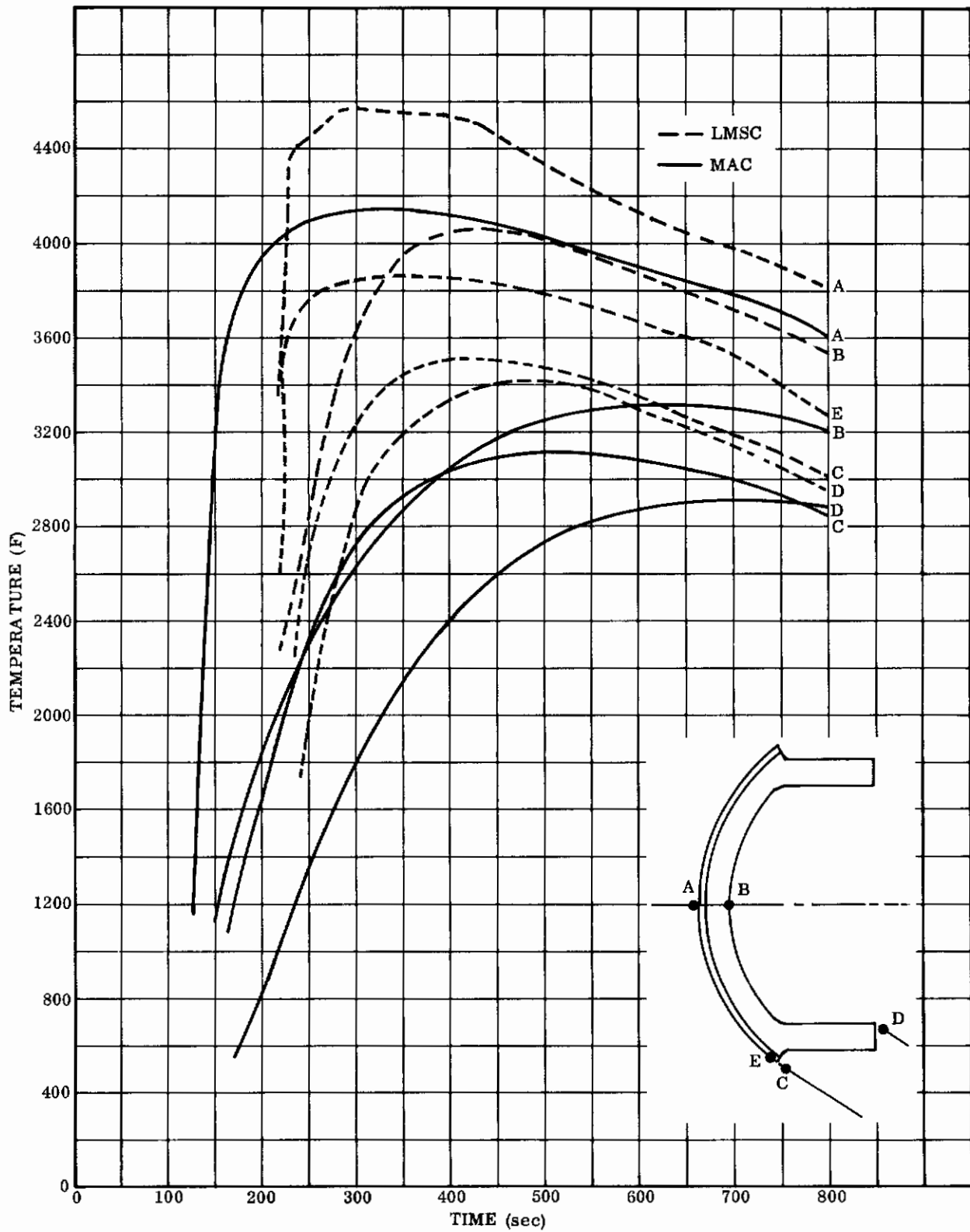


FIGURE 31. TEMPERATURE HISTORY OF VARIOUS POINTS ON THE NOSE AND SKIRT SECTIONS; ASV-4

2. Gradients through the thoria are higher in the MAC analysis than in the LMSC analysis. This can be apparently accounted for by slight differences in thoria thermal conductivity used. A comparison is as follows:

<u>Temperature (F)</u>	<u>LMSC</u>	<u>MAC</u>
400	2.1	2.25
800	1.35	1.70
1200	0.95	1.50
1600	0.80	1.45
2000	0.80	1.25
2400	0.80	1.20
2800	0.90	1.15
3200	1.10	1.10
3600	1.35	1.10
4000	1.60	1.25
4200	1.75	1.35

Taking a point at 300 seconds, according to Figure 31, the variation in gradient can be explained in gross fashion by this difference in conductivities.

At T = 300 seconds:

	Surface Temperature (F)	Tungsten Temperature (F)	Mean Temperature (F)	K at T _{mean}	ΔT	KΔT
LMSC	4540	3600	4070	1.7	940	1598
MAC	4120	2700	3410	1.1	1420	1560

This difference in thermal conductivity might also explain the differences in the lag between surface actual temperature and equilibrium temperature.

The question of choice of Fay & Riddell, in its several modifications, or Lee's approximate solution as the method for calculation of stagnation point convective heating rate is a difficult one. In fact, one reason for the ASSET project is to help in defining methods for predicting heating rates in hypersonic glide by obtaining accurate flight data. It is certainly assumed that both McDonnell and Lockheed gave consider-

able thought to the entire subject before choosing one method of analysis or another. Attempting to define the problem more completely for the Solar nose cap analysis therefore was a lengthy task of questionable result.

Circumstances surrounding the use of the Solar nose cap on ASSET allow a choice of analysis to be made on an other-than-thermodynamic basis. MAC designed the ASSET vehicle stagnation areas for all flights other than ASV-4 and AEV-1 using Lee's approximate analysis. The zirconia nose cap, used for all flights but ASV-4 and AEV-1, and the molybdenum forging, used on all six ASSET flights, were designed to temperatures resulting from that analysis. When the zirconia cap is used, both the cap and the molybdenum forging reach a higher temperature than with the Solar cap for the same glide trajectory, because of differences in cap emittance and in heat sink available. Therefore, the Solar nose cap can be considered thermo dynamically interchangeable with the zirconia cap for any flights being flown by the zirconia cap.

In addition, since the maximum use temperature for coated molybdenum is not much in excess of 3100 F, the zirconia cap cannot be used for ASV-4. This follows, since the Solar cap results in a forging temperature of 3100 F and the zirconia cap in something considerably higher by MAC's analysis. A factor of safety therefore results from the use of the Solar cap for ASV-4. Finally, if the ASV-4 trajectory is to be flown at all, it must be flown at a heat flux rate no greater than that shown by the MAC analysis for ASV-4 or the forging will be overheated and, in all likelihood, would be unsatisfactory. If the LMSC analysis is correct, ASV-4 must be flown at reduced conditions to maintain molybdenum temperatures below 3100 F. From the preceding comments, then, the following thermodynamic factors can be summarized:

1. Solar nose cap can be substituted for the zirconia cap for any flight conditions.
2. ASV-4 can only be flown with the Solar nose cap, and at a heat flux no greater than resulting from the MAC analysis.
3. If the Solar nose cap is qualified to the MAC analysis, it will not be the component limiting the maximum performance of the vehicle.

The results of the MAC analysis were therefore chosen to define the thermal environment for the tests of the Solar cap. Should this choice be proved wrong by the earlier flights of ASV, either an adjustment of the flight trajectory of ASV-4 or a re-qualification of nose cap and vehicle must occur.

4.2 STRENGTH ANALYSIS

A thermal stress analysis was performed by LMSC on the Solar nose cap. The complete analysis is presented in Appendix C. Maximum thermal stresses occurred at 220 seconds after launch, and reached a maximum of 27,000 psi in compression and 21,000 psi in tension. The analysis demonstrates that the tungsten forging is structurally sound under the LMSC analytical temperature profiles.

The thoria coating is not considered as contributing to the thermal stress behavior of the forging. The pinned joining method used and the lack of chemical or metallurgical bond of thoria coating to tungsten substrate make this assumption reasonable. Thermal stress analysis of the thoria coating was not performed. Proof of the ability of the thoria overlay to resist the thermal environment was demonstrated by the consistently successful plasma-arc tunnel tests.

Contrails

V. TEST PROGRAMS FOR ASSET NOSE CAP

The requirements for the flight nose cap being furnished by Solar for the ASSET ASV-4 vehicle were defined in MAC Specification Control drawing 51-30012. In accordance with that SCD, a series of flight qualification tests were required to demonstrate the integrity of the final design. The results of these tests are reported and discussed in this section. It covers the development and test of the nose cap for ASV-4 flight vehicle, and contains:

- Comparison of environmental requirements with test conditions
- Results and discussion of subscale tests
- Results of discussion of full-scale tests

The second nose cap delivered by Solar was for the AEV-1 vehicle. The configuration was identical to the ASV nose cap with the exception of one additional pressure-port tube and plug. Since flight trajectories for AEV's are less critical than that for ASV's, this report also demonstrates the flightworthiness of the nose cap built for AEV-1.

Environmental conditions to be simulated are defined in Sections 1.1 and 1.2.

Thermal analyses of the nose cap were performed by both Lockheed Missiles and Space Company and McDonnell Aircraft Corporation. The results of these analyses are discussed in Section 4.1. In summary, LMSC analysis indicated a maximum stagnation point hot-wall convective heat flux of 273 Btu/ft² sec. The MAC analysis resulted in 206 Btu/ft² sec for the same point. The reasons for this difference are discussed in Section 4.1.

Qualification of a nose cap for an ASV flight was the prime goal of the analytical and test programs. It was therefore only necessary to qualify the nose cap to the MAC analysis, since that analytical technique was also used by MAC on the nose cap afterbody forging. Such qualification assured that the cap was compatible with the vehicle to which it is attached. Should the vehicle flight conditions be made more severe, both the vehicle and the nose cap would most likely require re-qualification.

5.1 TEST FACILITIES AND CONDITIONS

5.1.1 Load Test

The nose cap was installed in a molybdenum ring simulating actual vehicle mounting mechanism. A foamed plastic loading jig was made, allowing the nose cap to load uniformly over its entire area. Weights were placed on the loading jig in 20-pound increments to design ultimate load.

5.1.2 Acceleration Tests

Though not required by the MAC SCD, acceleration tests were run on subscale test specimens. The tests were conducted at Stellardyne Laboratories, Inc., El Cajon, California. Specimens were mounted on a universal jig that allowed loading in tension, compression, or shear. The jig was mounted on a Stellardyne 60-inch centrifuge and submitted to 12 g for 3 minutes. A photograph of the facility is shown in Appendix D.

5.1.3 Acoustic Tests

The full-scale specimen was tested by Wyle Laboratories, El Segundo, California, using the acoustic facility at Norair. A description of the facility is included in Appendix G. Overall sound pressure level achieved during test was 155 db.

5.1.4 Vibration Tests

Full-scale vibration tests were conducted at Wyle Laboratories, El Segundo, California, using the test equipment described in Appendix G. The vibration levels required by MAC SCD 51-30012 were achieved.

5.1.5 Thermal Test

Thermal qualification tests of the Solar nose cap were performed in a plasma-arc tunnel. This mode of testing was chosen since it provided a more representative gas environment than a combustion-burner facility. In addition, plasma-arc testing allows the simulation of environmental parameters--gas enthalpy and heat flux--without major regard to material properties such as emittance and conductivity, which may not be known accurately. Most oxyacetylene facilities monitor surface temperature, matching it to design temperatures calculated for the material system. Errors in the analysis or in the chosen material properties can result in an invalid test.

Testing on both subscale and full-scale nose caps was performed at Plasmadyne Corporation, Santa Ana, California. This facility consists of an air arc, operating at power levels up to 1000 kw, installed in a vacuum chamber. Hot gases are expanded through a convergent-divergent nozzle. Exit velocity of the gas is Mach 3.0.

Simulation of all variables of the re-entry environment in the Plasmadyne facility was not possible. Since simulation of the maximum heat flux conditions at the stagnation point was required for the full-size test article, neither stagnation point enthalpy nor model stagnation point pressure could be simulated at the same time. Table 3 lists the maximum values calculated for actual flight conditions at the stagnation point, compared with the values obtained in the plasma-arc test. For full-scale tests, model pressure was low, and stagnation enthalpy was high. Since the nose cap is a non-ablating design, simulation of heat flux was of prime importance. The effect of enthalpy in test higher than that in flight is an increase in the slope of the temperature curve during boost, and a higher hot-wall flux for a given cold-wall flux (smaller hot-wall correction). Table 3 illustrates the hot-wall correction effect, noting that cold-wall heat flux was less in the test than for flight, but hot-wall flux was higher in the test than for flight.

Simulation of the flight trajectory was made at two steady-state points. Table 4 lists the test profiles used, and Figure 32 compares the test profiles with calculated flight inputs. For the full-scale tests, the rate of temperature rise is correct, the maximum stagnation hot-wall convective heat flux is correct, and all other temperature-time inputs are conservative.

The Plasmadyne facility has been calibrated extensively when operating a 3.0-inch nozzle with both high and moderate enthalpy plasma generators. Much of this calibration was performed under Contracts AF 33(616)7110 (report ASD-TR-61-304) and AF 33(616)8476 with RTD. Re-calibration of the 3.0-inch nozzle was therefore not required for the subscale tests. The prior method of calibration, taken from ASD-TR-61-304 is summarized below. However, all full-scale tests were run in a Mach 3 nozzle with a 5-1/8-inch exit diameter. This nozzle required calibration for those tests. Details of the calibration data are presented in a report by Plasmadyne⁽¹⁾ and are summarized below.

Subscale tests were accomplished in the Mach 3 nozzle with a 3.0-inch exit diameter. The test conditions obtained are shown in Table 4. Heat flux values were measured with a copper cold-wall calorimeter 5/8-inch diameter hemisphere. Measured heat flux values were converted to hot-wall model stagnation point heat flux values by:

-
1. Evaluation of Thermal Protective Systems Under Simulated Lift Re-Entry Conditions Produced in Advanced Arc Tunnels. Fifth Quarterly Progress Report under Contract No. AF33(657)-8476 by the Plasmadyne Corporation (30 August 1963).

$$\frac{\dot{q}_s \text{ model}}{\dot{q}_s \text{ calor}} = \left(\frac{R_o \text{ calor}}{R_o \text{ model}} \right)^{1/2} \left(\frac{h_T - h_w \text{ model}}{h_T - h_w \text{ calor}} \right)$$

Where: \dot{q}_s = stagnation point cold-wall heat flux
 R_o = radius
 h_T = gas stagnation enthalpy (Btu/lb)
 h_w = gas enthalpy at wall (Btu/lb)

TABLE 3
 MAXIMUM TEST CONDITIONS FOR PLASMA-ARC TESTS

Model	Model Stagnation Pressure (psi)	Stagnation Enthalpy (Btu/lb)	Stagnation Point Cold-Wall Heat Flux (Btu/ft ² sec)	Stagnation Point Hot-Wall Heat Flux (Btu/ft ² sec)
5 (Subscale)	1.54	7610	195.7 ⁽¹⁾	164
6 (Subscale)	1.54	7490	200.3 ⁽¹⁾	167
7 (Subscale)	1.54	7585	194.2 ⁽¹⁾	163
8 (Full-Scale)	0.479	15,120	225 ⁽²⁾ 198.2 ⁽¹⁾	208
9 (d) (Full-Scale)	0.479	14,914	198.4 ⁽¹⁾	206
10 (Full-Scale)	0.479	14,574	203.36 ⁽²⁾ 196.8 ⁽¹⁾	
Actual Conditions During Flight	2.5	7,600	245	206

1. Calculated
2. Measured

TABLE 4
PLASMA-ARC TUNNEL TESTS
Calibration Data

Number	Time (sec)	Model Stagnation Enthalpy (Btu/lb)	Model Stagnation Pressure (atm)	Stagnation Heat Flux Measured with 5/8-inch Calorimeter (Btu/ft ² -sec)	Calculated Cold-Wall Model Heat Flux (Btu/ft ² -sec)	Measured Cold-Wall Model Stagnation Heat Flux (Btu/ft ² -sec)
5	0	835	0.0605	Not Measurable	Approx. 7.0	-----
	0 - 200	Linear Increase to 7,610	7,610 Btu/lb			
	200- 371	7,610	0.1050	610.8	195.7	-----
6	0	815	0.0606	Not Measurable	Approx. 7.0	-----
	0 - 200	Linear Increase to 7,490	7,490 Btu/lb			
	200- 500	7,490	0.1050	612.5	200.3	-----
	500- 650	Linear Decrease to 4,985	4,985 Btu/lb			
	650-1050	4,985	0.0785	365.4	115.8	-----
1050-1080	Linear Decrease to 830	830 Btu/lb				
7	0	810	0.0606	Not Measurable	Approx. 7.0	-----
	0 - 200	Linear Increase to 7,585	7,585 Btu/lb			
	200- 500	7,585	0.1050	609.9	194.2	-----
	500- 650	Linear Decrease to 5,000	5,000 Btu/lb			
	650-1050	5,000	0.0785	365.6	115.9	-----
1050-1080	Linear Decrease to 800	800 Btu/lb				
8	0	785	0.0250	Not Measurable	-----	-----
	0 - 120	Linear Increase to 15,120	15,120 Btu/lb			
	120- 300	15,120	0.0326	640.5	198.2	225.16
	300- 440	Linear Decrease to 9,990	9,990 Btu/lb			
	440- 920	9,990	0.0275	425.5	130.2	134.61
920- 950	Linear Decrease to 815	815 Btu/lb				
9 (d)	0	984	0.0250	Not Measurable	-----	-----
	0 - 120	Linear Increase to 14,914	14,914 Btu/lb			
	120- 300	14,914	0.0326	641.4	198.4	-----
	300- 440	Linear Decrease to 10,210	10,210 Btu/lb			
	440- 920	10,210	0.0275	424.5	129.9	-----
920- 950	Linear Decrease to 895	895 Btu/lb				
10	0	1025	0.0250			53.53
	0-120	Linear Increase to 14,574	14,574 Btu/lb			
	120-300	14,574	0.0326	645.5	196.8	203.36
	300-400	Linear Decrease to 1,0162	1,0162 Btu/lb			
	400-920	1,0162	0.0275	410.5	133.0	129.91
920-990	Linear Decrease to 1,025	1,025 Btu/lb				

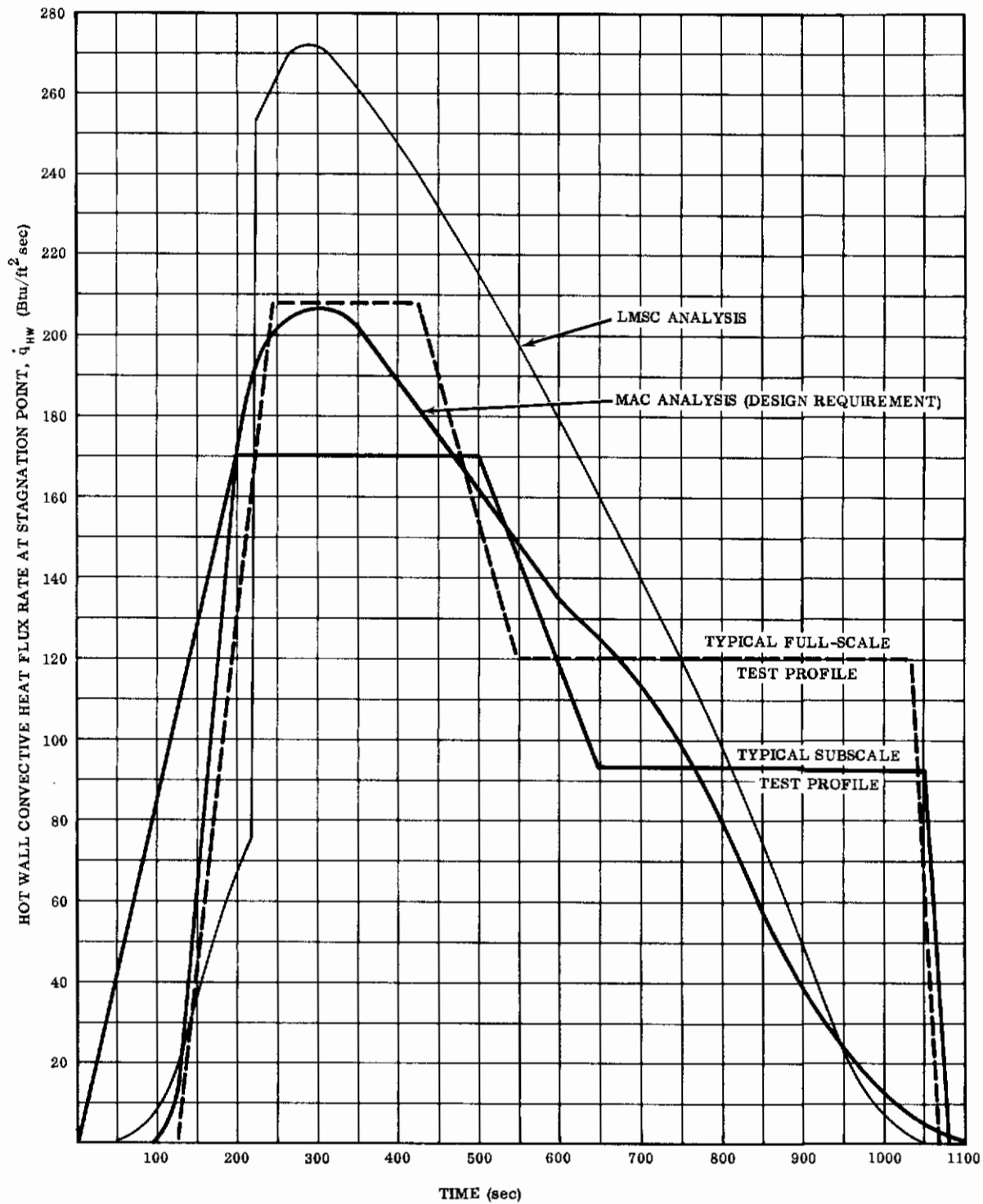


FIGURE 32. COMPARISON OF TEST INPUTS WITH DESIGN REQUIREMENTS; Hot-Wall Convective Heat Flux at Stagnation Point, ASV-4

Cold-wall values were calculated neglecting the enthalpy difference terms. Stagnation point enthalpy was measured directly using a specially designed enthalpy probe. The probe measured the local total enthalpy by

- extracting a known amount of gas from the free stream
- cooling the gas to approximately 100 F
- measuring the heat extracted

Radial traverse of the 3.0-inch nozzle showed decreases in local stagnation enthalpy of up to 20 percent from the centerline to the edge of the jet, excluding the boundary layer area.

Model stagnation pressure was measured with a water-cooled pitot tube. Model stagnation pressures appeared to be about 10 percent lower on the jet centerline than at one inch from the centerline.

Full-scale tests were conducted in a specially constructed 5-1/8-inch exit diameter nozzle. Test conditions achieved with this nozzle are shown in Table 4. The 5-1/8-inch diameter nozzle was calibrated for this program using similar instrumentation and calibration procedures as for the 3.0-inch nozzle. A plot of model stagnation pressure versus radial position in the stream is shown in Figure 33. The pressure survey did not include the boundary layer, which was approximately 5/8-inch thick at operating conditions.

Cold-wall heat flux values were measured with a copper calorimeter, and converted to model stagnation heat flux by the equation shown above. These values are shown in Table 4.

Graphite models of both the full-scale and sub-scale test articles were constructed and instrumented with small copper-slug calorimeters to check the heat flux values obtained on an actual shape. The actual heat flux to the model surface was measured at the test points that were used in simulating the re-entry trajectories. The heat flux measured was actually the cold-wall convective heat flux, since the average copper-slug temperature for the most severe test point at the stagnation point was 590 F. Results of these test runs are presented in Table 5 for the full-scale

TABLE 5
 CALORIMETER DATA - MODEL CALIBRATION TEST
 5-1/8-Inch Diameter Nozzle

Stagnation Enthalpy (Btu/lb)	Model Stagnation Pressure (atm)	Slug Position (deg)	Cold-Wall Heat Flux to Calorimeter (Btu/ft ² sec)	Average Copper Calorimeter Temperature (F)
15,120 (For test No. 8 and 9d)	0.0275	Stag. Point	225.16	590
		42	61.65	
		42	60.38	
		42	64.65	
		25	222.86	
9,990 (For tests No. 8 and 9d)	0.0275	Stag. Point	134.61	372
		42	45.01	
		42	41.45	
		42	46.65	
		25	152.89	
1,025 (For test No. 10)	0.0250	Stag. Point	53.53	
		42	8.96	
		42	5.88	
		42	9.36	
		25	43.71	
14,574 (For test No. 10)	0.0326	Stag. Point	203.36	
		42	77.40	
		42	67.05	
		42	68.94	
		25	213.81	
10,162 (For test No. 10)	0.0275	Stag. Point	129.91	
		42	49.31	
		42	43.86	
		42	45.09	
		25	155.68	

models. The distribution of heat flux over the model surface does not agree with theoretical distribution. In fact, at a stagnation enthalpy of 9990 Btu/lb the stagnation point heat flux is lower than at a 25-degree angle. This nonuniformity of heat flux distribution was noted on actual test parts as well. Plasmadyne personnel attributed this phenomenon to the interaction of shock waves. The high heat flux area away from the stagnation point was apparently the intersection of a shock wave with the surface of the model, causing local overheating. If this explanation is correct, the stagnation point heat flux and temperature reached during the test will correspond to actual flight conditions. However, the hottest part of the model where shock impingement occurred was tested at a higher heat flux and temperature than will be experienced in flight.

Calibration data for the subscale specimens run in the 3-inch nozzle are shown in Table 6. Data are in reasonable agreement with theory.

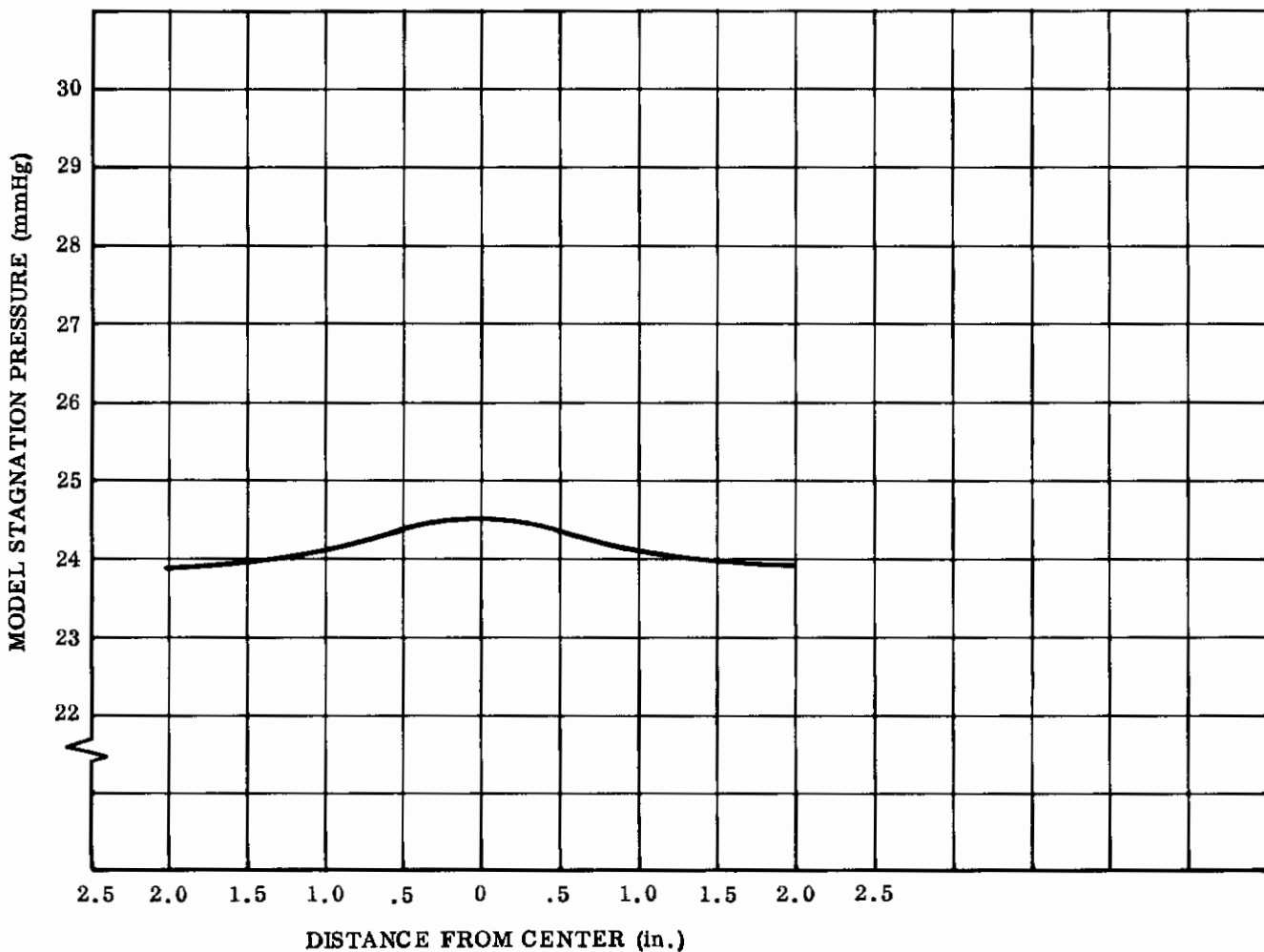


FIGURE 33. RADIAL MODEL STAGNATION PRESSURE SURVEY; 5/8-Inch Nozzle

TABLE 6
SUBSCALE CALORIMETER DATA

Gas Stagnation Enthalpy (Btu/lb)	Model Stagnation Pressure (atmospheres)	Slug Position (deg)	Heat Flux (Btu/ft ² sec)
7,584	0.1048	Stag. Point	198.23
		12.5	168.59
		12.5	166.29
		25.0	80.26
		25.0	85.15
		25.0	88.88
5,050	0.0786	Stag. Point	108.75
		12.5	98.82
		12.5	95.37
		25.0	55.37
		25.0	53.98
		25.0	53.38

} In conjunction with Models A-2 and A-3

5.2 SUBSCALE TEST PROGRAM

A series of subscale tests was conducted to evaluate the ASSET nose cap design concept prior to full-scale flightworthiness tests. The subscale form chosen for evaluation was a 0.250-inch thick tungsten plate, formed to the same contour as the actual nose cap, but measuring only 3.85 inches in diameter. This specimen, therefore, duplicated the area within 2 inches of the stagnation region. The following tests were run:

<u>Test Number</u>	<u>Coating</u>	<u>Test</u>
1	SO-52 (as cured)	Acceleration and vibration
2	SO-52 (tested at 4100 F for 5 min)	Acceleration and vibration
3	SO-71 + SO-84 (as cured)	Vibration
4	SO-71 + SO-84 (as cured)	Acoustic

5	SO-71 + SO-84 (as cured)	Plasma arc (aborted at 6 min due to equipment failure)
6	SO-86 (as cured)	Plasma arc
7	SO-71 + SO-84 (as cured)	Plasma arc

Each of these tests is discussed in the following paragraphs.

5.2.1 Test No. 1 and 2 - Acceleration and Vibration

Subscale tests 1 and 2 were conducted simultaneously. Since they were performed early in the program, they utilized the sine-wave reinforcement technique. This form of reinforcement was shown to be inefficient by subsequent testing and is no longer used. The coating SO-52 was also replaced by higher-strength coatings. However, since acceleration tests were not run on other coating systems, those early results are presented, and serve to indicate that the stronger composites are satisfactory.

The specimens for tests 1 and 2 were reinforced with tungsten sine-wave ribbon and 0.010-inch tungsten wire coils. One specimen had been exposed to 4100 F for 5 minutes in an oxyacetylene torch facility; the other was as cured. For testing, the shapes were mounted on a right-angle fixture by removing small sections of the coating and clamping to the tungsten substrate.

The acceleration tests were conducted by Stellardyne Laboratories on a 60-inch centrifuge obtaining a centrifugal force of 12 g for 3 minutes in each of the three major axes (compression, shear, and tension). The test report and a photograph of the test apparatus are contained in Appendix II. No deleterious effects were observed in the coating or reinforcements for either of the nose shapes. The success of the low-strength SO-52 formulation on the acceleration test indicated no major problem in qualifying the high-strength SO-71 coating selected for ASSET.

Vibration tests were conducted on the two SO-52 coated ASSET nose shapes that successfully passed the acceleration test. The tests were conducted by Solar on a Calidyne (Model A174) shaker under vibration and g loads expected during boost:

<u>Frequency (cps)</u>	<u>Load (g)</u>
5 to 15	0.3 inch D.A.
15 to 100	± 3.0
100 to 500	± 5.0
500 to 2000	± 10.0

The test fixture, with the nose shapes attached, was mounted to the shaker. The tests were performed by slowly scanning through the frequencies at the required g loads, while making visual inspection of the effect on the coating and reinforcements.

Frequencies of 1000 and 1500 cps at 10 g produced resonance in the shapes and caused powdering of the coating in small areas above the reinforcements on the "as cured" nose shape. Negligible effects were observed on the shape which had been tested in the oxygen-acetylene torch because of the increased hardness of the coating. The powdering of the "as cured" coating accelerated the development of high-strength coating formulations, leading to the development of coatings SO-71 and SO-86. After exposure to 4100 F, the increased hardness of the coating due to sintering prevented failure of the coating in vibration. This indicates, as would be expected with such material systems, that vibration loads encountered during glide are not significant, being smaller in magnitude than those during boost, when acting on a strengthened material system.

5.2.2 Test No. 3 - Vibration

Two specimens of the stronger coating SO-71 + SO-84 were prepared for vibration testing. One specimen was reinforced with tungsten sine-wave ribbon; the other with tungsten mesh similar to the finally chosen reinforcement system. These two caps were vibrated at Stellydyne Laboratories on a Ling A-246 shaker under the conditions described in Section 5.2.1 Resonance was detected on each cap at 10 g and 1000 cps, but no failure occurred; however, the cap with the sine-wave reinforcement did show a slight hairline crack. A copy of the Stellydyne Laboratories report is included with this report as Appendix III.

This series of tests indicated that the SO-71 + SO-84 system with wire mesh reinforcement had sufficient strength to withstand vibration loads occurring during boost.

5.2.3 Test No. 4 - Acoustic Vibration

Acoustic noise tests were conducted on one ASSET subscale nose shape fabricated using coating SO-71 + SO-84 and tungsten-mesh reinforcement. The model was exposed to an overall sound pressure level of $153 \pm 0/-2$ db at a frequency range of 37.5 to 9600 cps. The test produced no evidence of damage to the model.

Testing was performed at Rototest Laboratories, Inc. The test report and a photograph of the test installation are included as Appendix IV to this report.

5.2.4 Test No. 5 - Plasma-Arc Tunnel

The successful results obtained on vibration, acceleration, and acoustic testing with the strong SO-71 + SO-84 coating system led to its tentative choice as the ASSET composite overlay. Subscale thermal tests were then scheduled to verify torch testing of the overlay, already accomplished at Solar. Further, initial plasma tunnel exposure tests of pressure port fittings, pressure port tubes, and thermocouple were planned.

The specimen for test number 5 utilized SO-71 + SO-84 coating system. Coating thickness was 0.230 inch. Instrumentation plugs of 80, 90, and 95 percent density were arranged symmetrically around the specimen.

Testing was performed at Plasmadyne Corp., Santa Ana, California, in a 3.0-inch diameter plasma-arc tunnel, nitrogen stabilized and having air simulation capabilities. Calculated maximum heat flux to the model at the stagnation point was $195.7 \text{ Btu/ft}^2 \text{ sec}$, model stagnation pressure was 0.105 atmosphere, and stagnation point gas enthalpy was 7610 Btu/lb. Test conditions achieved are shown in Table 7.

Surface temperature was monitored with an L&N pyrometer. A temperature-time curve for this test is shown in Figure 34. The test was terminated at 371 seconds due to overheating of the chamber.

The test produced no evidence of serious damage to the model. Minor cracking of the overlay and craze of the SO-84 cover coat are shown in Figure 35. A cross-section of the overlay taken after test is shown in Figure 36, and indicates the tungsten

TABLE 7
TEST CONDITIONS
Plasma-Arc Tests

Test No.	h Stagnation Enthalpy (Btu/lb)	h_W cal (Btu/lb)	h_W model (Btu/lb)	T_W (F) Corrected For ϵ	\dot{q}_{CW} (Btu/ft ² sec)	\dot{q}_{HW} (Btu/ft ² sec)
5 (Subscale)	7610	160	1170	3710	195.7	169
6 (Subscale)	7490	160	1220	3670	200	171
	4985	160	1040	3235	115.8	95
7 (Subscale)	7585	160	1220	3795	194.2	167
	5000	160	1075	3354	115.9	94

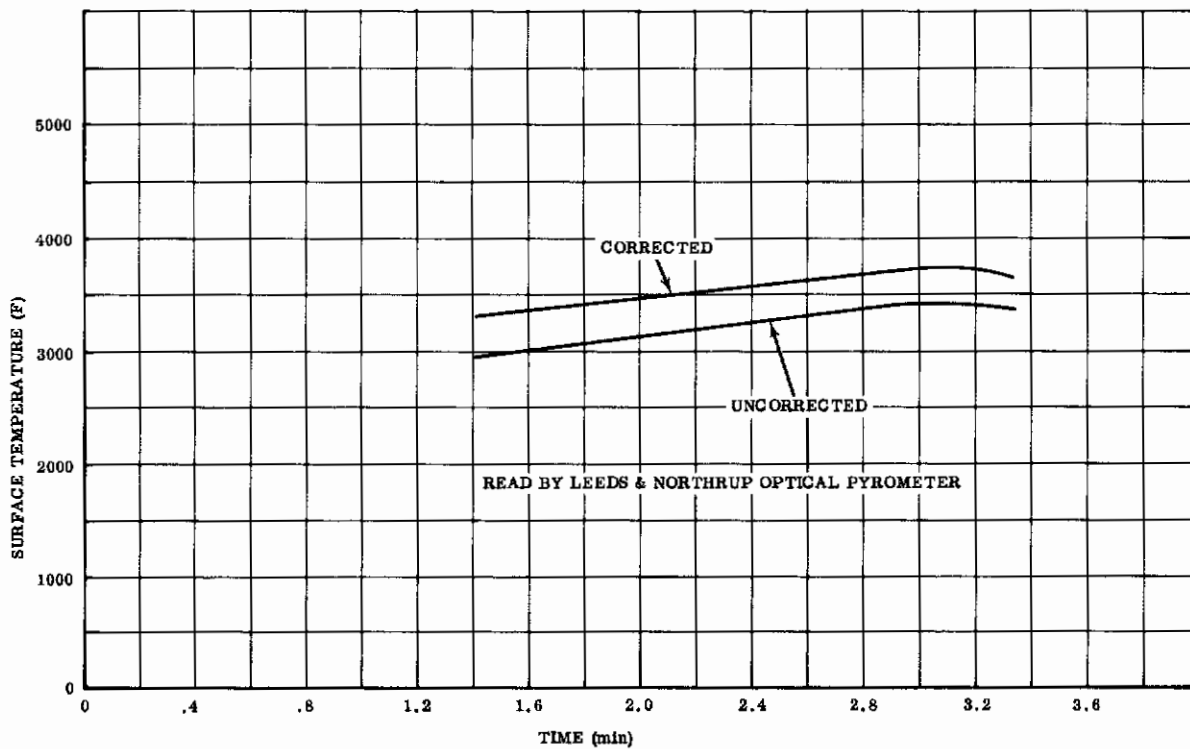
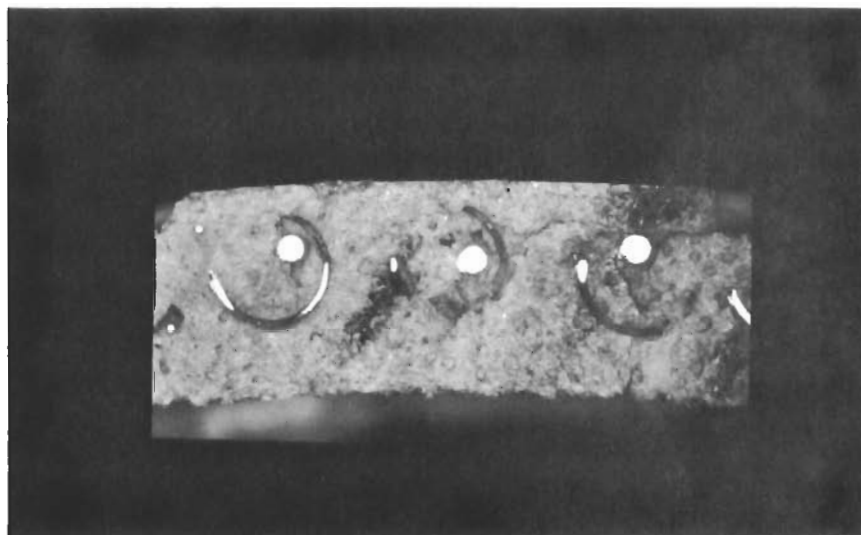


FIGURE 34. STAGNATION POINT TEMPERATURE; Test No. 5



FIGURE 35. ASSET NOSE SHAPE AFTER PLASMA-ARC TESTING



Magnification: 4X

FIGURE 36. REINFORCED SO-71 COATING AFTER PLASMA-ARC TESTING TO 3500 F FOR 3 MINUTES

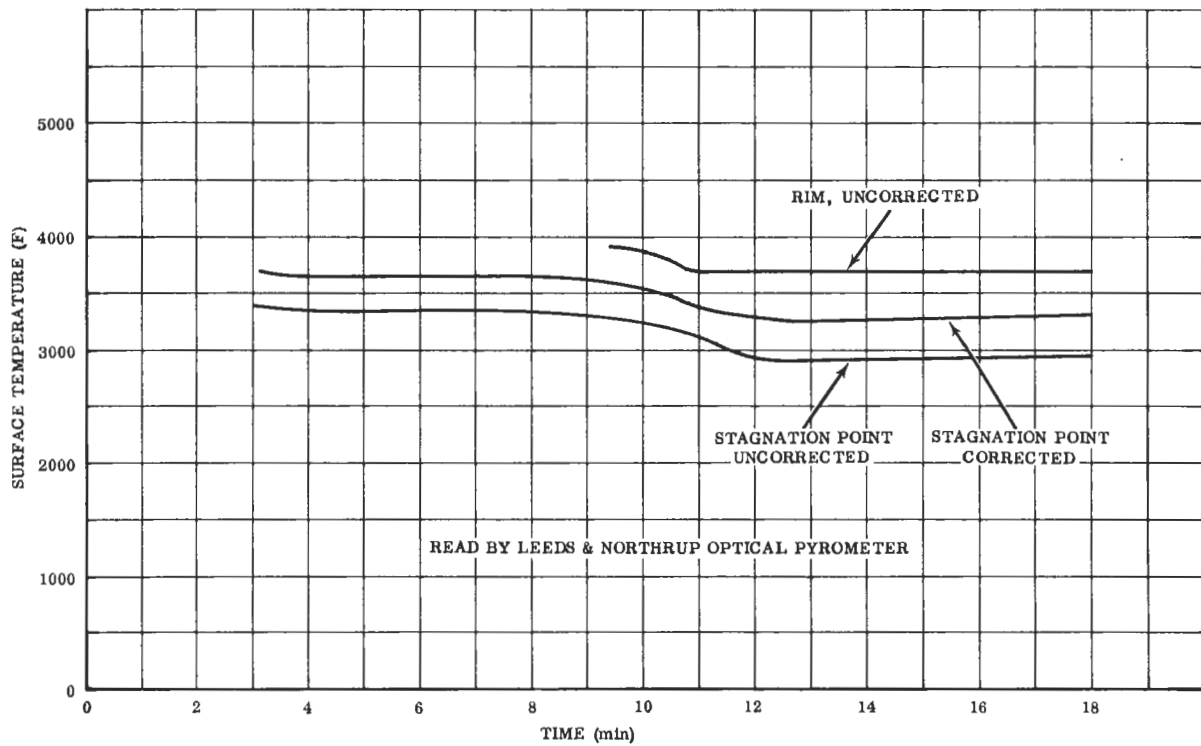


FIGURE 37. MODEL SURFACE TEMPERATURE; Test No. 6



FIGURE 38. SO-86 COATED SUBSCALE ASSET SHAPE AFTER PLASMA-ARC TESTING

reinforcement was protected from oxidation during exposure at 3500 F. Inspection of the instrumentation plugs showed longitudinal cracks emanating from the surface of the 90 and 95 percent dense plugs. Since the model received a severe thermal shock of cold gas at the termination of the test, further evaluation of instrumentation plugs was considered necessary.

5.2.5 Test No. 6 - Plasma-Arc Tunnel

Cure cycle analyses of coating SO-71 led to a reduction in the amount of binder used from 10 percent to 5 percent. Laboratory tests in oxyacetylene facilities indicated this reduction produced a more workable coating. The coating, designated SO-86, was applied to a subscale specimen. The tungsten plate and reinforcing wire and the grid from the specimen used in test No. 5 were reused for this test. Thoria plugs of 80, 90, and 95 percent density were again used. Molybdenum tubes, approximately 2 inches in length and coated with Durak B, were installed into each thoria plug to simulate the pressure port tubes. Each tube-to-plug joint was coated with SO-84.

The specimen was tested in the 3.0-inch plasma-arc tunnel at conditions shown in Table 7. The surface temperatures are shown in Figure 37. A hot ring developed that was approximately 3/4 inch wide and 2 inches from the center of the specimen. This ring attained a temperature of 3900 F at the maximum heat flux conditions of 195 Btu/ft² sec. The center and edges of the specimen were much cooler, with a surface temperature of 3360 F. The subscale specimen exhibited a phenomenon which caused nonuniform heating over the surface. A glowing cone of gas was noted forward of the stagnation region in the area that remained cool. A general blacking of the surface coincided with the hot ring. Plasmadyne attributed this effect to shock wave interaction.

The test was successful, however; and the test specimen is shown in Figure 38. No oxidation of the molybdenum tubing occurred, and the joint wash coat of SO-84 was intact. The only failure was a longitudinal crack in the 95 percent dense thoria plug.

5.2.6 Test No. 7 - Plasma-Arc Tunnel

The test specimen utilized the SO-71 + SO-84 coating system. Two pressure port plugs, 90 percent dense, were installed to simulate BL and SF locations on ASV-4. In addition, a molybdenum-sheathed, W-3-coated thermocouple with BeO insulation and W5Re/W26Re elements was installed at the stagnation point with the tip located 0.025 inch from the surface. Test conditions achieved in the 3.0-inch plasma-arc tunnel are shown in Table 7. Surface temperature-time curves and thermocouple readings are presented in Figure 39.

The same unsymmetrical heating pattern noticed on test No. 6 occurred on this sample; however, the test produced no evidence of damage to the subscale shape. Minor cracking of the overlay, the glazed coating surface caused by the hot ring, and the black surface deposit of unknown origin are shown in Figure 40. Inspection of the 90 percent dense instrumentation plugs showed no evidence of failure.

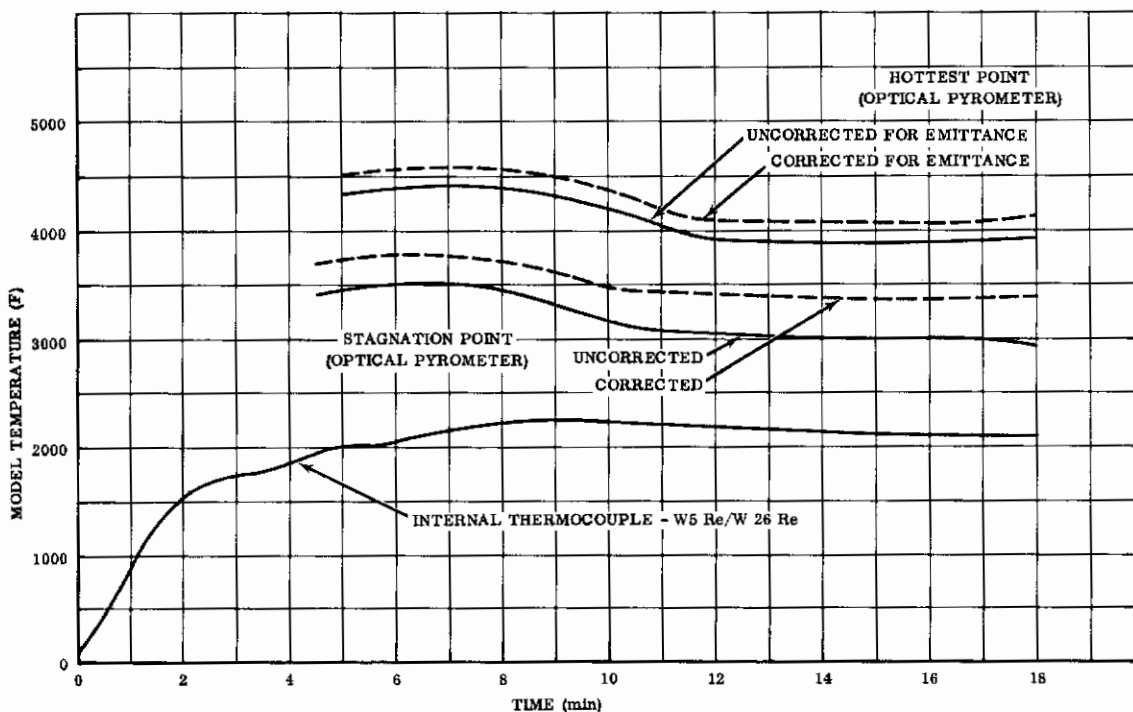


FIGURE 39. MODEL SURFACE TEMPERATURE; Test No. 7



FIGURE 40. SO-71 + SO-84 COATED SUBSCALE ASSET SHAPE; After Plasma-Arc Testing

5.3 FULL-SCALE TEST PROGRAM

The materials system developed and checked by the subscale tests was tested on full-scale ASSET hardware. The following tests were conducted:

<u>Test Number</u>	<u>Coating</u>	<u>Test</u>
8	SO-86 (as cured)	Plasma-Arc
9 (a)	SO-86 plus SO-84 (as cured)	Load
(b)	Same specimen	Acoustic
(c)	Same specimen	Vibration
(d)	Same specimen	Plasma-Arc

Each of these tests is discussed in the following paragraphs.

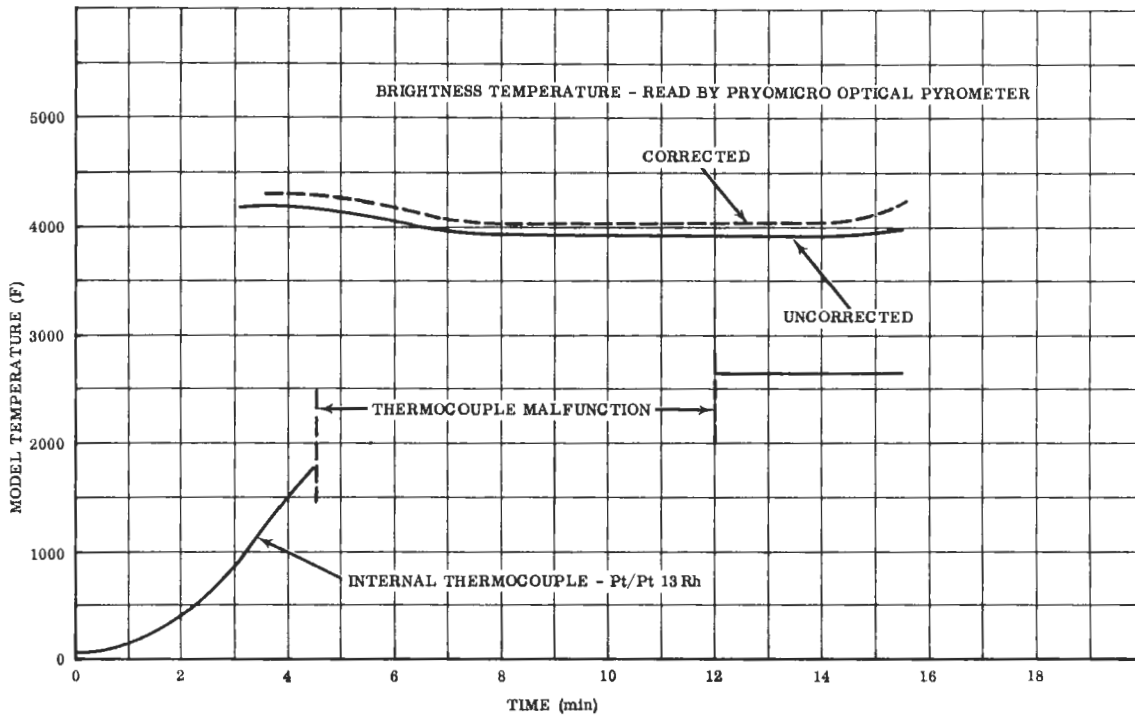


FIGURE 41. MODEL SURFACE TEMPERATURE; Test No. 8

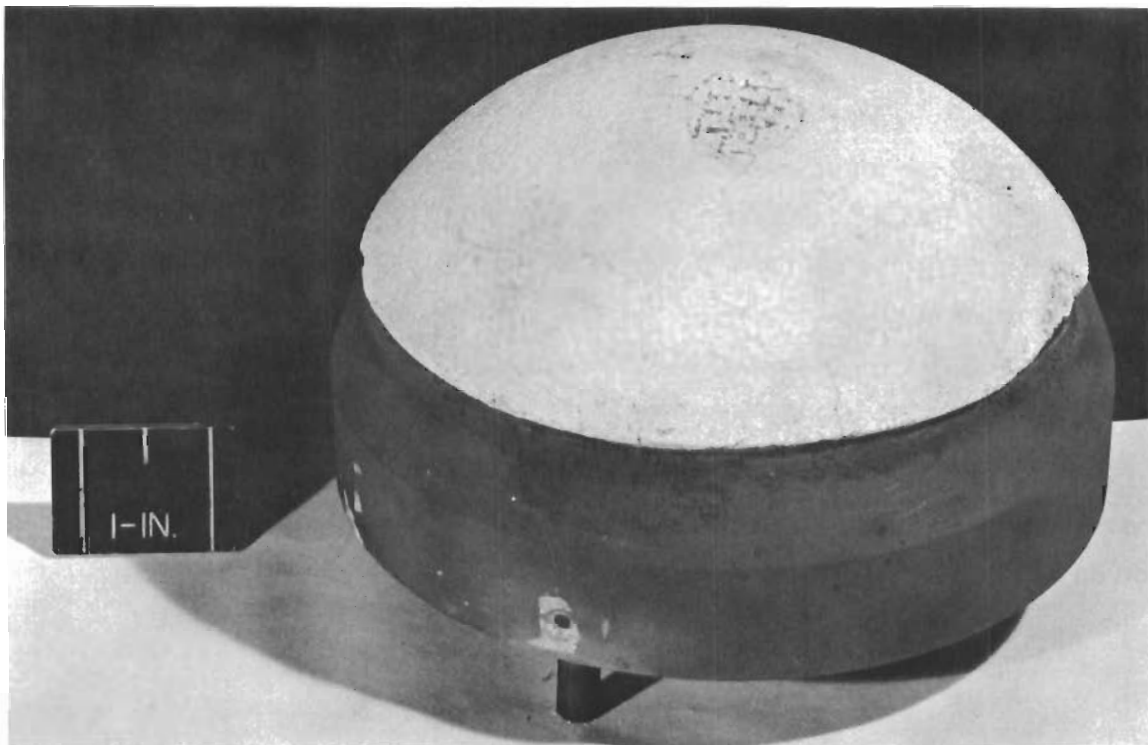


FIGURE 42. SO-86 COATED ASSET CAP MOUNTED IN MOLYBDENUM SKIRT; After Plasma-Arc Testing

5.3.1 Test No. 8 - Plasma-Arc Test

The success of the one-coat SO-86 coating in the subscale test led to its choice for the full-scale ASSET test cap. A finish-machined tungsten forging was fitted with wire-mesh reinforcement. The SO-86 coating was applied to the cap and machined to a final thickness of $0.200^{+0.005}_{-0.000}$ inch. The curing process was accelerated for this cap to meet the test schedule, and two defects that required patching were encountered during the cure. A bubble formed during the low-temperature cure causing a small coating separation at the top of the reinforcements, and an edge was chipped during handling. Both repaired areas showed evidence of hairline cracks after high firing to 2200 F, indicating that the repair was only partially successful. It was decided to proceed with the test, allowing an evaluation of repair procedure.

The coated cap was installed in the front section of a molybdenum skirt and the cavity at the back of the cap was filled with graphite cloth insulation. A Pt-Pt/13Rh thermocouple was inserted in a hole drilled 1/8-inch deep in the tungsten behind the stagnation point. No pressure ports or molybdenum tubes were used for this test.

The temperatures recorded on the specimen during test are shown in Figure 41. The specimen after test is shown in Figure 42. The two repaired areas show evidence of cracking during the test and they separated from the cap during removal from the test fixture after the test. In all other respects, the coating and reinforcement performed satisfactorily during the test. Results of the thermocouple measurement was erratic, and believed to be in error. It is possible the thermocouple was not in intimate contact with the tungsten throughout the test run.

The successful test of the SO-86 coating and wire-mesh reinforcement on the ASSET cap led to the choice of this overlay system for the final test article. The failure of patch areas to survive the plasma-arc test precludes the use of this repair method on subsequent ASSET caps.

5.3.2 Test No. 9 - Flight Qualification Tests

In accordance with MAC SCD 51-30012, Section 4.2, a series of tests were performed on a full-scale ASSET nose cap to establish flightworthiness. The tests in the specified order were:

- Load Test
- Acoustic Test
- Vibration Test
- Thermal Test

The specimen to be used for this test was to be identical to the ASV-4 flight cap in all respects. However, limitations in the plasma-arc tunnel equipment available at Plasmadyne required that certain modifications be allowed. The first deviation from actual flight configuration was required because the chamber at Plasmadyne did not allow the installation and test of the full-size molybdenum afterbody forging used on ASSET. Therefore, a short molybdenum forging supplied by MAC was used for all full-scale testing. This forging simulated the mounting method actually used, and was adequate for those tests. The shortened length, however, did not permit the use of full-length molybdenum pressure port tubes for this test so the tubes were cut off just aft of the nose cap closure plate. MAC submitted verbal agreement on allowing this deviation for all of the tests to be performed on the final qualification specimen.

The second deviation concerned the installation of the flight thermocouple. The only path available for passing thermocouple wire through the chamber wall was through the specimen holder. This holder terminates in a water-cooled sting 2.0 inches in diameter with a 0.607-inch diameter hole down the centerline. The centerline of the sting coincides with the stagnation point of the nose cap, thus, a straight thermocouple of any length can be accommodated if it is mounted at the stagnation point. That arrangement was used on subscale test No. 6 (Sec 5.2.5). The flight thermocouple however, is not straight, does not go through the stagnation point, and is too long to be included completely within the short molybdenum support forging used for flight tests. The flight arrangement could therefore not be checked. An attempt was made to adapt the straight thermocouple used in subscale test No. 6. This thermocouple

was bent into a configuration that allowed installation in the proper location on the nose cap. However, the rigid portion of the thermocouple passed through the back plate of the complete test assembly, and outside of the water-cooled sting. The flexible thermocouple leads were then passed back into the specimen and through the hole in the sting. The portion of the thermocouple outside the test assembly was wrapped with Fiber Frax in an attempt to shield the thermocouple against heating. Because of the awkward physical arrangement, the thermocouple was not installed for the load, acoustic, and vibration tests. Instead, a steel rod of the same outside dimensions was installed and cut off just aft of the nose cap closure plate. The steel pin was removed after load and vibration tests, and the thermocouple was installed just prior to the thermal test. The general arrangement of the test specimen with the steel pin installed is shown in Figure 43.

Test No. 9 (a) - Load Test

Maximum dynamic pressure on the nose cap is 22.2 psi, occurring during boost. Total pressure on the nose cap was obtained by integration, assuming $P = P_{\text{stag}} \cos^2 \Theta$. Total force parallel to the axis was obtained by

$$F_N = 2\pi r^2 P_{\text{st}} \int_0^{\pi/3} \sin \Theta \cos^3 \Theta d\Theta$$

resulting in a total force of 317 pounds. The load test was run to 320 pounds. The test specimen and foam loading pad are shown in Figure 44. Load was applied with 20-pound lead weights in 60-pound increments to 300 pounds, and then to 320 pounds, held for 3 minutes, and removed. The specimen showed no signs of damage upon completion of the test.

Test No. 9 (b) - Acoustic Test

The test specimen was installed in the Norair 150-cubic-foot reverberant chamber using a spring-mount system. The specimen was subjected to a random sound field of 155 db intensity for 5 minutes. The sound pressure level in each octave band and a photograph of the test set up are presented in the combined vibration and acoustic test report included as Appendix V. No evidence of damage to the specimen could be found after the test.

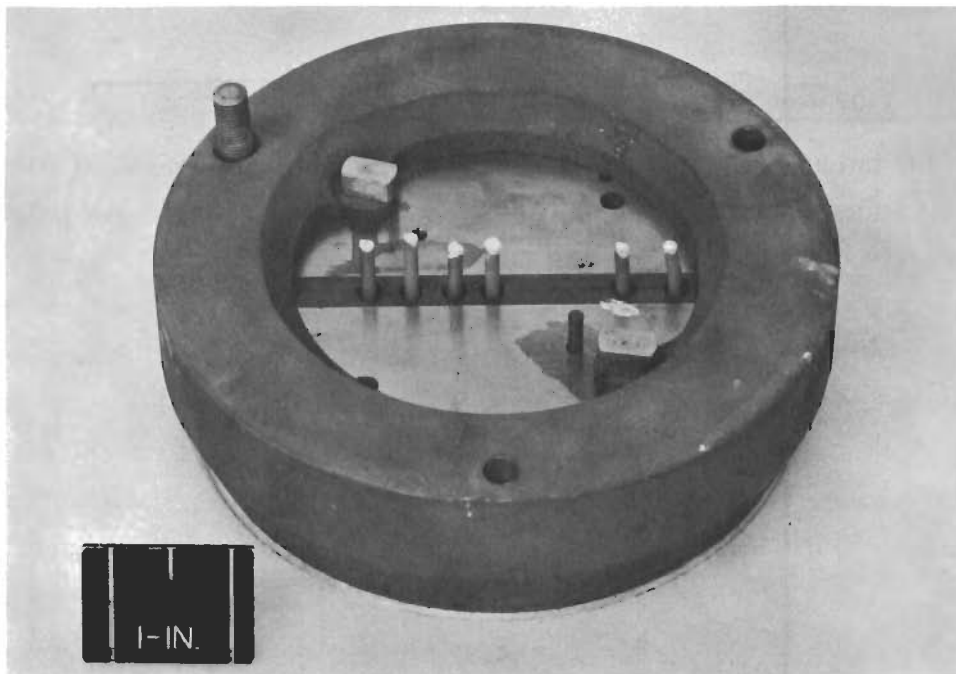


FIGURE 43. ASSET NOSE CAP IN MOLYBDENUM SKIRT SHOWING INSTRUMENTATION TUBES

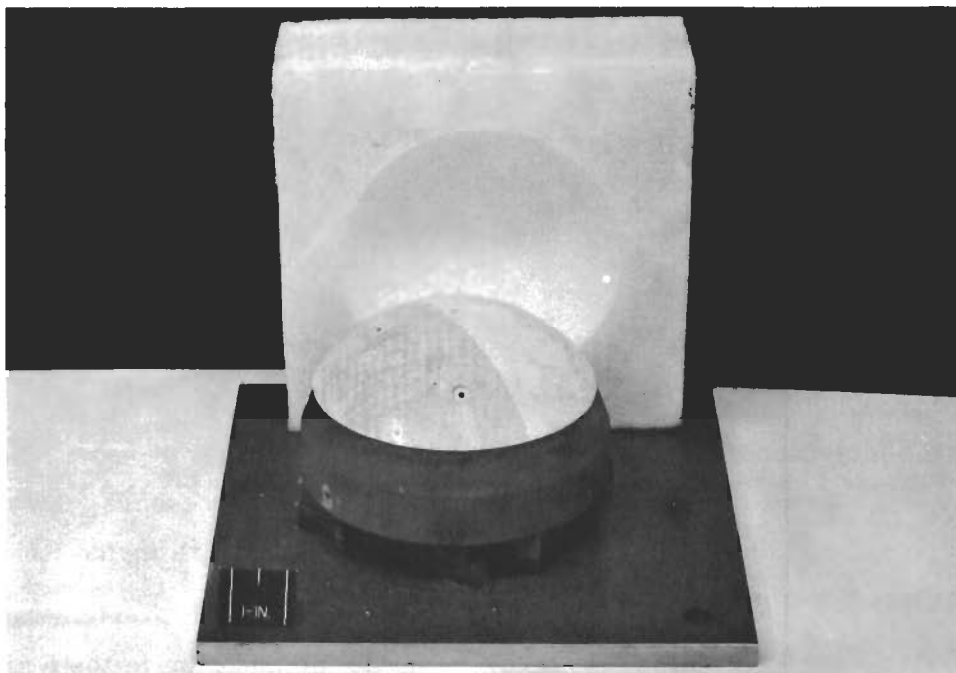


FIGURE 44. ASSET NOSE CAP AND LOAD BEARING TEST FIXTURE

Test No. 9 (c) - Vibration Test

Following the acoustic test, the part was mounted on a mechanical vibration table. The cap was subjected to sinusoidal vibration along its axis at the following conditions:

<u>Frequency (cps)</u>	<u>Load (g)</u>
5-15	0.3 inch D.A.
15-100	3.0
100-500	5.0
500-2000	10.0

Total test time was 7.5 minutes. There was no evidence of damage to the test specimen. The test report and a photograph of the test setup are contained in Appendix V.

Test No. 9 (d) - Plasma-Arc Test

After completion of all mechanical tests, the test cap was fitted with the W5Re/W26Re thermocouple as described in Section 5.3.2. The cap was then installed in the plasma tunnel facility using the 5-1/8-inch diameter nozzle, and tested under the same conditions as test No. 8. Surface temperatures are shown in Figure 45.

The test was completely successful; the specimen after test is shown in Figure 46. The SO-86 coating was intact, the thoria plugs had no failures, and there was no evidence of oxidation on any internal nose cap details. The lack of oxidation is particularly interesting, since several internal molybdenum components were uncoated, specifically, the molybdenum support bolts and three of the pressure-port tubes. This lack of oxidation indicates that the combination of low ambient pressure, low mass flow over internal parts, and the presence of the chopped graphite cloth inside the nose cap either eliminates or minimizes the oxidation problem.

The thermocouple installed outside the test cap did not survive the test. Burn-out occurred early in the test resulting in no useful data.

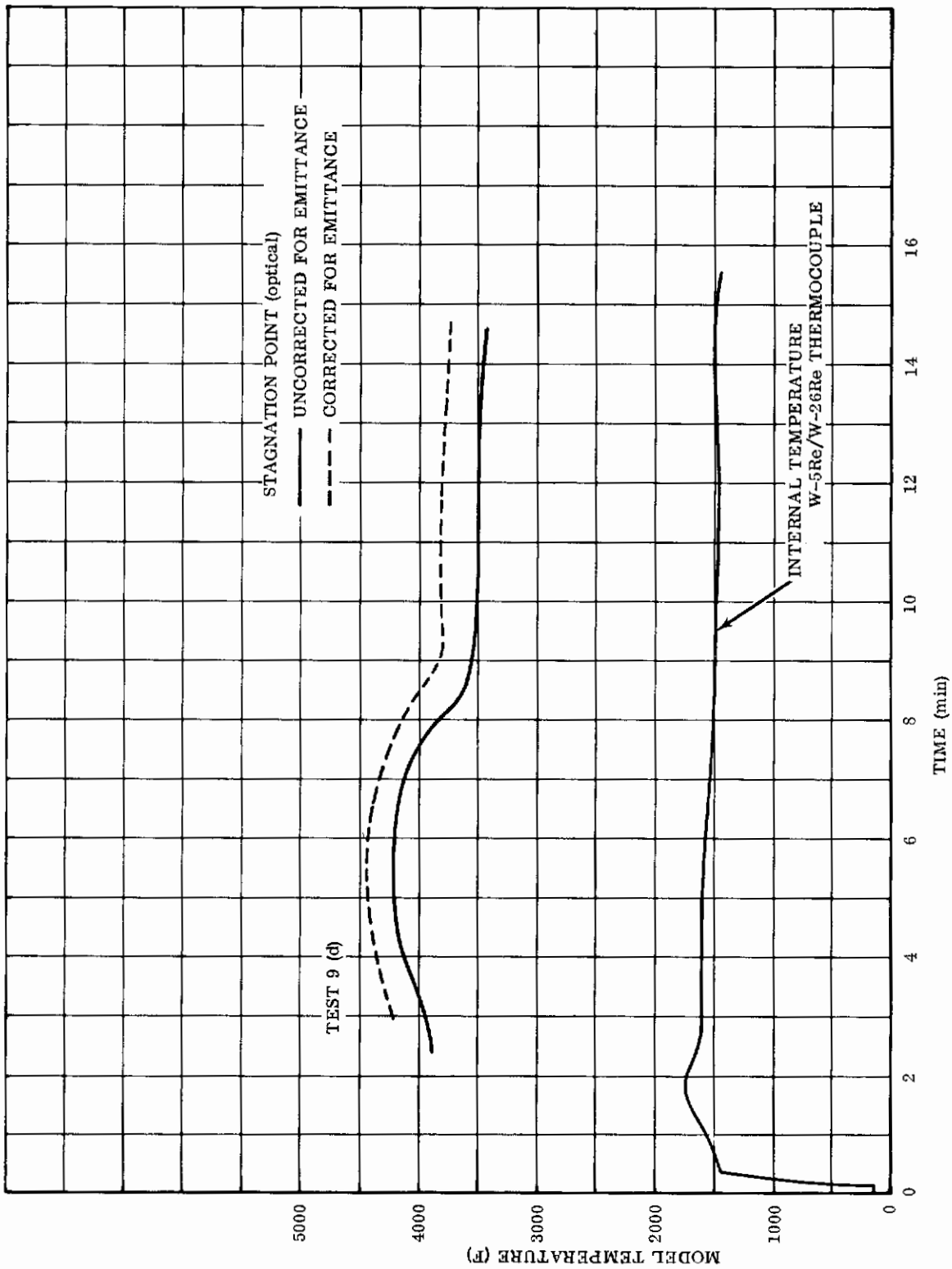


FIGURE 45. MODEL SURFACE TEMPERATURE

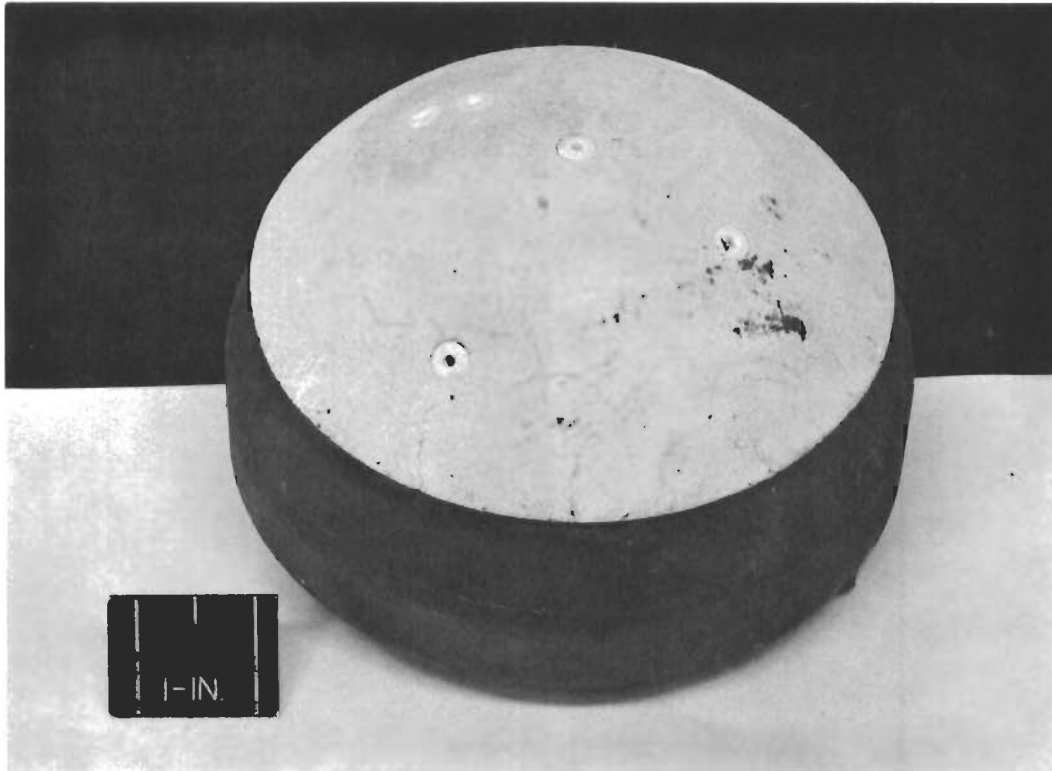


FIGURE 46. ASSET NOSE CAP AFTER THERMAL TEST; Coating SO-86 with Half of Cap Covered With Wash Coat of SO-84

5.3.3 Test Number 10 - Plasma Arc Test

The material system and detailed design of the ASSET nose cap had been verified by the series of tests reported above; however, the thermocouple installation procedure had not. A full scale ASSET nose cap was therefore prepared for test in the 5-1/8 inch diameter nozzle at Plasmadyne. Test conditions were the same as for tests 8 and 9d. All pressure ports were eliminated. A straight thermocouple was installed at the stagnation point, using an installation technique identical to that planned for the flight cap.

Surface temperatures recorded during the test are shown in Figure 47; the cap after test is shown in Figure 48. Motion pictures taken during the test indicated that a small hole opened almost immediately in the thoria, just over the thermocouple end. This hole, shown in Figure 48, did not enlarge during the test. Subsequent examination indicated that the thermocouple had been retracted into the cap approximately 0.5-inch from its proper location. The excellent condition of the thermocouple end

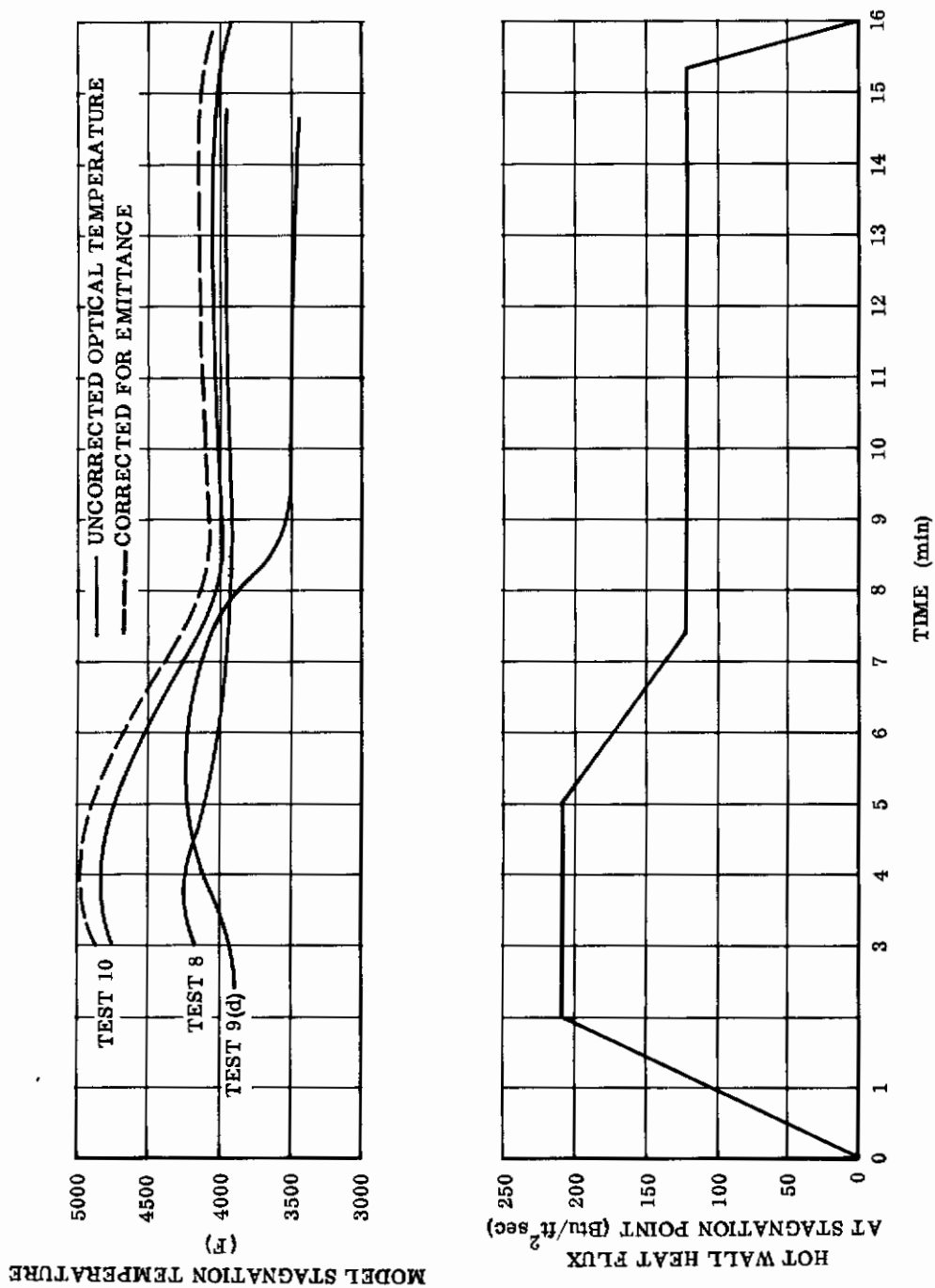


FIGURE 47. COMPARISON OF SURFACE TEMPERATURES; Full-Scale Test



Outside Surface



Inside Surface

FIGURE 48. SPECIMEN AFTER TEST; Test No. 10

indicated that this retraction must have occurred prior to the test. The small covering of thoria, only 0.025 inch thick, over the thermocouple area failed immediately, exposing the inside of the cap. The hole in the tungsten forging through which the thermocouple was intended to pass had enlarged in diameter from 1/8-inch to 1/4-inch by oxidation during the test, (Fig. 48). Even under these conditions, no failure of the cap occurred. The temperature recorded by the thermocouple is fictitious, since it was not in contact with the cap during the test. A heavily glazed area surrounded the stagnation point, as shown in Figure 48. Previous testing did not show such behavior at temperatures less than 4700 F, which lends credence to the almost 5000 F temperature recorded optically for this specimen.

5.3.4 Combined Temperature/Vibration Test

Following qualification of the Solar nose cap through the tests described above, McDonnell requested that the Solar nose cap be subjected to a combined temperature/vibration test. A special test rig, shown in Figure 49, had been built by MAC specifically for the ASSET caps. It consists of a vibration table mounted behind a water-cooled shield. The specimen is coupled with the vibrator through the shield. A bank of six oxy-acetylene torches move along a track to vary specimen temperature. Any desired combination of temperature and vibration spectrum can be obtained (within limits).

A full-scale ASSET nose cap with ASV-4 instrumentation layout was assembled for thermal vibration test. The pressure tubes on this cap were terminated at the graphite inserts. The thermocouple was full length so temperature could be recorded during test. The following test conditions were to be used in the temperature/vibration test:

Heat to 2000 F, hold 7-1/2 minutes, then run following sinusoidal spectrum:

Boost

<u>Load</u> (g)	<u>Frequency</u> (cps)
0.3 inch D. A.	5 to 15
±3.0 g	15 to 100
±5.0 g	100 to 500
±10.0 g	500 to 2000

Increase temperature to 4100 F, hold 7-1/2 minutes, and run the following sinusoidal spectrum:

Glide

<u>Load</u> (g)	<u>Frequency</u> (cps)
0.3 inch D. A.	5 to 15
±3.0 g	15 to 30
±1.0 g	30 to 500
±2.0 g	500 to 2000

In the actual test, the boost test was conducted inadvertently at 2000 C (3632 F) rather than 2000 F. Figure 50 show the cap and fixture after test. Edge failure was visually observed during the boost phase of the test (3632 F). Thoria plugs also failed

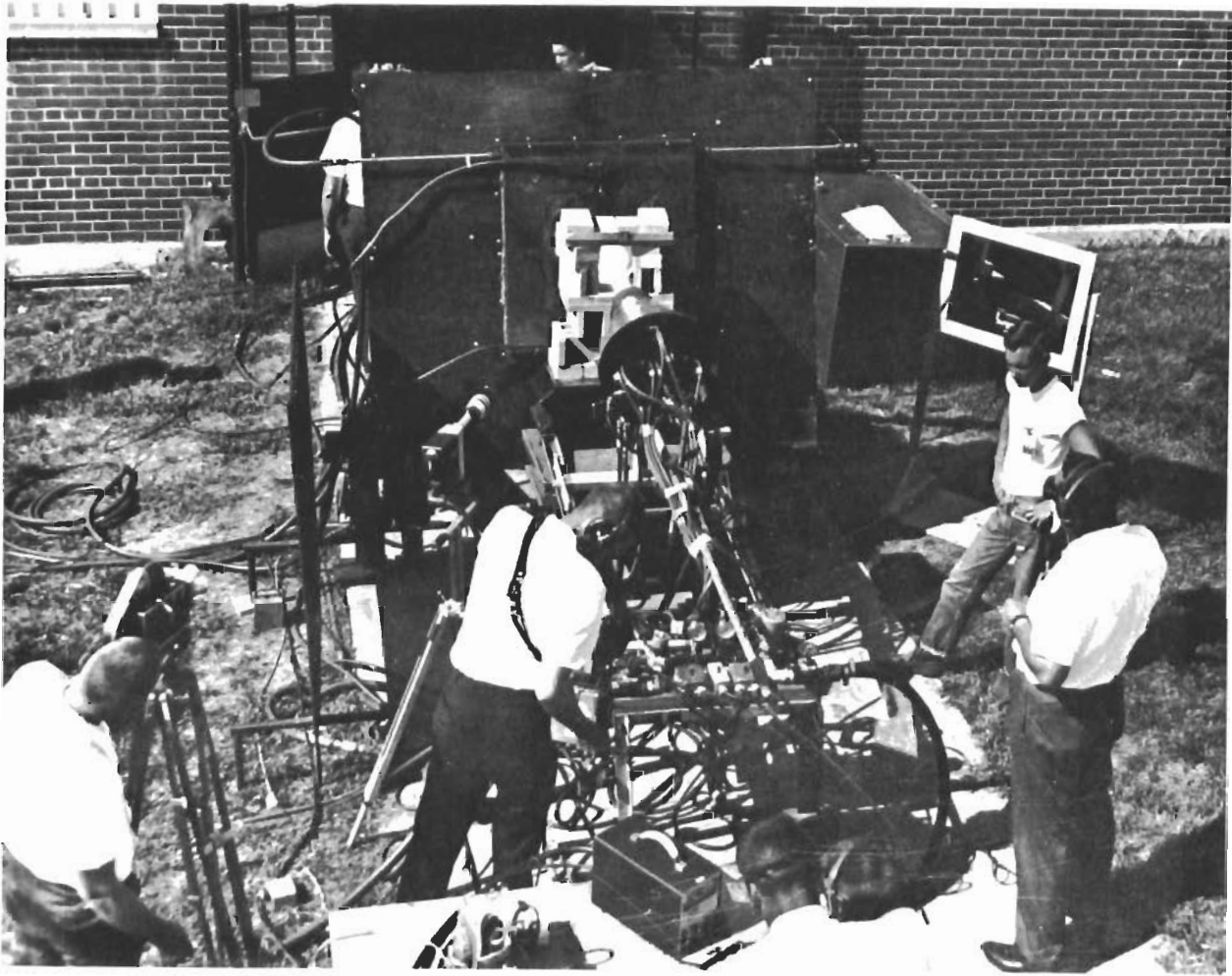
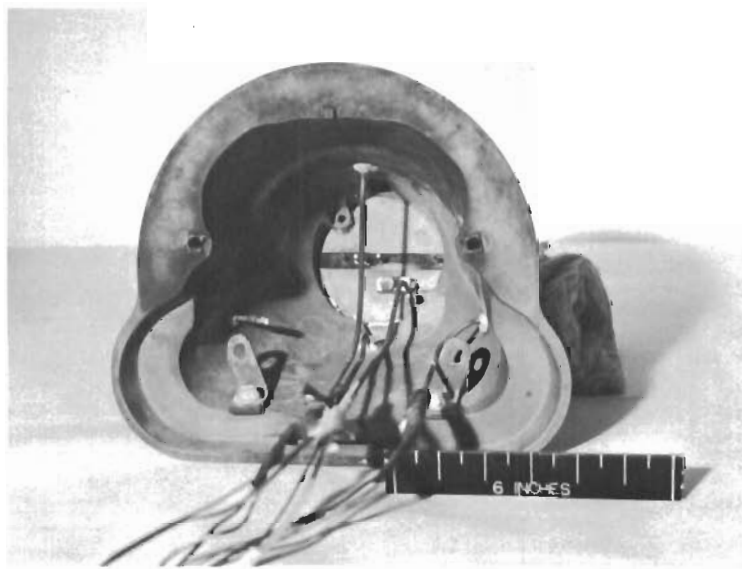
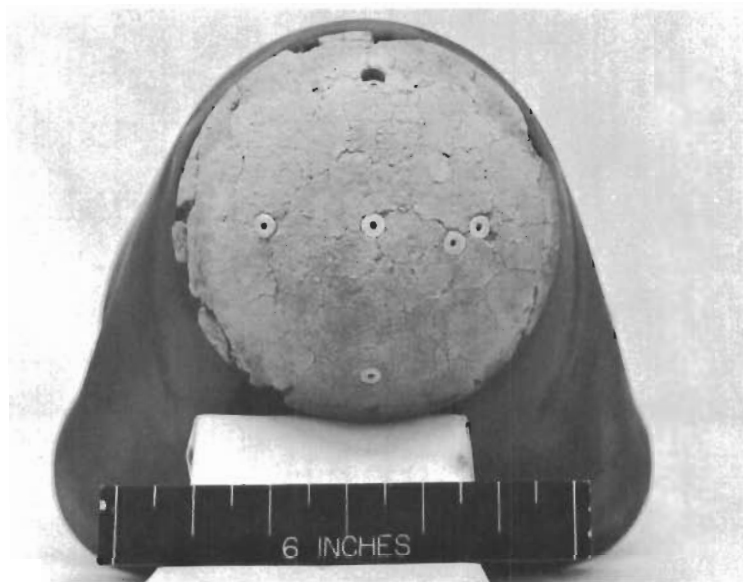


FIGURE 49. COMBINED TEMPERATURE/VIBRATION TEST FACILITY

during this phase of the test. The glide portion of the test resulted in no further failure. Considering the severity of the test, the nose cap material system performed very satisfactorily. The thermocouple installed in the cap performed perfectly, even at the overly severe test conditions. A comparison of corrected optical surface temperature and thermocouple reading is shown in Figure 51. The lag between readings is due to heat capacity of the system and insulating qualities of the overlay.

Examination of the cap indicated that corrective steps could be taken to strengthen the areas that failed. The coating loss at the edges of the cap occurred in areas where the wire mesh was not supported by pins, or where a small length of the wire making up the mesh was not adequately secured. Thoria instrumentation plugs sheared at a change in cross-sectional area. Hence, the sheared section was not held in the coating and readily fell free from the coating.



Rear View Showing Mounting

FIGURE 50. ASSET CAP AFTER TEMPERATURE/VIBRATION TEST

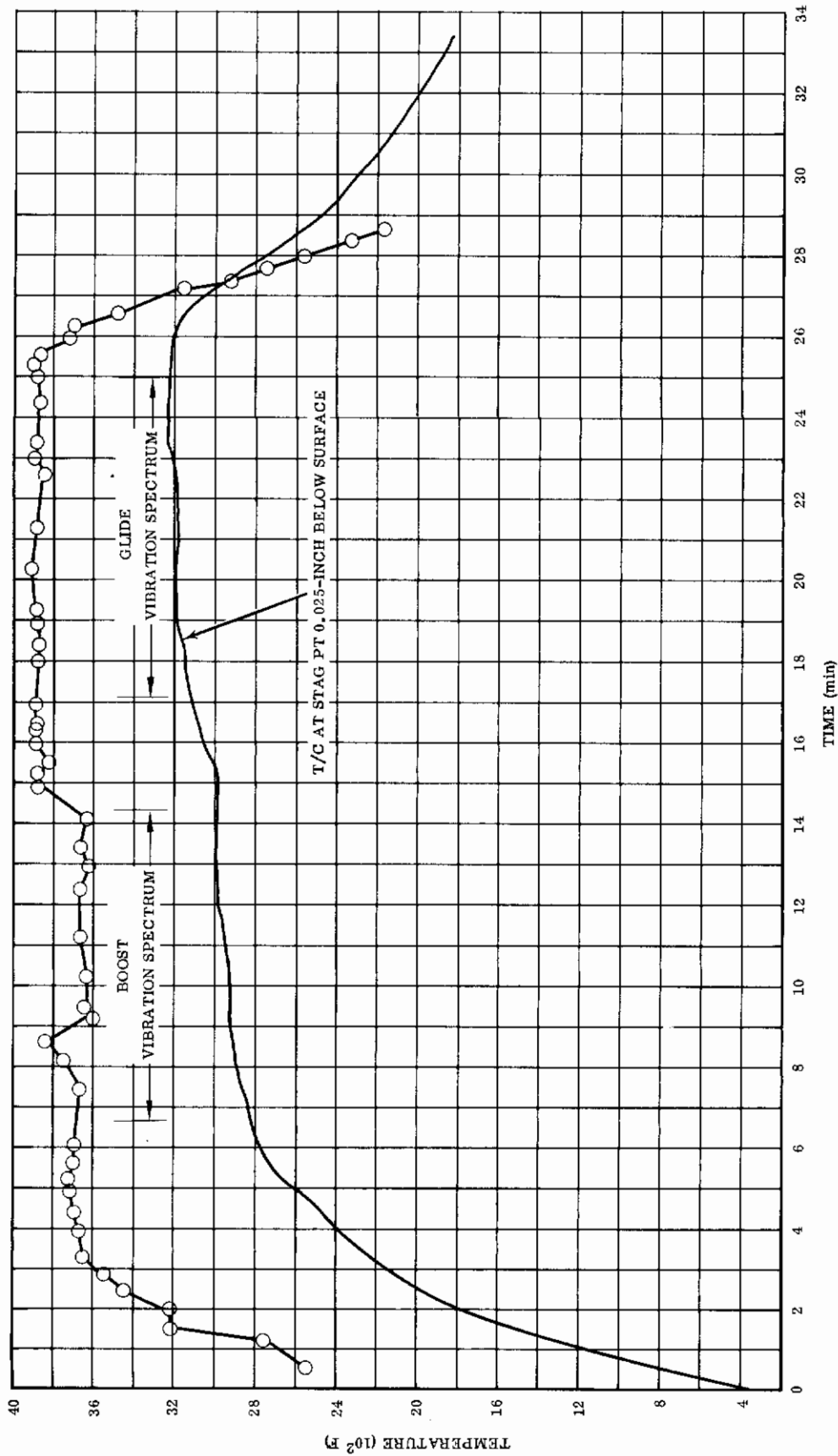
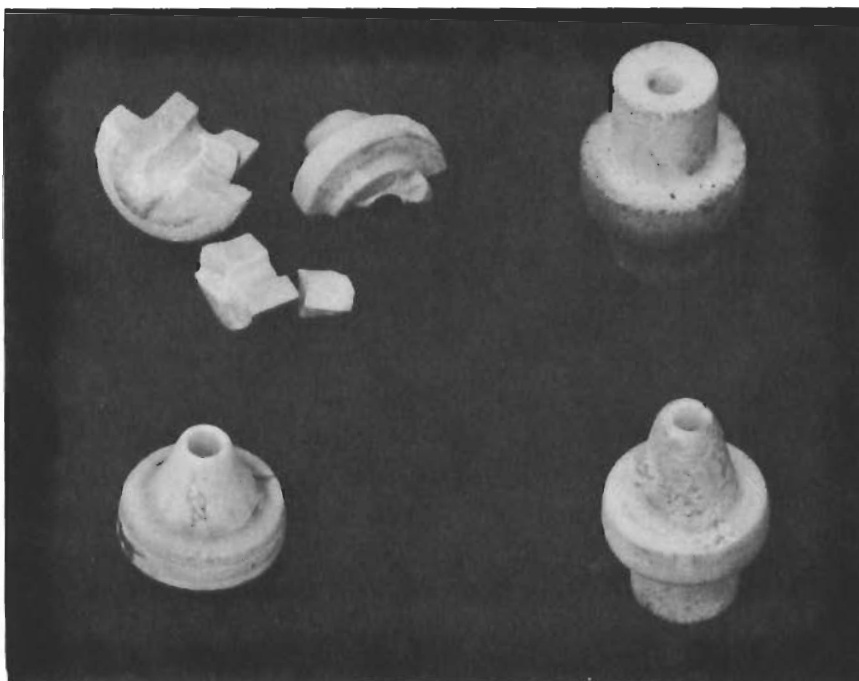


FIGURE 51. TEMPERATURE HISTORY; ASSET Nose Cap

A series of thermal shock tests were conducted on various plug shapes and fits of plug into cavity to improve their strength. Table 8 contains a summary of these tests and Figure 52 shows examples of the various plugs. The failure of the standard plugs in a tight-fitting cavity indicated that the plugs fail due to a combination of excessive compressive loads and rapid changes in cross-section. A tapered plug with adequate diametric clearance was tried.



Upper Left: Standard Plug in Tight Hole (0.004 in. Clearance)
Upper Right: Standard Plug in Open Hole (0.024 in. Clearance)
Lower Left: Tapered Plug in Open Hole (0.022 in. Clearance)
Lower Right: Tapered Plug in Open Hole (0.022 in. Clearance)
(All plugs tested in Oxygen Acetylene Torch with SO-86 coating.
Plug mounted in copper block. Optical temperature of plugs
was 4900 F.)

FIGURE 52. THERMAL SHOCK TESTS ON THORIA PLUGS

TABLE 8

SUMMARY OF TEST ON THORIA INSTRUMENTATION PLUGS

All plugs were heated with an oxygen acetylene torch to peak temperatures in 45 seconds, held at temperature for 3 minutes and cooled. Temperature observed with optical pyrometer was 4900 F.

Plug Shape	Diametrical Clearance Between Cavity ⁽¹⁾ and Plug	Remarks
Standard	0.004	Badly shattered
Standard	0.008	Badly shattered
Standard	0.002 (3 each)	Two plugs shattered One plug cracked (Two plugs cemented in place with SO-84)
Standard	0.024	Cracked
Tapered	0.022 (3 each)	Small crack in two plugs. (One plug cemented in place with SO-84)

¹ Cavity machined in a copper block and SO-86 thoria coating applied over copper and plug.

A small longitudinal crack appeared in most of the plugs due to thermal stresses. The tapered plug will allow the tungsten reinforcement and thoria coating to hold the plug in place. In addition, pressure loss through any cracks would be greatly suppressed by the tight fitting coating.

A second cap was built for testing at MAC and modified as follows:

1. Eight additional pins were added near the edge decreasing the distance between the pins to roughly 3/4 inch.
2. The shapes of the pressure plugs were changed to tapered, and the diametrical clearance between the plug and shell was increased to 0.024 inch.

The coated cap (Fig. 53) was installed in the same test device as for the first test. Test conditions were as outlined above. Figure 54 shows the cap during test, and Figure 55 was taken immediately after shut down of the torches.

No failures were experienced during this test. The thermocouple performed in much the same manner as it had during the first test. No edge cracking or pressure port failures occurred. The cap after test is shown in Figure 56. Surface checking was due to the thin wash coat of thoria applied to smooth the surface prior to test, and was expected to occur.

Based on the successful tests at Plasmadyne and McDonnell, the Solar nose cap was accepted for flight.

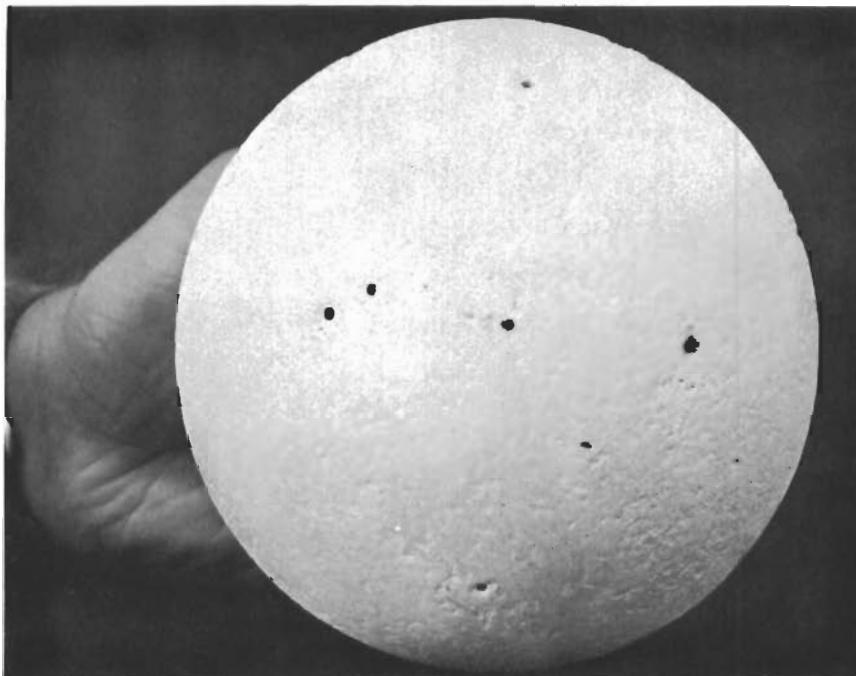


FIGURE 53. COATED ASSET CAP FOR TEMPERATURE/VIBRATION TEST

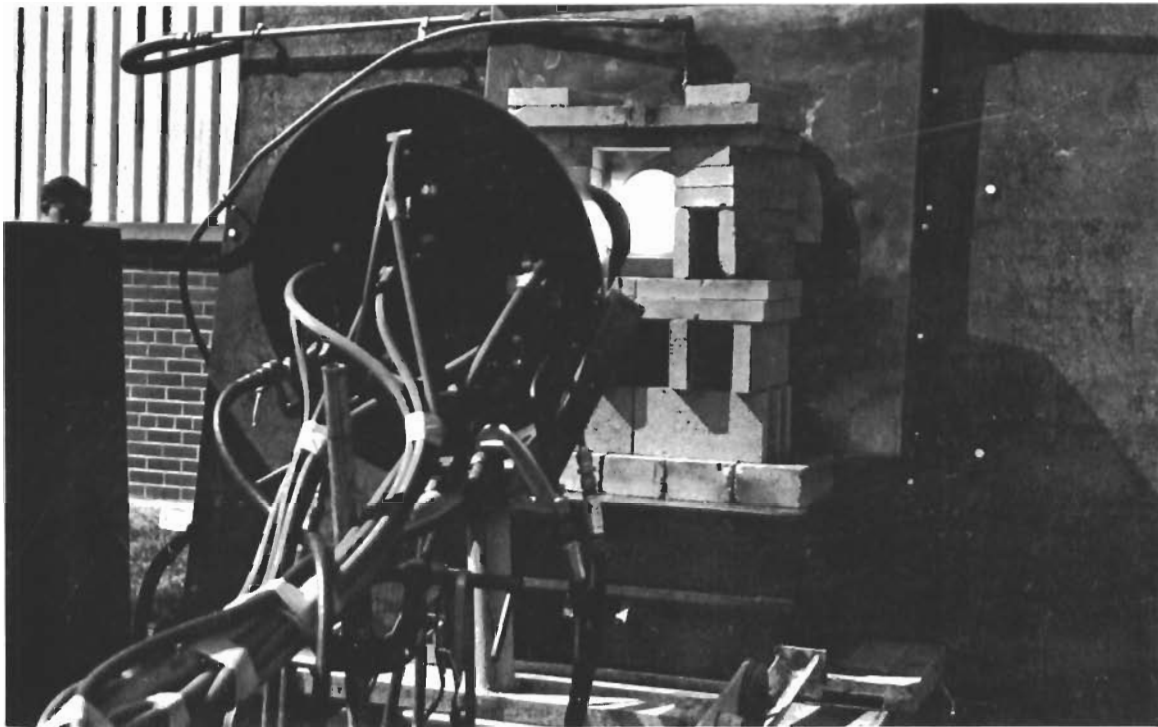


FIGURE 54. ASSET CAP DURING TEST AT MAXIMUM TEMPERATURE

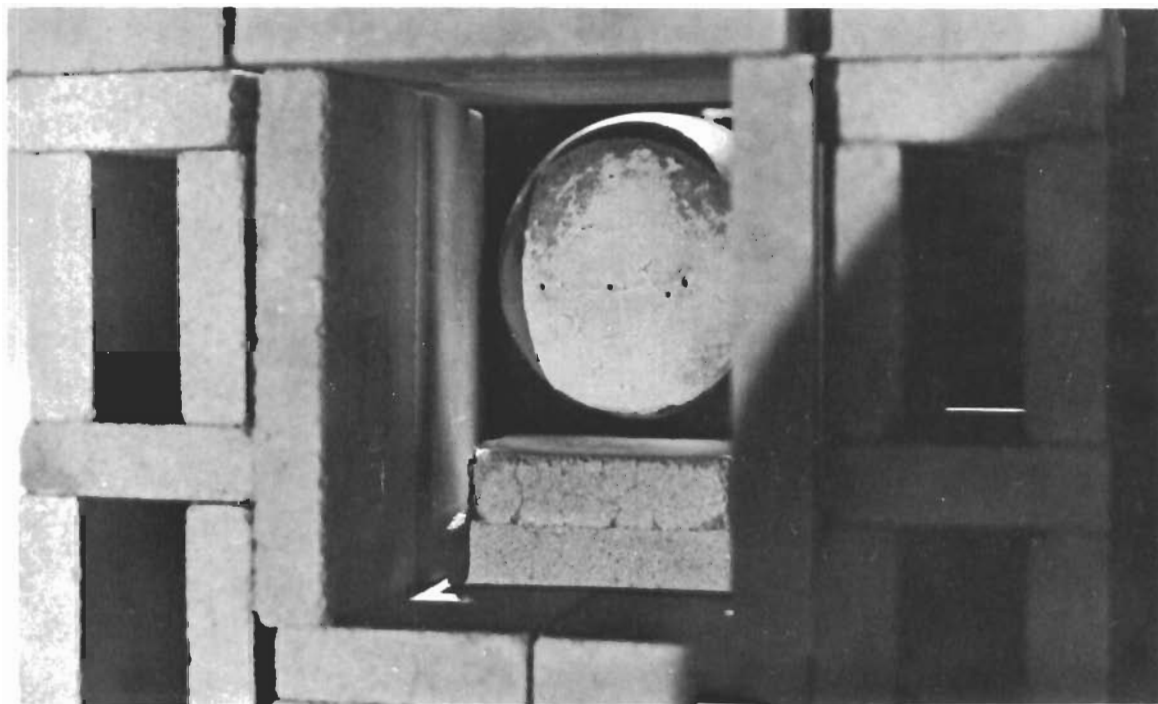


FIGURE 55. ASSET CAP PRIOR TO COOL DOWN

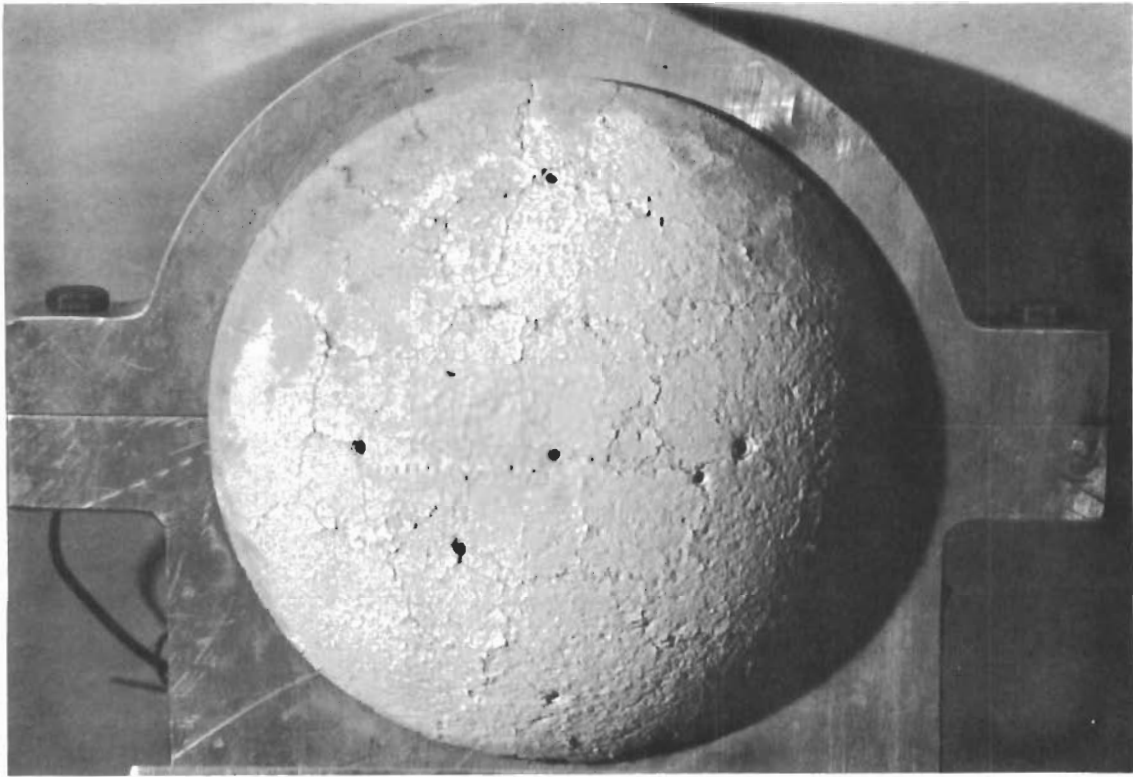


FIGURE 56. ASSET CAP AFTER TEMPERATURE/VIBRATION TESTING

VI. CONCLUSIONS

The primary goal of this portion of the overall program was to demonstrate the usefulness of high-temperature metallic/ceramic composite structures on re-entry vehicle nose caps. Certainly the final evaluation of this material system will be derived from data gathered during the actual flight tests. Certain conclusions are apparent, however, from the ground qualification tests conducted on the ASSET nose caps:

1. Mesh reinforcement systems impart a high degree of mechanical strengthening to porous ceramics at both room temperature and elevated temperatures.
2. Thoria reinforced with tungsten mesh can withstand vibration and shock loads associated with missile launch and nose cone re-entry.
3. Plasma-arc tunnel testing of re-entry shapes up to 6 inches in diameter is feasible, with good simulation to near-orbital conditions.

Contrails

APPENDIX I
THERMO-STRUCTURAL ANALYSIS

Contrails

THERMO-STRUCTURAL ANALYSIS OF
TUNGSTEN NOSE CAP FOR
ASSET ASV-4 FLIGHT VEHICLE

by

W. E. Jacobsen
and W. S. Wolff

Report No. 3-10-03-1

July 1, 1963

Subcontract to Solar Aircraft Company
No. 4840 - 29067-VHL(CR) - Revision No.3

ASD Contract AF 33(616) - 8497

LOCKHEED MISSILES AND SPACE DIVISION
Lockheed Aircraft Corporation
Sunnyvale, California

Contrails

SUMMARY

This report presents a thermo-structural analysis of a tungsten nose cap to be flight-tested as part of the ASSET program on vehicle ASV-4. The 0.25-in-thick spherical frontal portion of the cap is protected against oxidation by an overlay of 0.20-in. tungsten-reinforced thoria. Transient distributions of temperature throughout the structure, as well as elastic/plastic thermal stresses and deformations, were determined. Moreover, a strength analysis of molybdenum alloy fasteners is presented.

From a temperature and stress-deflection standpoint the cap design appeared satisfactory. However, an extended temperature analysis of a molybdenum nose skirt to which the cap is bolted indicated very severe temperatures.

Contrails

CONTENTS

<u>Section</u>		<u>Page</u>
	SUMMARY	ii
	ILLUSTRATIONS	iii
	NOMENCLATURE	iv
1	INTRODUCTION AND DISCUSSION	1-1
2	TRANSIENT TEMPERATURE ANALYSIS	2-1
	2.1 Thermal Tables	2-7
	2.2 Figures	2-11
3	THERMAL STRESS AND DEFLECTION ANALYSIS	3-1
	3.1 Figures	3-6
4	FASTENER ANALYSIS	4-1
	4.1 Figures	4-4
5	CONCLUSIONS	5-1
6	REFERENCES	6-1

ILLUSTRATIONS

<u>Figure</u>		<u>Page</u>
2-1	Nodal Arrangement for Heat Transfer Analysis	2-7
2-2	ASV-4 Design Trajectory	2-8
2-3	Temperature History of Various Points on the Nose and Skirt Sections, Descent	2-9
2-4	Temperature History of Various Points on the Bottom and Top of the Nose and Skirt Sections, Ascent	2-10
2-5	Pressure Port Detail	2-11
2-6	Stagnation Point Heat Flux	2-12
3-1	Forged Tungsten Nose Cap, Spherical	3-6
3-2	Tungsten Mechanical Properties	3-7
3-3	Tungsten Effective Stress Versus Effective Plastic Strain	3-8
3-4	Tungsten Effective Plastic Strain Versus Effective Strain	3-9
3-5	Shell Mid-Surface Temperatures	3-10
3-6	Shell Temperature Differential for Various Times	3-11
3-7	ASSET Nose Cap Meridional Stresses, Flight Time 220 Seconds	3-12
3-8	ASSET Nose Cap Circumferential Stresses, Flight Time 220 Seconds	3-13
3-9	Tungsten Nose Cap Shell Mid-Surface Deflection	3-14
4-1	Dynamic Pressure, Fastener Temperature, and Molybdenum Strength Variation	4-4

NOMENCLATURE

h	convective coefficient, $\text{lbm}/\text{ft}^2\text{-sec}$
I	enthalpy, Btu/lbm
I_r	recovery enthalpy, Btu/lbm
Nu	Nusselt number
Pr	Prandtl number
\dot{q}	convective heat flux, $\text{Btu}/\text{ft}^2\text{-sec}$
Re	Reynolds number
r	radius of surface point from axis of symmetry, ft
S	boundary layer length, ft
T	temperature
u	velocity, ft/sec
ϵ	emittance
μ	dynamic viscosity
ρ	density

Subscripts

*	evaluated at reference enthalpy conditions
e	evaluated at boundary layer edge
l	laminar boundary layer
o	evaluated at stagnation point (total conditions behind normal shock)
t	turbulent boundary layer
w	evaluated at wall

Contracts

THERMO-STRUCTURAL ANALYSIS OF TUNGSTEN NOSE CAP
FOR ASSET ASV-4 FLIGHT VEHICLE

1.0 INTRODUCTION AND DISCUSSION

By supplemental agreement with the prime contractor, Solar Aircraft Company, San Diego, work commenced in April, 1963, on a technical study to determine temperatures and stresses which will occur in a forged tungsten nose cap to be exposed to a boost ascent-glide descent trajectory as a portion of the forthcoming ASSET program at the Atlantic Missile Range (Aerothermodynamic/Elastic Structural Systems Environmental Tests). To expedite this technical support effort structural work on a preceding subcontract to Solar to analyze and assist in the development of refractory metal frontal sections for various super-orbital glide reentry vehicles has been held in abeyance.

Solar is fabricating for imminent ASSET-testing an instrumented nose cap of forged tungsten, protected against oxidation by a tungsten grid-reinforced overlay of trowelled thorium oxide. This specific cap structure will be attached to a molybdenum nose skirt and flown on the aerothermostructural ASSET flight article, ASV-4. A Thor-Delta boost system will inject the test glider into a lifting reentry trajectory at an initial velocity of 19,800 fps and an initial altitude of 196,700 ft. The flight duration analyzed herein (including ascent and descent) was 1260 sec. During entry, which commenced at 220-sec flight, a vehicle pitch-up attitude of 20° was maintained.

The trajectory data (Ref. 1) were obtained from copies of correspondence received by Solar from the McDonnell Aircraft Corporation; cap geometry and attachment details, as well as required thermo-physical and mechanical properties of the materials, were provided by Solar (Refs. 2, 3, and 4).

Transient temperature distributions throughout boost and glide reentry were determined for the cap, thoria overlay, and disilicide-coated molybdenum afterbody. Unsymmetric air stream impingement on the nose cap during ascent flight was also included.

An analysis of elastic/plastic thermal stresses and displacements based upon the derived temperatures was conducted. Moreover, a load-temperature study was performed to determine the strength of molybdenum fasteners utilized in attaching the cap to the afterbody.

Lockheed Missiles and Space Company Research Laboratory personnel who contributed principally to this study are William S. Wolff of Fluid Mechanics and Willis E. Jacobsen of Solid Mechanics. Dr. Robert R. Johnson of the Mechanical and Mathematical Sciences Laboratory directed the overall effort.

2.0 TRANSIENT TEMPERATURE ANALYSIS

The following information required for the thermal analysis was supplied by Solar Aircraft Company:

- (1) A drawing of the nose cap (Ref. 2) is shown in Fig. 2-1.
- (2) The trajectory information, velocity, altitude, and angle-of-attack are presented in Fig. 2-2.
- (3) Properties of thoria (ThO_2) coating developed by Solar, are presented in Table 2-1, Section 2. The properties listed are specific heat, thermal conductivity, density, and emittance.
- (4) The emittance values of a W-3 coating for the molybdenum skirt were taken from McDonnell Memo No. 242-151C-2319 in accordance with Solar's instructions. These values are listed in Table 2-2.

The specific heat, thermal conductivity and density of the molybdenum skirt were obtained from an AVCO Manufacturing Corp. report by James A. Collins entitled "Thermo-Physical Properties of Pure Metals, Alloys, Non-Metals, and Plastics," dated 15 December 1958. These are listed in Table 2-2. The specific heat, thermal conductivity and density of tungsten were obtained from Solar Quarterly Progress Report No. 1 dated 1 December 1961, designated ER1115-5 (Table 2-3).

The Solar nose cap and molybdenum skirt were divided into a network of nodes so that LMSC's transient temperature prediction program could be used. The network of nodes is shown in Fig. 2-1. The thoria section was divided into three layers in the radial direction, and the tungsten was divided into two layers. The thoria has a much smaller thermal conductivity than the tungsten, and, in order to duplicate the effects of the large temperature gradients in the thoria, it had to be more finely divided.

The tungsten wire mesh is physically located within the middle layer of the three thoria layers. Therefore the specific heat, thermal conductivity, and density of the middle layer were adjusted to account for the combination. These values are listed in Table 2-4.

A contact resistance was included between all nodes along the interface of the nose cap and molybdenum skirt. A value of $10 \text{ ft}^2\text{-sec}^{-\circ}\text{R/Btu}$ was used for the contact resistance (Ref. 7).

The entire nose cap and the front portion of the molybdenum skirt are backed by insulation; thus for all practical purposes there is no heat transfer from the inner surfaces of the structure.

During the ascent portion of the trajectory the vehicle angle-of-attack varies between zero degrees and minus 10 degrees as shown in Fig. 2-2. Since the computer program cannot account for a variable angle-of-attack it was decided to assume a constant value of zero degrees during the boost portion of the trajectory. This condition places the nose cap centerline at an angle-of-attack of minus twenty degrees. Therefore, the lower section of the molybdenum skirt will assume a plus 10° angle-of-attack and the top outermost portion of the skirt will be flown at an angle-of-attack of minus twenty degrees. In order to account for the asymmetry of flow, the boost portion of the trajectory was investigated by separate solutions (two-dimensional) for the lower section and upper section. The boost trajectory required the initial 220 seconds. IMSC's computer program provides the temperature for each node at each time interval. Temperatures for corresponding nodes, top and bottom, at 220-sec flight were then averaged and used as input temperatures for the reentry portion of the trajectory.

During reentry the vehicle holds a plus 20° angle-of-attack, aligning the nose cap at zero angle-of-attack. The highest temperatures will occur on

the lower section of the molybdenum skirt. Consequently, only the lower section was used for the reentry trajectory, giving conservative results. The nose cap and skirt were, however, assumed to be axially-symmetric during reentry.

For the boost portion of the trajectory only the forward-half of the molybdenum skirt was considered in order to conserve machine time. For reentry the full length of the molybdenum skirt was included in the analysis.

The IMSC digital computer program uses the Fay and Riddell solution of the stagnation point boundary layer equations (Ref. 8). If the convective heat transfer coefficient "h" is defined by the general convective heat transfer equation

$$\dot{q} = h(I_r - I_w) \quad (1)$$

then, according to Fay and Riddell,

$$h_o = \frac{1}{Pr} \left(\frac{Nu}{\sqrt{Re}} \right) \sqrt{\rho_w \mu_w \left(\frac{du_e}{dx} \right)_s} \quad (2)$$

The results of Lee's (Ref. 9) are utilized to obtain the local laminar convective coefficients in terms of the stagnation point coefficient:

$$\frac{h_l}{h_o} = \frac{\rho_e u_e \mu_e r}{2 \left[\int_0^s \rho_e u_e \mu_e r^2 ds \right]^{1/2}} \left[\rho_o \mu_o \left(\frac{du}{ds} \right)_o \right]^{-1/2} \quad (3)$$

The transition phenomenon is, unfortunately, ill-defined in the reentry environment. Some degree of correlation of the momentum thickness Reynolds

number at transition and local body inclination has been established. The correlations, however, are not conclusive because of the paucity and scatter of the available data. The transition criterion available is either based on the assumption that a critical value of the local momentum thickness Reynolds number exists below which the flow is always laminar and above which the flow is always turbulent, or by checking both values of laminar and turbulent coefficient and using the higher value, the conservative approach. IMSC's program has both options, and for this analysis the highest heat transfer coefficient was used. This assumption is recommended in Ref. 10.

The method for predicting the turbulent heat transfer coefficient was developed by Bromberg, Fox and Ackerman (Ref. 11):

$$h_t = \frac{0.0225 (r^{1/4} \rho_* \mu_*^{1/4} u_e)}{\left\{ \frac{5}{4} (0.0225) \frac{0.71}{7} \int_{S_t}^S r^{3/4} \rho_* \mu_*^{1/4} u_e ds + \left(\frac{72}{7} (0.071) \left[\int_0^{S_t} r^2 \rho_* \mu_* u_e ds \right] \frac{1}{2} \right)^{1/5} \right\}^{1/5}} \quad (4)$$

The cited authors indicated that only small error is incurred by neglecting the effect of the laminar run, incorporated as the second integral in the denominator of Eq. (4). Upon introducing this simplification Eq. (4) reduces to

$$h_t = \frac{0.0225 (r^{1/4} \rho_* \mu_*^{1/4} u_e)}{\left(\frac{5}{4} (.0225) \frac{0.71}{7} \int_0^{S_t} r^{3/4} \rho_* \mu_*^{1/4} u_e ds \right)^{1/5}} \quad (5)$$

Pressure distribution around the surface of the body was required so that flow properties at the edge of the boundary layer could be evaluated. Lee's "Modified Newtonian" method (Ref. 12) for the spherical section was matched to the pressure coefficient of the conical skirt section.

The heat conduction network is shown in Fig. 2-1. The masses of the exterior surface nodes are assumed to be located at the surface of the thorium coating rather than at the centroid of the node, improving the accuracy of the surface temperature calculation. By placing the nodal mass at the surface a slight error arises in heat conduction length between the surface node and the next radially-inward node. To minimize this error the outside nodes were taken as thin as possible. The mass of all the remaining nodes was assumed to be concentrated at the centroid of the node.

The method used in the numerical integration of the equations is the "Forward Difference Technique." It is important when using this method to use a time increment value less than the minimum RC value of the network to insure convergence and keep oscillations to a minimum. The RC value is the product of the net resistance times the capacitance of a node. The program checks at each time increment all nodes and determines which node has the minimum RC value. This minimum resultant value is multiplied by a number less than one to insure convergence. The temperature history plot, Fig. 2-3, shows that no instability or significant oscillations occurred.

Figures 2-3 and 2-4 show the temperature histories of various nodes on the nose cap and molybdenum skirt. Figure 2-4 comprises the boost phase. For each node two curves are shown representing the corresponding node on the top and bottom sections of the nose cap and skirt. The reentry phase is shown in Fig. 2-3. The maximum nodal temperature of 4540°F occurred at the stagnation point on the surface of the thorium coating. The maximum temperature attained throughout the molybdenum skirt, 3520°F , occurred at the interface of the nose cap and skirt. A noticeable temperature drop prevailed between nodes 10-1 and 11-1 (Fig. 2-3). This drop was due to the contact resistance at the interface of the nose cap and molybdenum skirt.

The high temperature portion of the flight trajectory occurred between approximately 250 seconds and 850 seconds. During this time temperature differentials across the 0.2-in.-thick thoria coating varied between 450°F and 200°F at the stagnation point. There is approximately a 0.1-in. section between the tungsten shell and the molybdenum pressure port tube as shown in Fig. 2-5. The tungsten shell near the stagnation point exceeds 3600°F for approximately 500 seconds during the hyperthermal glide reentry. Therefore, allowing the same temperature gradient across the 0.1-in. thoria sleeve as across the 0.2-in. thoria shell one can conservatively estimate that the molybdenum tube attached to the stagnation point pressure port will reach approximately 3400°F.

Figure 2-6 presents the cap stagnation point convective heat flux as a function of time. A step change in the function at 220 seconds may be noted. This is caused by the vehicle angle-of-attack modulation from zero degrees to plus twenty degrees at boost termination. The maximum convective heat flux of 271 Btu/sec-ft² occurred at 290 seconds. For equilibrium conditions

$$q_{\text{radiation}} = q_{\text{convection}} \quad (6)$$

The radiation heat flux can be approximated by

$$q_r \approx \frac{\epsilon}{2} \left[\frac{T_w}{10^3} \right]^4 \quad (7)$$

where the wall temperature T_w is given in °R.

Using relationships (6) and (7) T_w is equal to 4640°F for equilibrium conditions at the stagnation point. This temperature is 100°F above the maximum temperature reached by the thoria coating.

2.1 THERMAL TABLES

Table 2-1

PROPERTIES OF THO₂ COATING SO-71

Thermal Conductivity

400 ^o F	2.1	Btu/hr-ft- ^o F
800	1.35	
1200	.95	
1600	.80	
2000	.80	
2400	.80	
2800	.90	
3200	1.10	
3600	1.35	
4000	1.60	
4200	1.75	

Specific Heat

.065 Btu/lb-^oF

Density

0.2 lb/cu in. = 345.6 lb/ft³

Emittance

3000 ^o F	0.35
3500	.50
3700	.61
4000	.78
4200	.82
4500	.82

Table 2-2
PROPERTIES OF MOLYBDENUM

Thermal Conductivity		Specific Heat	
50°F	.0261 Btu/sec-ft-°F	50°F	.061 Btu/lb-°F
100	.0256	100	.0615
400	.0242	400	.064
800	.0208	800	.066
1200	.0189	1200	.0682
1600	.0172	1600	.072
2000	.0161	2000	.077
2400	.0147	2400	.081
2800	.0139	2800	.086
3200	.0139	3200	.092
3600	.0139	3600	.098

Density

50	638	lbm/ft ³
100	637	
400	635	
800	633	
1200	630	
1600	628	
2000	625	
2400	623	
2800	621	
3200	621	
3600	620	

Emittance of a W-3 coating on molybdenum

$0 < T < 1910^{\circ}\text{R}$	0.6
$1910^{\circ}\text{R} < T$	$.000138T(^{\circ}\text{R}) + .336$

Table 2-3

PROPERTIES OF TUNGSTEN

Thermal Conductivity

60°F	.0247 Btu/sec-ft-°F
1830	.0181
3630	.0168
4500	.0168

Specific Heat

60°F	.033 Btu/lb-°F
1830	.039
3630	.044
4500	.044

Density

1190 lbm/ft³

Table 2-4

PROPERTIES OF THORIA PLUS TUNGSTEN MESH

Thermal Conductivity

60°F	.002275	Btu/sec-ft.°F
1830	.001476	
3630	.001529	
4500	.001529	

Specific Heat

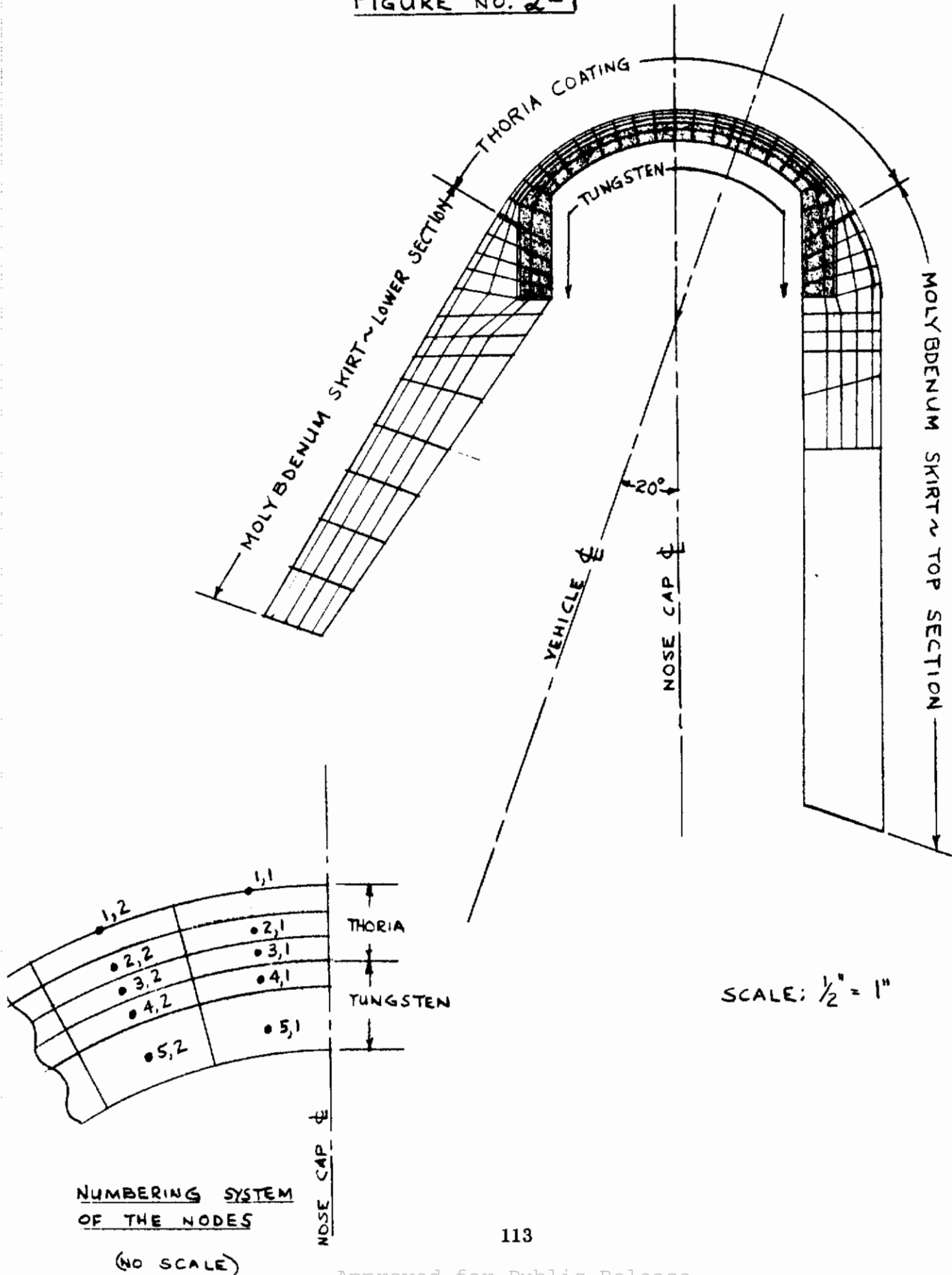
60°F	.05875	Btu/lbm-°F
1830	.05994	
3630	.06090	
4500	.06090	

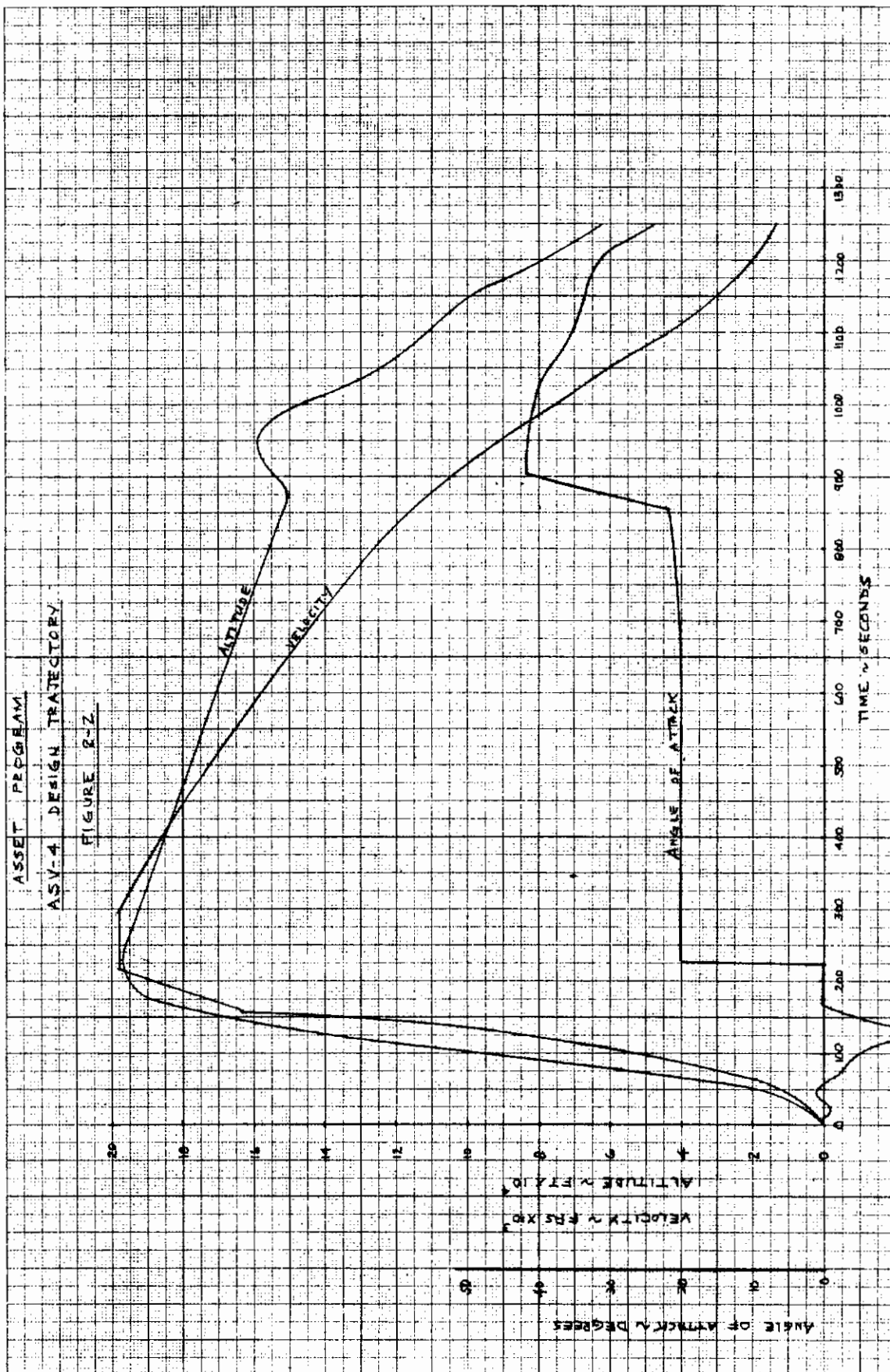
Density

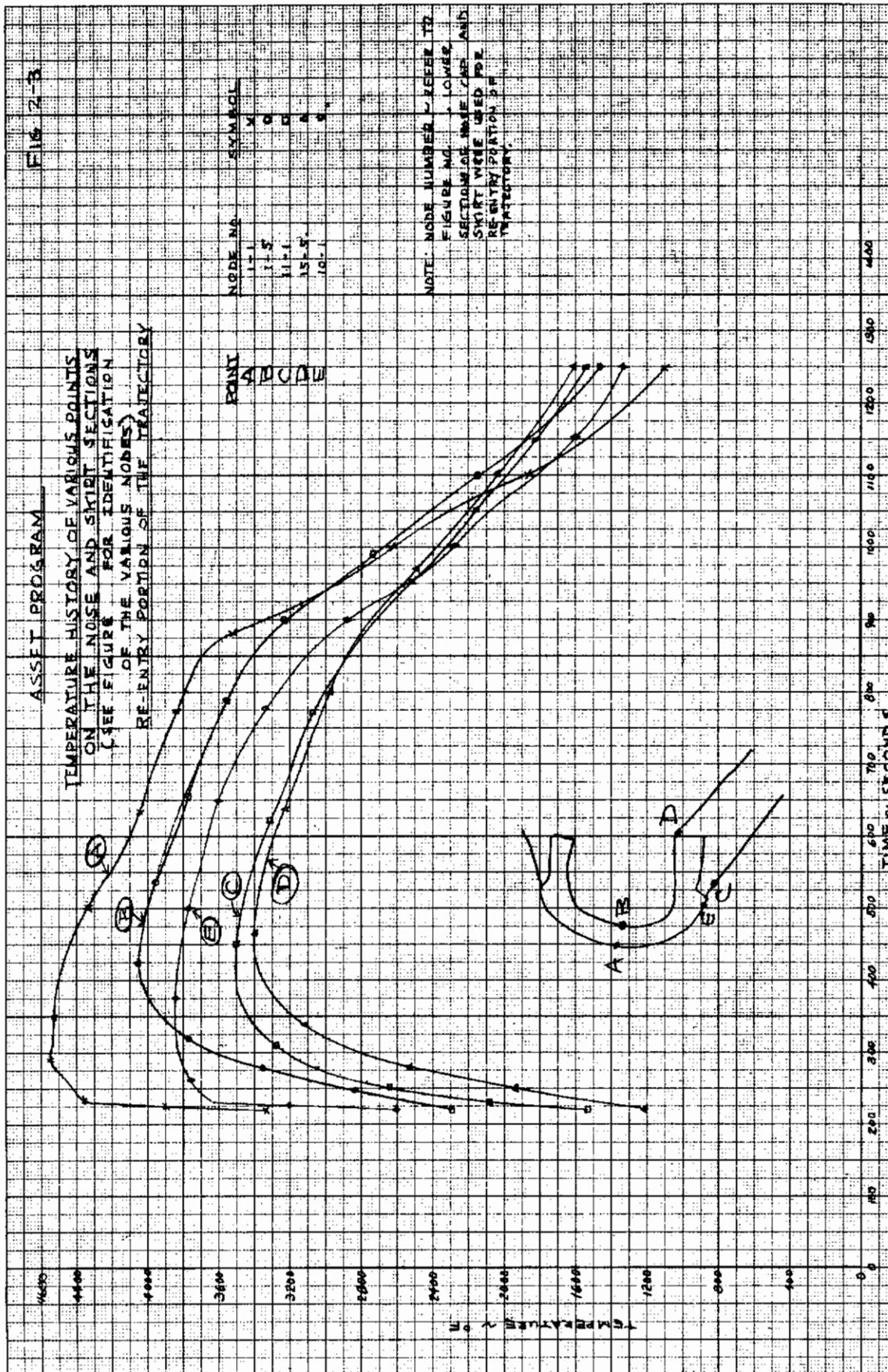
430 lbm/ft³

NODAL ARRANGEMENT FOR HEAT TRANSFER ANALYSIS

FIGURE NO. 2-1



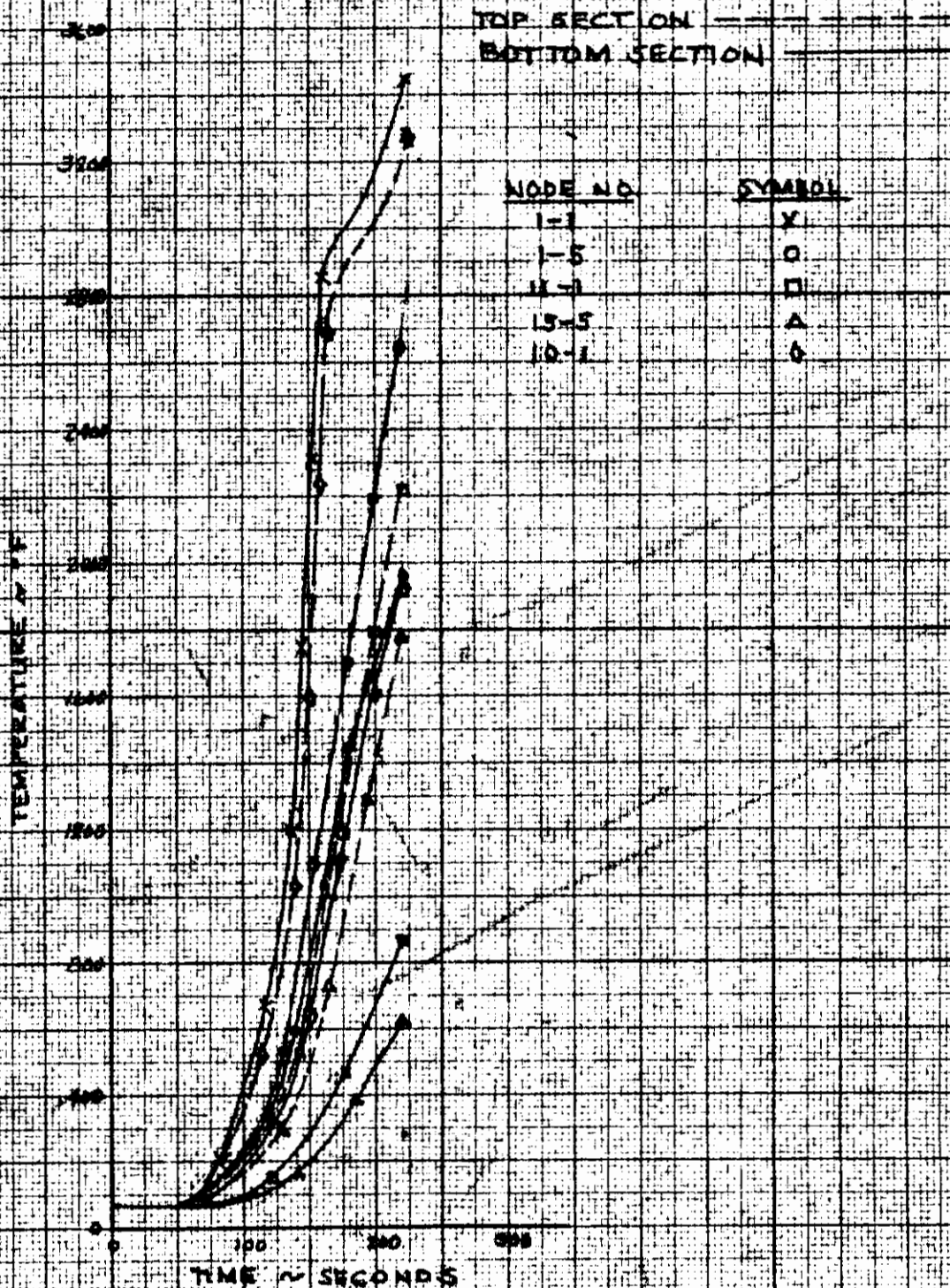




ASSET PROGRAM

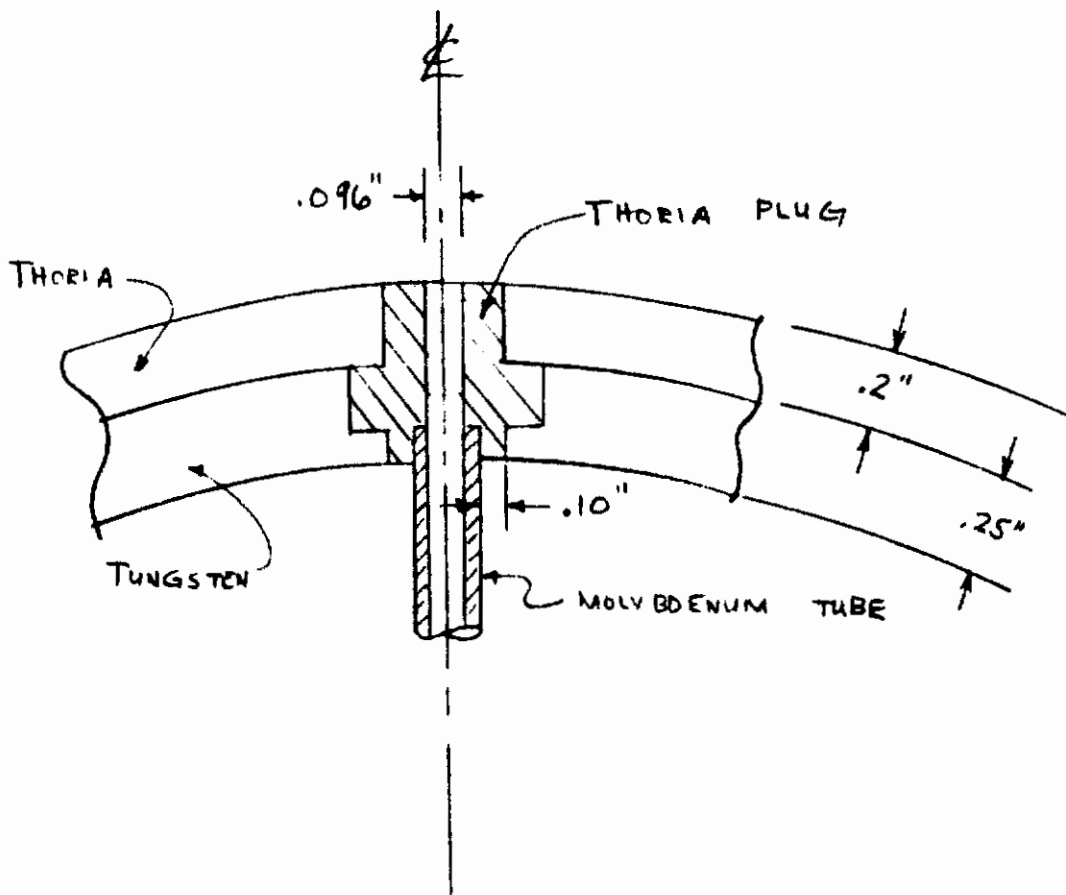
FIG 2-4

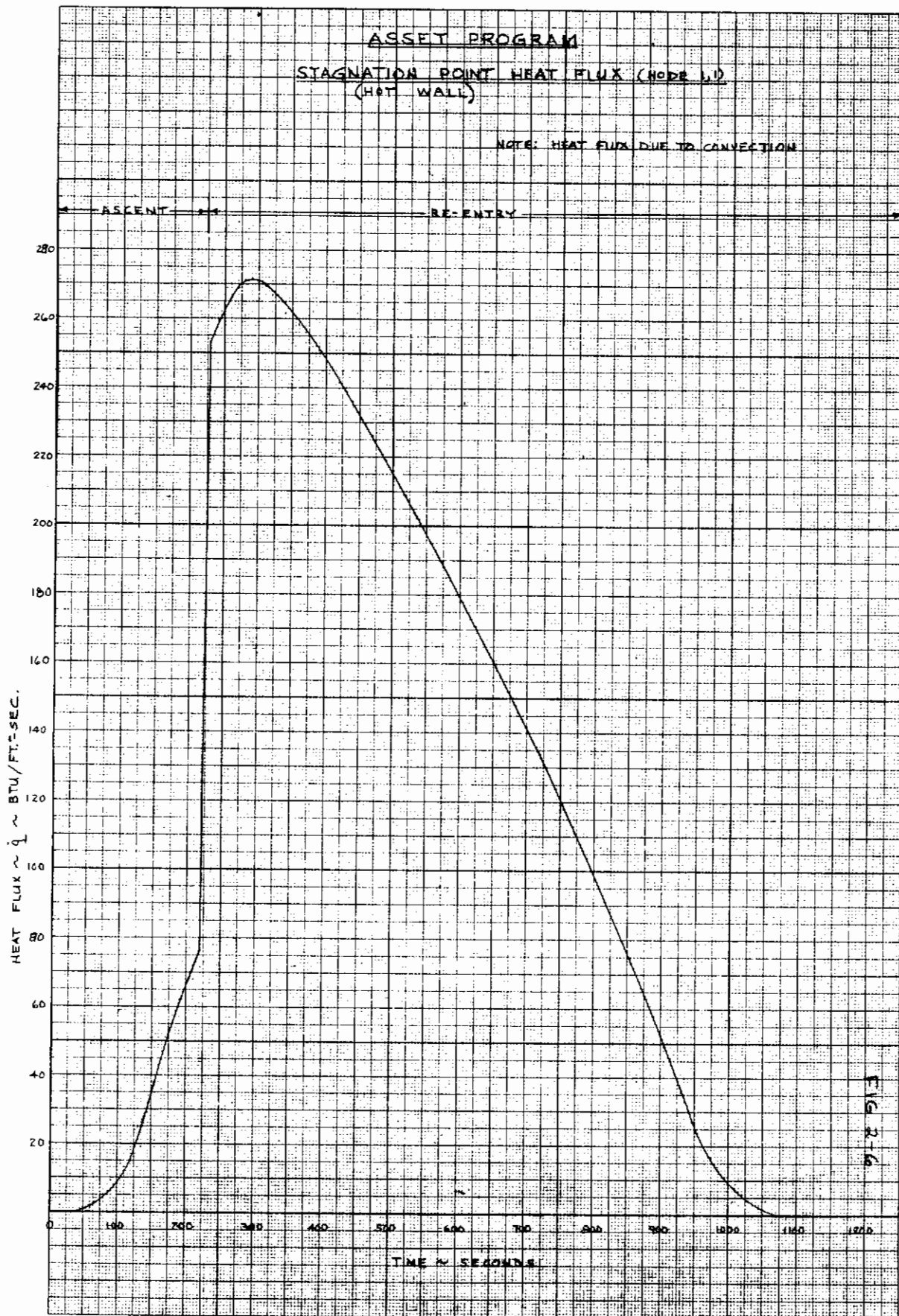
TEMPERATURE HISTORY OF VARIOUS POINTS
ON THE BOTTOM AND TOP SECTIONS OF THE
NOSE AND SKIRT SECTION
ASCENT PORTION OF THE TRAJECTORY



ASSET PROGRAM
PRESSURE PORT DETAIL

FIG 2-5





3.0 THERMAL STRESS AND DEFLECTION ANALYSIS

Temporal and spatial variations of temperature within the forged tungsten nose cap were utilized to determine the stress-deflection history. A full-scale layout of the cap geometry, a shell of revolution with an assumed rotationally-symmetric application of load and temperature, is shown in Fig. 3-1. The mid-surface of this body is described as a frontal spherical segment of 2.785-in. radius joined at the shoulder region to a 2.15-in.-radius cylinder by a tangent circular transition of approximately 0.8-in. radius of curvature. The shell thicknesses are a uniform 0.25 in. for the spherical section, a uniform 0.50 in. throughout the aft cylindrical portion, and a nearly linear increase in thickness with station over the shoulder transition section.

Stationing for stresses and deflections is listed sequentially from unity at the stagnation point through eighteen at the rear edge. In zones of stress discontinuities and anticipated steep meridional temperature gradients the station interval was purposely decreased for better definition of structural behavior.

Because of the low relative magnitude of air loads (to be discussed in the fastener analysis, Section IV) only stresses of thermal origin were considered. Expected inelastic behavior of the shell was to be described by plasticity theory and assumed as independent of viscous effects. An isotropic material was furthermore assumed for the solution. The flow rules invoked were associated with the von Mises loading function for a temperature-dependent workhardening material. It was presumed that the equations of thin-shell theory (Ref. 5).described with sufficient accuracy any plastic action under the restriction of small deformations.

The stress solution was formulated as a boundary-value problem in terms of time-rates of the variables. The equations were reduced to two governing

differential equations in which plastic strain rates are retained as implicit functions to be determined as the loading history progresses. An analytical solution of the equations appeared impossible; therefore, a numerical step-by-step integration in time was employed on a digital computer. Results include displacements, stresses, and elastic-plastic interfaces for given times.

The governing differential equations (Ref. 5) are

$$a_1 \frac{\partial^2 \dot{U}}{\partial s_1^2} + a_2 \frac{\partial \dot{U}}{\partial s_1} + a_3 \dot{U} + a_4 \frac{\partial^2 \dot{\beta}}{\partial s_1^2} + a_5 \frac{\partial \dot{\beta}}{\partial s_1} + a_6 \dot{\beta} = \phi_1$$

$$a_4 \frac{\partial^2 \dot{U}}{\partial s_1^2} + a_5 \frac{\partial \dot{U}}{\partial s_1} + a_6 \dot{U} + a_7 \frac{\partial^2 \dot{\beta}}{\partial s_1^2} + a_8 \frac{\partial \dot{\beta}}{\partial s_1} + a_9 \dot{\beta} = \phi_2$$

where the first dependent variable is $\dot{U} \equiv r_2 \dot{\psi}$, with $\dot{\psi}$ being the rate of change of shear resultant, lb/in.-sec, and r_2 a principal radius of curvature (circumferential) of the middle surface of the shell; and the second dependent variable $\dot{\beta}$ is the element rotational rate, rad/sec.

For this analysis a monocoque tungsten shell of revolution was assumed; that is, the reinforced thorium overlay, attached at discrete points to the shell by stand-off pins, was considered to be completely free-floating and offering, through bonding or attachment, no restraint whatsoever. The elevated-temperature mechanical properties of tungsten utilized in this analysis, namely, elastic modulus, shear modulus, Poisson's ratio, and coefficient of linear thermal expansion, are presented in Fig. 3-2. The stress-strain characteristics, plotted from uniaxial tensile tests of tungsten specimens, are shown in Figs. 3-3 and 3-4. These temperature-dependent values, applicable to the plastic regime, were incorporated into the computer solution in tabular form.

For the specific cap-skirt connection design little or no mechanical fixity was presented at the base of the cap, and freedom of thermal growth of the cap was similarly afforded by the mounting system.

Temperature distributions with time were calculated in the analysis described in detail in Section II. A plot of the mid-surface temperature about the tungsten shell for various flight times is presented in Fig. 3-5. Boost flight extended between zero time (lift-off) and glide injection (220 sec). During that interval pitch modulation maneuvers were programmed; such flight causes a non axi-symmetric upper and lower surface temperature distribution on the frontal structure. An artifice for this period of flight to provide thermal symmetry for the stress analysis was an averaging of the temperature obtained from both upper and lower surface flow impingement. This averaging process was an assumption of high radial heat conduction about the tungsten body. As can be seen from Fig. 3-5 the peak meridional mid-surface temperature drop, approximately 1000°F , occurred at 220 sec ($\bar{T}_{\text{stag. pt.}} = 2310^{\circ}\text{F}$ and $\bar{T}_{\text{rear}} = 1320^{\circ}\text{F}$). The meridional arc length measured from the stagnation point is denoted as s , and the total arc length about the body is termed s_l . The highest temperature attained in the tungsten shell, 4060°F , occurred at 440-sec flight near the stagnation point. Late in reentry (past 600 sec) the shell attained a uniformly-high temperature throughout. The negligible gradients are due to the length of exposure and the relatively-high thermal conductivity. With minimal gradients the resultant thermal stresses at later times also assume insignificant magnitudes. Whereas the meridional temperature variation was considerable at boost termination, radial gradients throughout the entire flight were small, again because of the conductivity of tungsten. The maximum temperature differential, less than 60°F outer-to-inner surface, occurred at 240-sec flight in the cylindrical portion of the shell, as shown in Fig. 3-6.

Radial temperature profiles were determined utilizing higher-degree curves to represent the variation in potential through the thickness. The gradients were so nearly linear and of such small magnitudes that a straight-line variation radially was a valid approximation for the stress solution. The increase in temperature differential slightly aft of the stagnation point, as shown by the dashed curve of Fig. 3-6, was due to the non-symmetric flow impingement during boost. The increase in differential near station $s/s_l \approx 0.6$ was due to the local divergence in shell thickness and accompanying increase in thermal

resistance; this, however, does not necessarily indicate an increased temperature gradient, $dt/d\xi$. Note that on the rearward portions of the shell an actual reversal of gradient occurs past 400 sec—hotter on the inside, cooler on the outside. This condition, as well as the reversed slope of the meridional temperature gradient, is attributable to the shell heat storage capacity and ultimately to the reduced heat transfer to the outer surface.

For the specific cap geometry initial trial thermal stress solutions were made to check relative effects of instantaneous radial and meridional temperature distributions. A check of stresses in the spherical frontal zone due to a uniform temperature over the surface and a constant radial gradient indicated good agreement between machine results and an exact analytical thick shell solution. Trial solutions proved that the predominant influence upon thermal stresses was the temperature variation along the cap. When the spherical center segment is hot compared with the cylindrical afterbody, thermal strains are of dissimilar magnitudes. Also, the cylindrical portion presents considerable stiffness or fixity to the hot frontal segment due to the former's higher modulus (relatively cool operating temperature) and higher moment of inertia (increased thickness of section).

The principal normal stresses σ_1 (meridional) and σ_2 (circumferential) which resulted from the severe temperature distribution at 220-sec flight are presented in Figs. 3-7 and 3-8, respectively. Since all calculated stresses were confined to the elastic range of the forged tungsten except for a localized region on the inner and outer surfaces near the hot stagnation zone, time effects were of little consequence. In these specific analyses the time-deformational response was thus not required. Comparative stresses were checked at instants of time slightly preceding and slightly following boost termination (220 sec) to ascertain that peak stress values were actually obtained.

Near-symmetry of the meridional stress pattern through the shell thickness is apparent in Fig. 3-7; also, a reduction of stresses to zero toward the rear of the shell was indicated, according to expectations. A peak compressive stress of 27,000 psi occurred at the outer surface shoulder discontinuity. The circumferential or hoop stresses shown in Fig. 3-8 were equal to the orthogonal stresses at the stagnation point, approached zero at the sphere-circular shoulder transition, thence became tensile at the forward portion of the cylinder and hoop compressive at the rear.

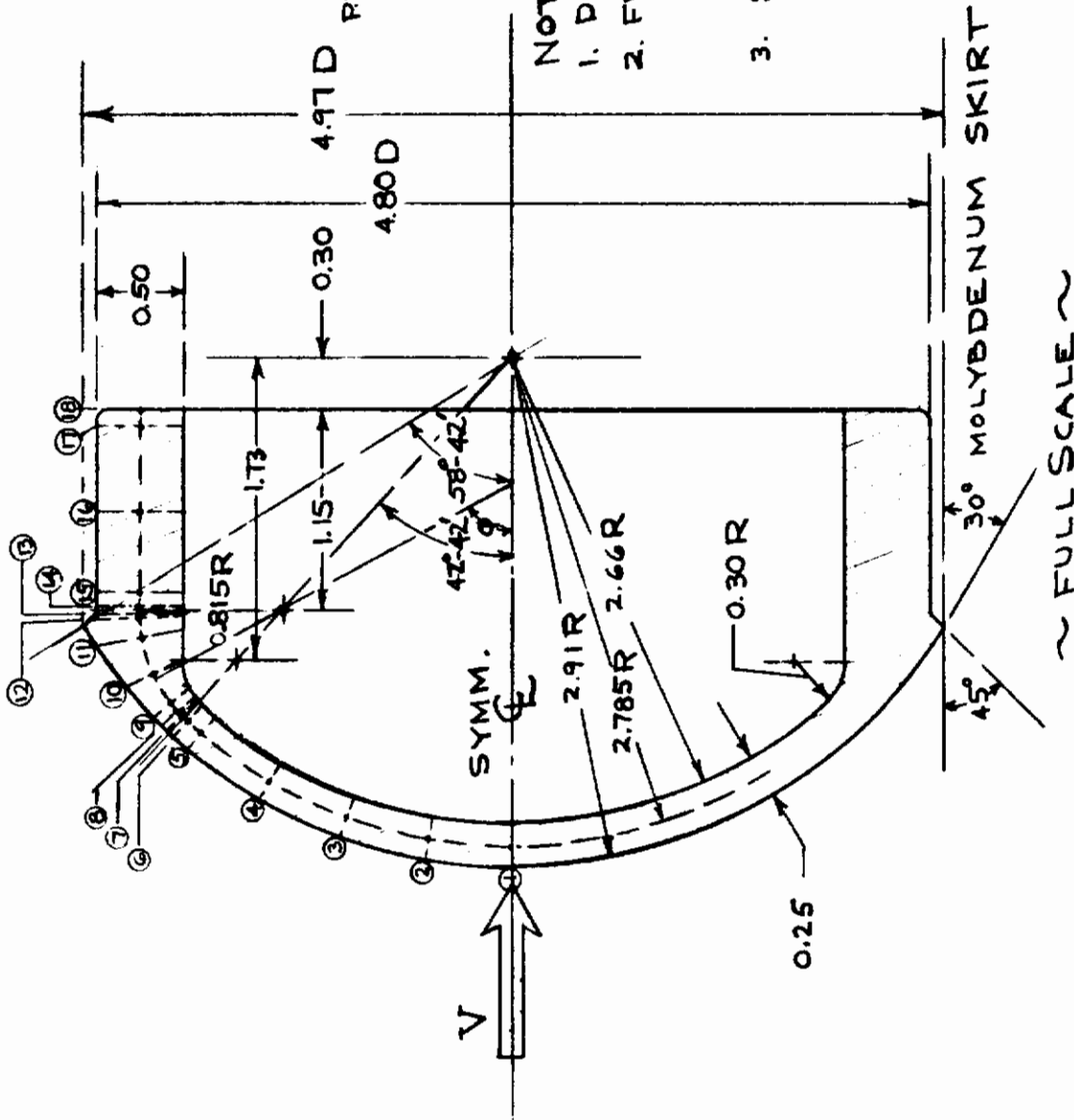
The thermal deformation of the shell mid-surface is presented in Fig. 3-9. The true direction and amplified magnitude of the deflection is superposed upon a full-scale undistorted plot of the original mid-surface geometry. Radial growth at the rear is 0.0068 in.; axial growth along the centerline is 0.0172 in.

Prepared	NAME JACOBSEN, B.	DATE 5-7-63	LOCKHEED AIRCRAFT CORPORATION MISSILES and SPACE DIVISION	Page	TEMP	PERM
Checked				ASSET Model ASY-4		
Approved			TITLE FORGED TUNGSTEN NOSE CAP, SPHERICAL	Report No.		

FIG 3-1

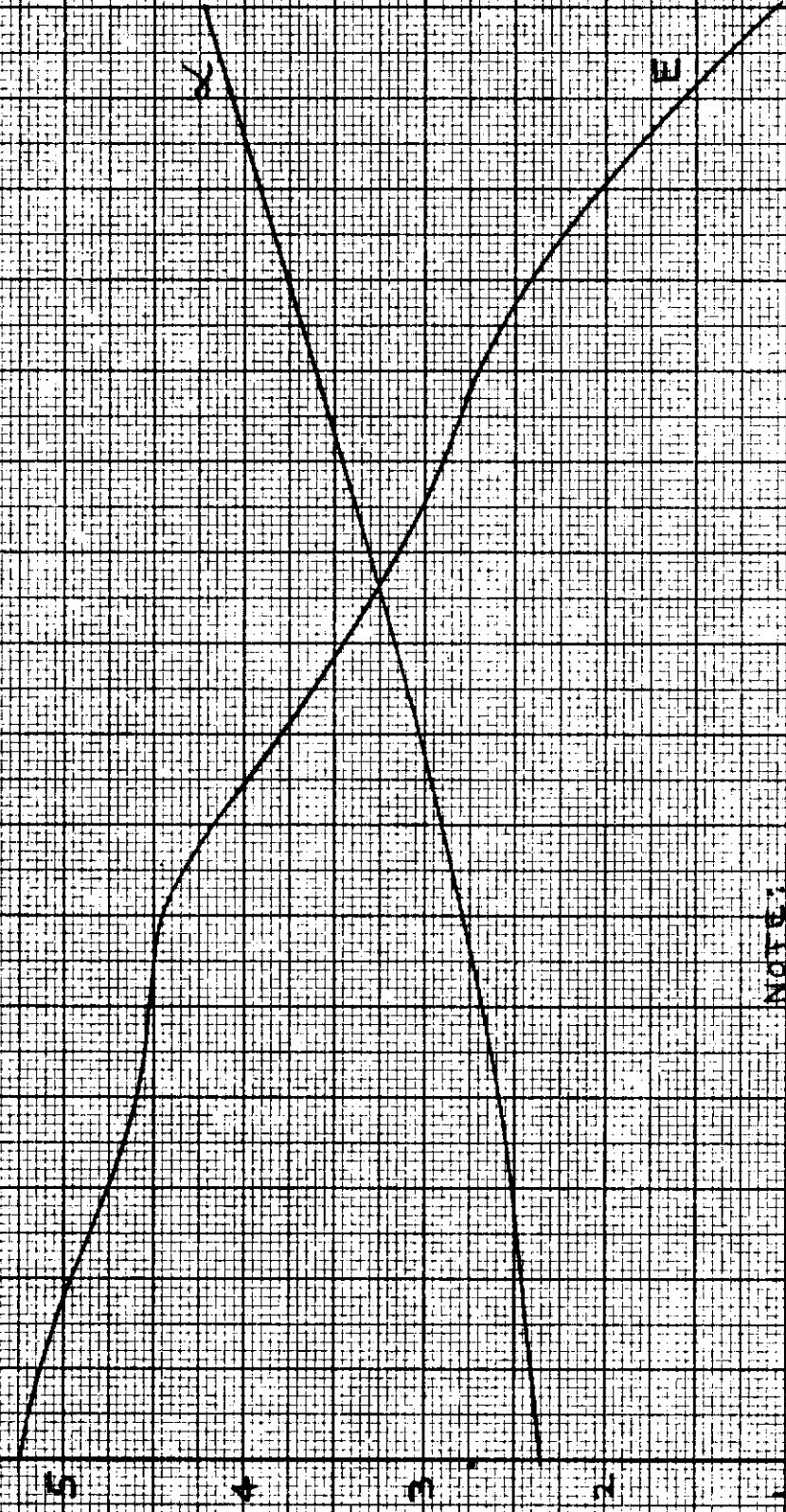
STA.	S/S _L	STA.	S/S _L
1	0	10	.614
2	.1245	11	.669
3	.2490	12	.698
4	.3735	13	.703
5	.4980	14	.707
6	.523	15	.732
7	.535	16	.854
8	.541	17	.974
9	.559	18	1.000

- NOTES:
1. DIMENSIONS IN INCHES.
 2. FILLETS 0.125-IN DIAM. UNLESS DENOTED OTHERWISE.
 3. S_L = 3.90 IN.



TUNGSTEN MECHANICAL PROPERTIES

COEFFICIENT OF THERMAL EXPANSION, α , $10^{-6}/IN/IN/°F$
 MODULUS OF ELASTICITY, E , 10^5 PSI
 MODULUS OF ELASTICITY, G , 10^5 PSI



NOTE:

- (1) POISSON'S RATIO, $\nu = 0.284$ FOR ALL TEMPERATURES.
- (2) SHEAR MODULUS, $G = E / 2(1 + \nu) = 0.389 E$.

TEMPERATURE, °F	1000	1500	2000	2500	3000	3500	4000
α	1.2	3.8	4.2	3.8	2.8	2.2	1.8
E	4.8	4.2	3.5	2.8	2.2	1.8	1.2

Central

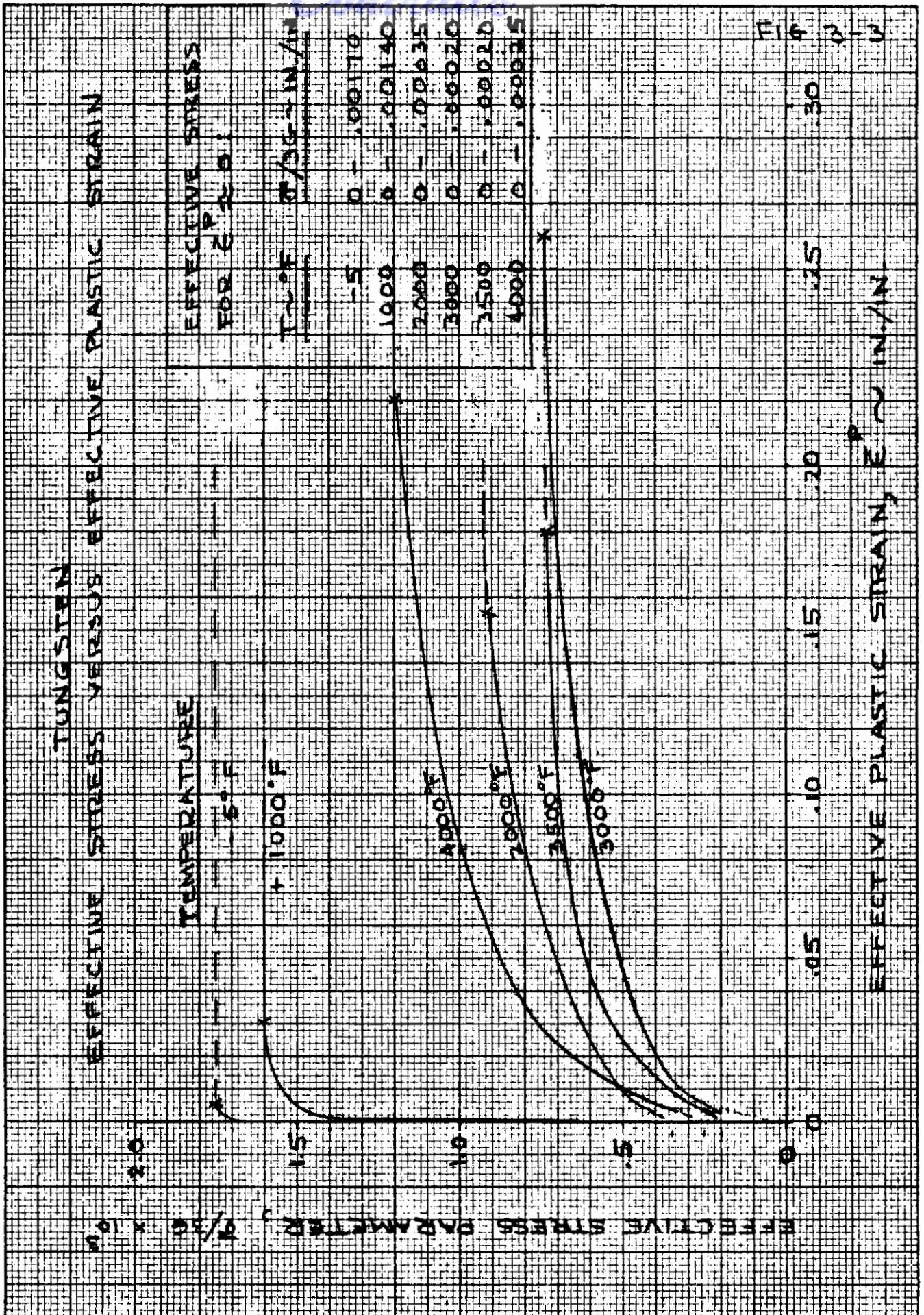
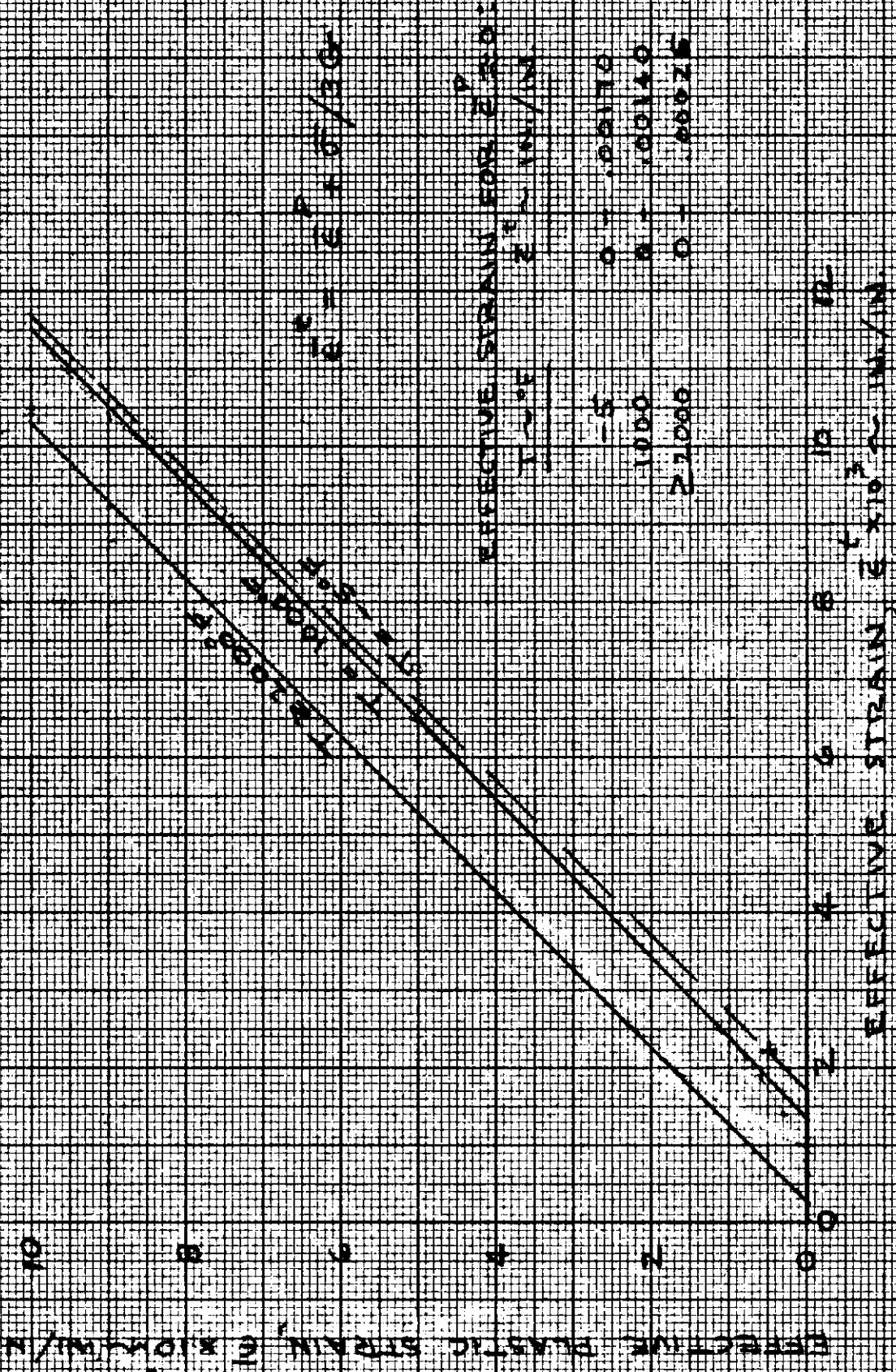


FIG 3-4

TUNGSTEN
EFFECTIVE PLASTIC STRAIN VERSUS EFFECTIVE STRAIN

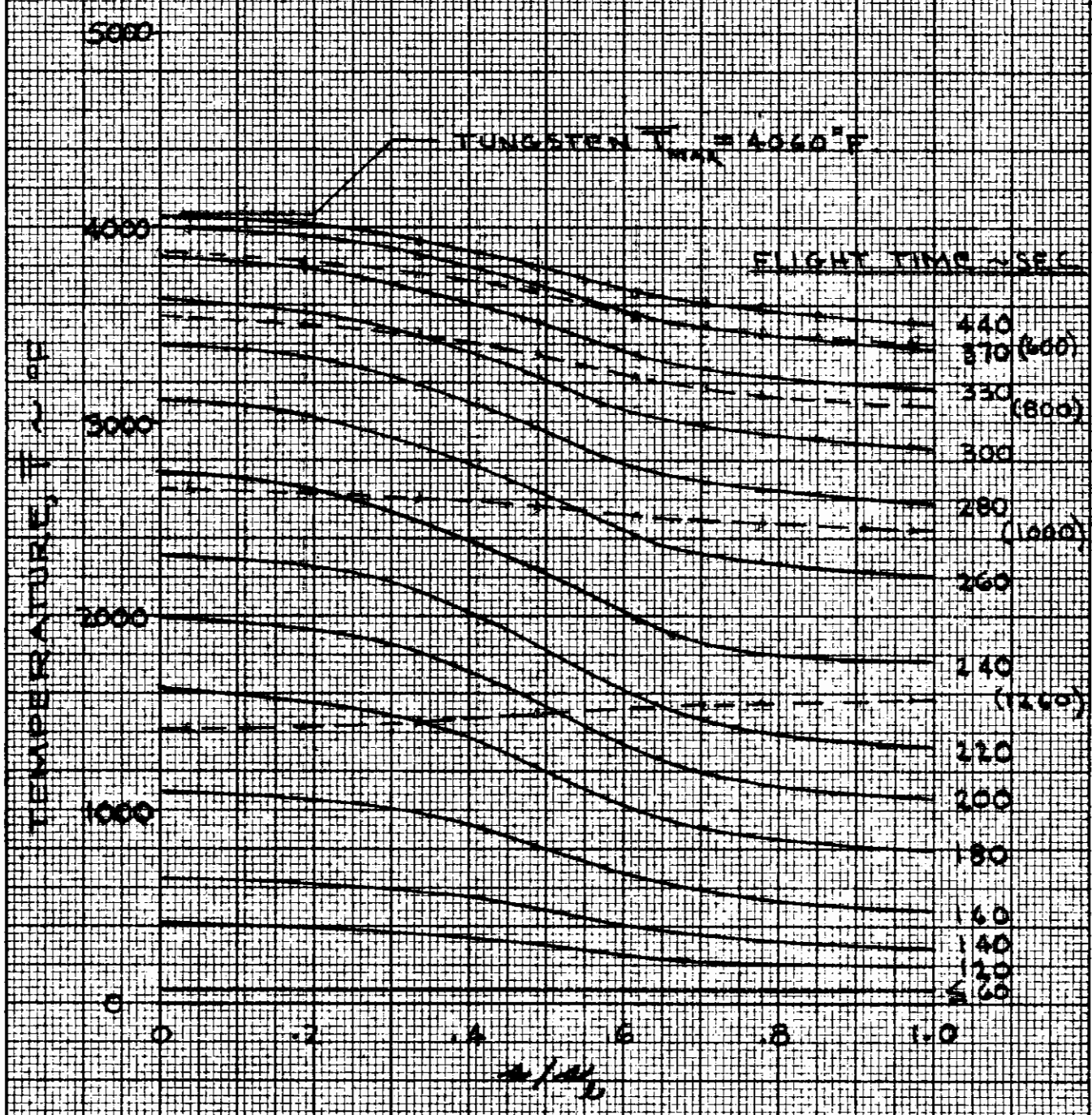


Continuity

FIG 3-5

ASV-4

SHELL MID-SURFACE TEMPERATURE



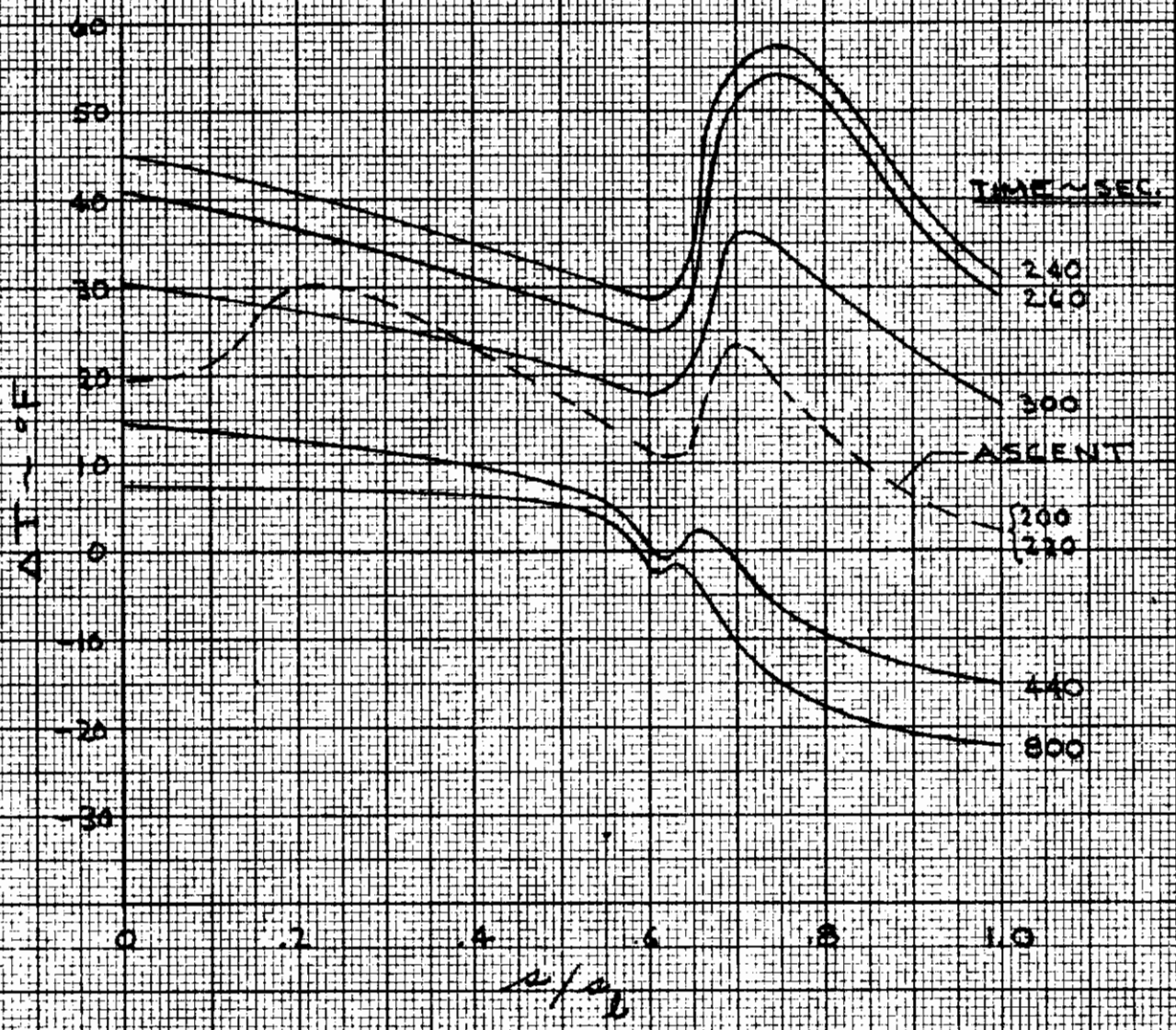
LEGEND:
—— TEMPERATURE DURING HEATING
- - - - (TEMPERATURE DURING COOLING)

Continuity

FIG 3-6

ASV-4

SHELL TEMPERATURE DIFFERENTIAL FOR VARIOUS TIMES



ΔT = AVERAGE RESULTANT TEMPERATURE DIFFERENCE, FRONT FACE - TO - REAR FACE

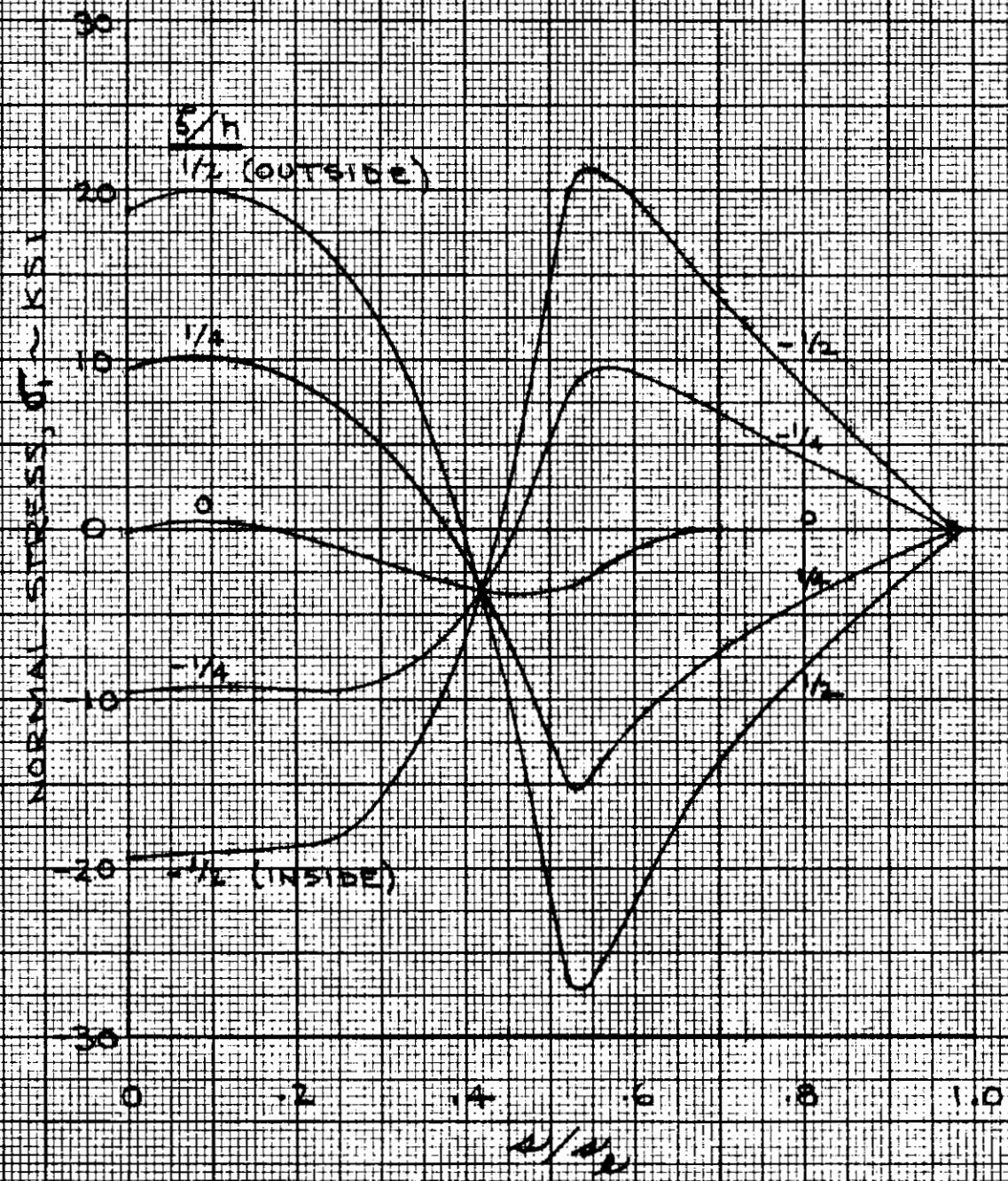
Continued

FIG 3-7

ASV-4
ASSET NOSE CAP
MERIDIONAL STRESSES

FLIGHT TIME 230 SEC.

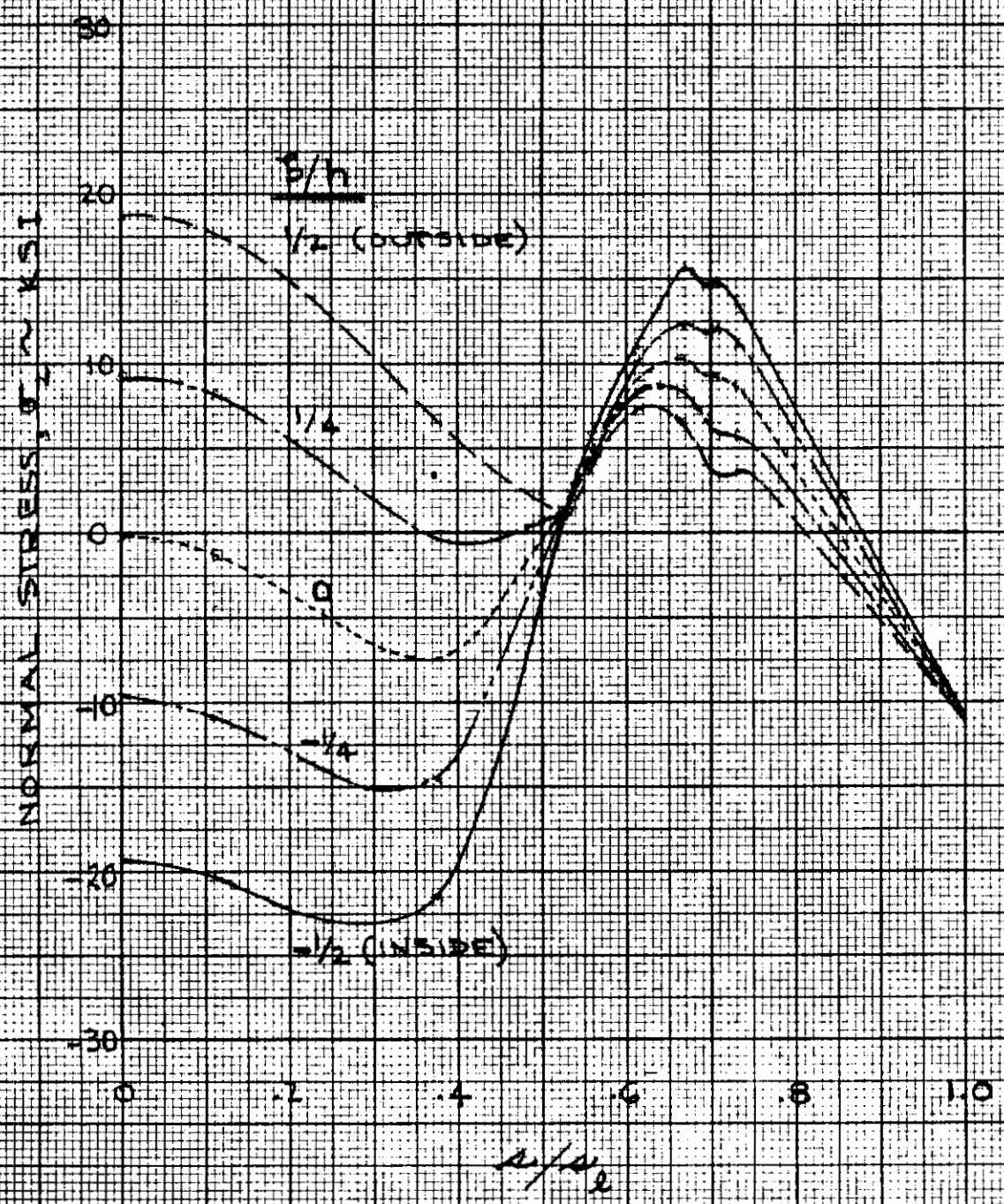
δ = NORMAL DISTANCE FROM SHELL
MID-SURFACE.
 h = SHELL THICKNESS.



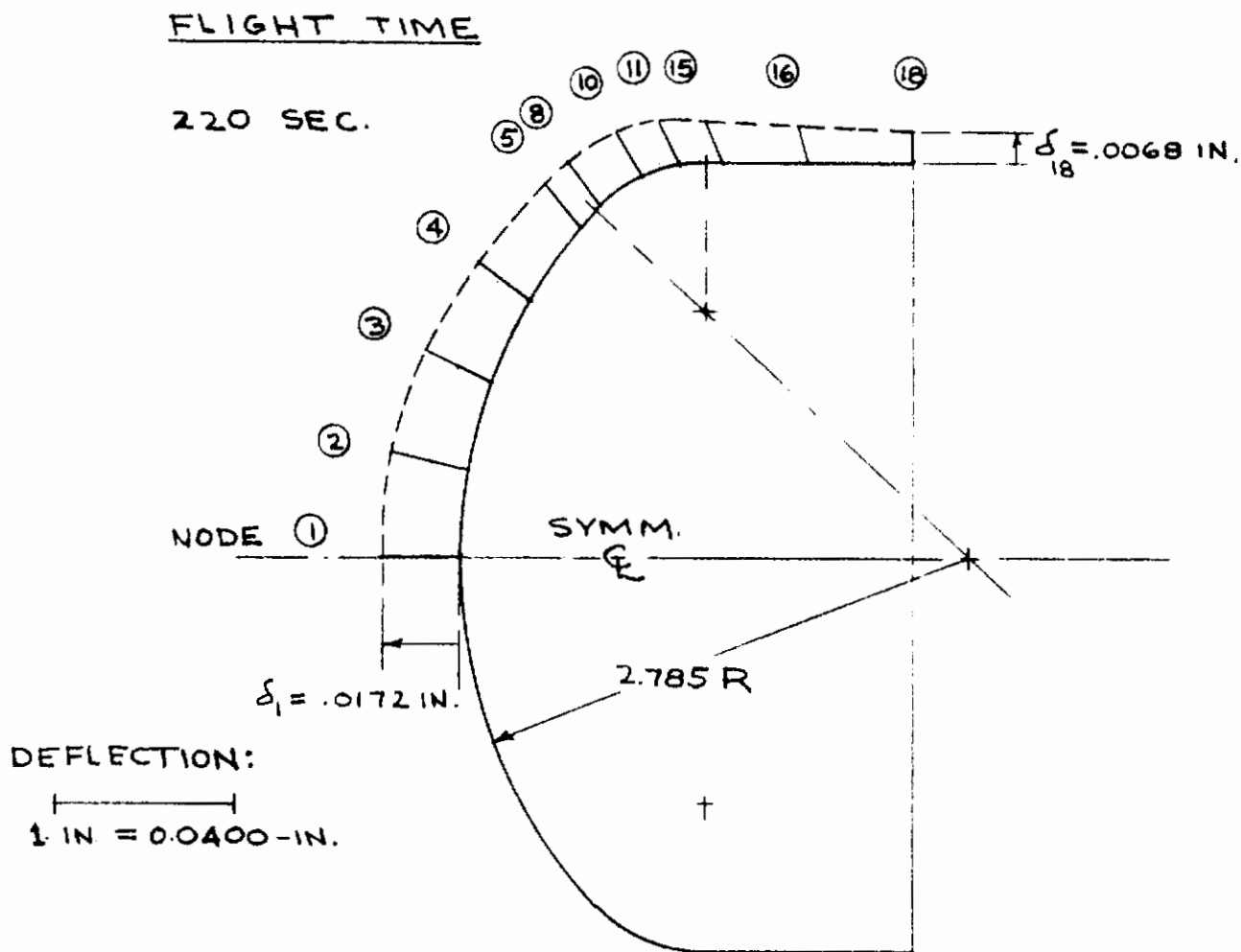
ASV-4
ASSET NOSE CAP
CIRCUMFERENTIAL STRESSES

FLIGHT TIME 220 SEC

y = NORMAL DISTANCE FROM SNELL MID-SURFACE
 h = SNELL THICKNESS



ASV-4 TUNGSTEN NOSE CAP SHELL MID-SURFACE DEFLECTION



FULL SCALE UNDEFLECTED NOSE SHAPE
(MEDIAN SURFACE)

4.0 FASTENER ANALYSIS

The deformation compatibility at the hot tungsten cap-molybdenum skirt juncture must be assured. At 220-sec flight the rear mid-surface temperature is approximately 1300°F and the cylindrical radius is 2.15 in. From the tungsten coefficient of expansion curve a median value of α (650°F) is 2.5×10^{-6} in/in-°F. This gives for the radial thermal deformation

$$\begin{aligned} \delta_{18} &= r_{18} \alpha \Delta T = 2.15 \text{ in} (2.5 \times 10^{-6} \text{ in/in-}^\circ\text{F}) (1300^\circ\text{F}) \\ &= \underline{0.007 \text{ in.}}, \text{ tungsten} \end{aligned}$$

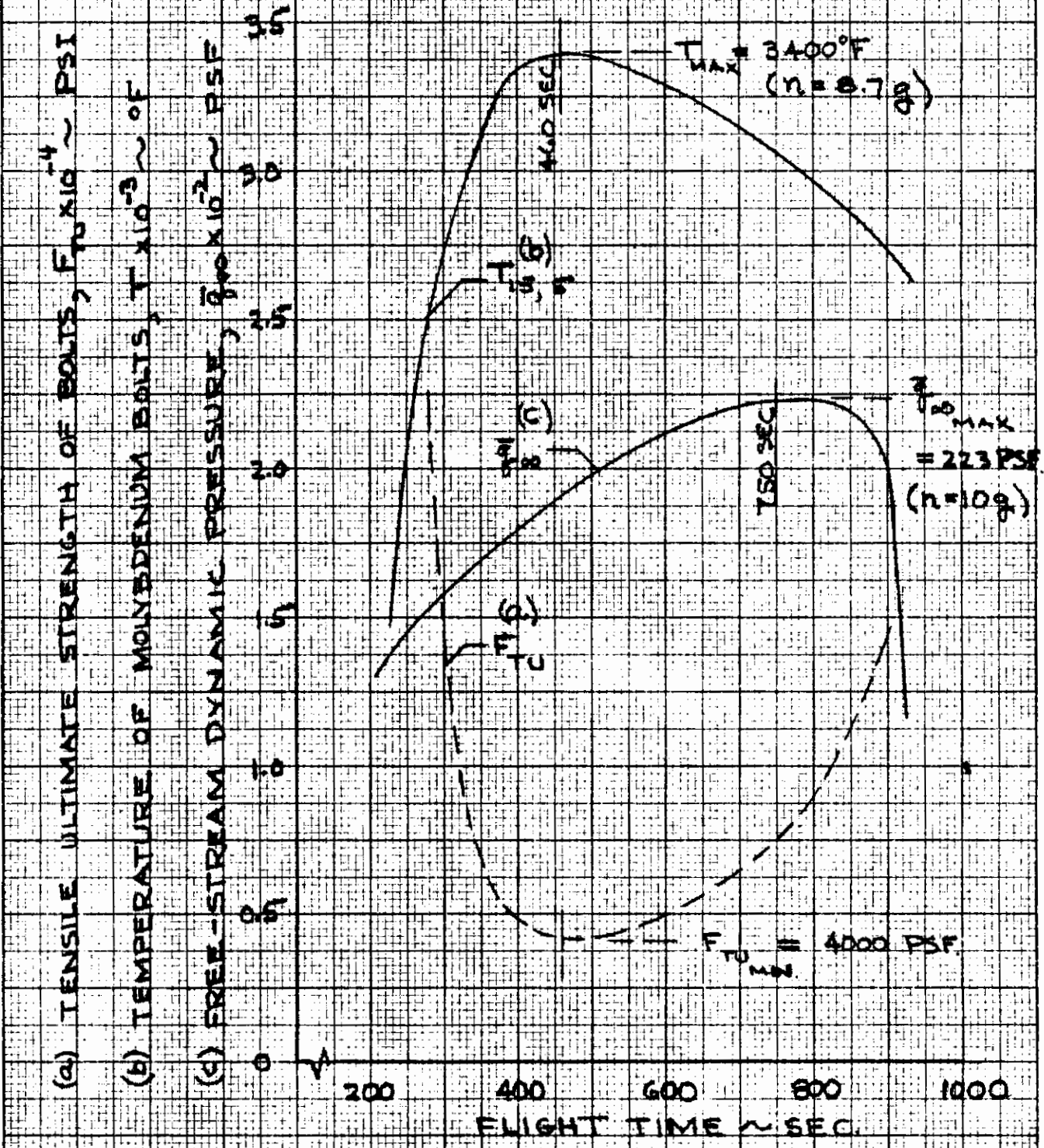
This agrees with the 0.0068-in. value from the machine solution, Fig. 3-7. The corresponding temperature in the molybdenum at the same station and time is 1340°F; for a mean local skirt radius of 2.8 in. and expansion coefficient (Ref. 6) of 3.3×10^{-6} in/in-°F for TZM alloy

$$\begin{aligned} \delta_{18} &= 2.8 \text{ in} (3.3 \times 10^{-6} \text{ in/in-}^\circ\text{F}) (1340^\circ\text{F}) \\ &= \underline{0.012 \text{ in.}}, \text{ molybdenum.} \end{aligned}$$

Thus, the skirt will actually expand away from the cap, offering no contact restraint to the thermal growth of the tungsten. At maximum temperature, 440-sec flight time, the same conclusion holds: a 3500°F tungsten temperature and 3440°F molybdenum temperature give radial growths of 0.022 in. and 0.038 in., respectively.

Finally, the strength at temperature of two molybdenum cap-attachment bolts was assessed. The weight of the cap was required to determine connector loading under various conditions. Volumes of 14.30 cu in. for the tungsten forging the 5.5 cu in. for the coating were obtained by integration. For a tungsten density of 0.693 lb/cu in. and an effective density of 0.361 lb/cu in. for the reinforced 80 percent-dense thoria resultant weights of substrate and overlay are 10 lb and 2 lb, respectively. Assuming that a graphite cloth internal insulation, rear molybdenum retaining bulkhead, and instrumentation

DYNAMIC PRESSURE, FASTENER TEMPERATURE, AND MOLYBDENUM STRENGTH VARIATION



tubes together weight 3 lb., the total weight of the frontal section is approximately 15 lb.

During boost acceleration a load factor of 15 is expected. The inertial loading plus an airload contribution of 50 lb provide a total aft-applied axial force of $15 (15) + 50 = \underline{275 \text{ lb.}}$ However, early in flight the fasteners are still approximately at room temperature, and the base of the cap bears uniformly against the skirt periphery at the juncture. Thus, no fastener problem exists during boost flight.

Reentry along the 10-g bound of the flight corridor indicates that the peak deceleration force will be 10 g's. With the vehicle angle-of-attack maintained at plus 20° the velocity vector, inertial force, and integrated pressure force will all be concurrent along the symmetric centerline of the cap. This gives a forward axial force of $15 (10) = \underline{150 \text{ lb.}}$

Peak free stream dynamic pressure coincides in time with peak deceleration, but peak incident heat flux precedes the maximum deceleration. However, temperatures in the fastener area are nearly at their peak during the high forward load application. An analysis of the ASV-4 design trajectory showed that, at 750-sec flight, a peak free stream dynamic pressure \bar{q}_∞ of 223 psf was achieved. For modified Newtonian flow and a hypersonic drag coefficient C_D of unity on a cap of 0.154- sq ft projected area, the total drag force is

$$D = 1.84 C_D \bar{q}_\infty A = 1.84 (1) (223) (0.154) = \underline{63 \text{ lb.}}$$

The net result of inertia and opposed airloading is a forward-directed force of 97 lb. Each of the two molybdenum bolts must sustain a tensile force of 48.5 while heated to 3050° F. The allowable tensile loading of a 3/16-in.-diam. TZM molybdenum alloy bolt at the temperature indicated is 135 lb.

Earlier in flight (460 sec) a peak temperature of 3400 F is attained in the fastener. Simultaneously, a load factor of 8.7 g's and a free stream dynamic pressure of 193 psf exist. The resultant load per bolt is slightly less but the allowable load per bolt is considerably less at the higher temperature. The actual tensile load is 35.5 lb.; the allowable is 72 lb. assuming 2 percent creep and two-minute exposure to the peak temperature.

A plot of the time variation of dynamic pressure, fastener temperature, and short-time tensile ultimate strength of recrystallized $M_0 + 0.5 Ti$ alloy is shown in Fig. 4-1. The pressure-temperature data were based upon the ASV-4 design trajectory, Fig. 2-2. The two design points, peak temperature at 460 sec and peak deceleration at 750 sec. are indicated on Figure 4-1.

5.0 CONCLUSIONS

The thermal analysis indicated that the trajectory is too severe for the molybdenum skirt section. The molybdenum protective coating will possibly deteriorate and fail at the high operating temperatures causing the exposed structure to oxidize. Finally, retention of the degraded skirt structure is questionable because the temperature environment appears to exceed the permissible strength and stiffness limitations of the material.

The most severe thermal stresses in the ASV-4 tungsten cap occur early in flight before the cap has attained peak (and uniformly-high) temperatures. At boost termination, when the meridional thermal gradient was highest, shell station $s/s_g = 0.53$ reached a maximum meridional stress of 27,000 psi compression at the outer surface and 21,000 psi tension at the inner surface. These principal values fell essentially within the elastic strain regime. The corresponding circumferential stress at the given station was negligible, 1200 psi tension acting uniformly across the shell thickness. Throughout the flight only minimal-amplitude strains in the plastic regime are developed and these are localized to the hotter frontal region of the cap. Fastener strength at elevated temperature appeared adequate to sustain cap loads.

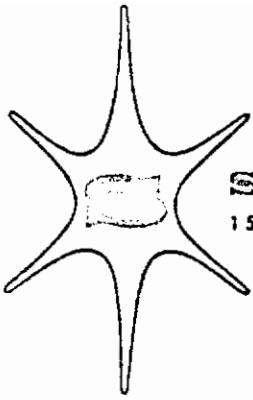
Considering the criticality of temperatures in the molybdenum — sufficient to weaken the skirt structure and cause loss of its disilicide coating by melting — either of two recourses are recommended: (1) Shroud the frontal structure during boost; (2) Reduce the trajectory heating intensity by altering the glide injection conditions.

6.0 REFERENCES

1. ASSET ASV-4 Design Trajectory, McDonnell Aircraft Corp., Inter-Office Memo No. 242-151C-2301, Enclosure (3), Fig. 12.
2. ASSET Nose Cap, Preliminary Drawing No. 36027, Solar, Undated.
3. ASSET Nose Cap Assembly, Drawing No. 36722, Solar, Undated.
4. Technical Data Sheets, Informal correspondence between Solar and IMSC, Palo Alto, April 16, 1963.
5. Stern, P., "Stresses and Displacements in Elastic/Plastic Shells of Revolution With Temperature-Dependent Properties," Lockheed Missiles and Space Company Technical Report: Solid Mechanics 6-90-62-123, Jan, 1963.
6. Structural Materials Handbook, IMSD 325441, Oct, 1960.
7. Barzelay, M. E. and Holloway, G. F., "Effect of an Interface on Transient Temperature Distribution in Composite Aircraft Joints," NACA TN 3824, Apr, 1957.
8. Fay, J. A. and Riddell, F. R., "Theory of Stagnation Point Heat Transfer in Dissociated Air," J.A.S., Vol. 25, No. 2, Feb 1958.
9. Lees, L., "Laminar Heat Transfer Over Blunt-Nosed Bodies at Hypersonic Flight Speeds," Jet Pro., Vol. 26, No. 4, Apr 1956.
10. Hankey, W. L. Jr., Neumann, R. D. and Flinn, E. H., "Design Procedures for Computing Aerodynamic Heating at Hypersonic Speeds," WADC Technical Report 59-610, June 1960.
11. Bromberg, R., Fox, J. L., and Ackermann, W. O., "A Method of Predicting Convective Heat Input to the Body of a Ballistic Missile," Trans. 1st Tech. Symposium on Ballistic Missiles, WDC, ARDC, and R-W Corp., June 1956 (Confidential).
12. Lees, L., "Hypersonic Flow," Fifth International Aeronautical Conference, Los Angeles 1955, Editor R. J. Turino, Published by IAS.

APPENDIX II
ACCELERATION TEST REPORT

Contrails



STELLARDYNE LABORATORIES, INC.

1525 CUYAMACA STREET • GILLESPIE FIELD • EL CAJON • CALIFORNIA

Dial Hickory 4-TEST

Los Angeles - STate 2-7679

ADDRESS MAIL TO:
P.O. BOX 366
EL CAJON, CALIFORNIA

REPORT NO. 2547 DATE 1-3-63

ACCELERATION TEST

ON

TWO (2) NOSE CONES

SPECIFICATION Per Customer Instructions

Prepared for:

Solar Aircraft Corp.
San Diego, California

State of California
County of San Diego

G. O. Kindt, being duly sworn,
deposes and says: That the information contained in this
report is the result of complete and carefully conducted
tests and is to the best of his knowledge true and correct
in all respects.

G. O. Kindt

Subscribed and sworn to before me this 3rd
day of January, 1963

Robert E. Sperry
Notary Public in and for the County of San Diego, State
of California.

My Commission expires 7-14-63

PURCHASE ORDER 53396 W.J.E.

CONTRACT NUMBER _____

CUSTOMER APPROVAL _____

TEST ENGINEER *C. B. King*

C. B. King

TEST WITNESS _____

SLIQC *J. C. McClure*
J. C. McClure

TEST SPECIMEN: Two (2) Nose Cones,

TEST PROCEDURE:

Acceleration:

Mount two (2) nose cones units in centrifuge and accelerate to 12g and retaining centrifugal force of 12g for 3 minutes in each of the three major axes (compression, shear and tension).

TEST RESULTS:

Test Set-Up

The two (2) nose cone units, in fixture, were mounted on Stellydyne Laboratories, Inc. 60 inch centrifuge and subjected to centrifugal force of 12g for a period of 3 minutes in each of three major axes.

Test No.	Specimen	Axis	Acceleration (g)	Duration (min)
1	"Cured"	Compression	12	3
	"Test Fired"	Shear	12	3
2	"Cured"	Shear	12	3
	"Test Fired"	Compression	12	3
3	"Cured"	Tension	12	3
	"Test Fired"	Shear	12	3

Note: Due to physical limitation of Solar's test fixture the "Test Fired" specimen was subjected to shear acceleration twice. This arrangement was acceptable to Solar's Inspection Representative.

Appendix "A" is a photograph of the test specimen in the centrifuge test set up.

Disposition:

The two (2) test units were delivered to Solar's representative upon completion of testing.



**TEST UNIT MOUNTED IN JIG ON 60-INCH CENTRIFUGE ARM
PRIOR TO TEST**

Contrails

APPENDIX III
VIBRATION TEST REPORT

Contrails



STELLARDYNE LABORATORIES, INC.

1525 CUYAMACA STREET • GILLESPIE FIELD • EL CAJON • CALIFORNIA

Dial Hickory 4-TEST

Los Angeles - State 2-7679

ADDRESS MAIL TO:
P.O. BOX 366
EL CAJON, CALIFORNIA

Solar Aircraft Corp.
San Diego 12, California

REPORT NO. 3290 DATE: 2-26-63

VIBRATION TESTING
OF
TWO (2) NOSE CONES

State of California
County of San Diego

G.O. Kindt, being duly sworn,
deposes and says: That the information contained in this
report is the result of complete and carefully conducted
tests and is to the best of his knowledge true and correct
in all respects.

G.O. Kindt

Subscribed and sworn to before me this 26th
day of February, 1963

Richard E. Henry
Notary Public in and for the County of San Diego, State
of California.

My Commission expires 7-14-63

PURCHASE ORDER 7232-57585-XJE

T. O. T. NUMBER 3290

PART NUMBER & DESCRIPTION _____

SLI O.C. J.C. McClure
J. C. McClure

TEST ENGINEER R. J. Leonard
R. J. Leonard

1. Vibration - Single Axis (two Units)

The unit will be mounted on the vibration head in the axis specified by Solar Aircraft.

A resonant search will be conducted with vibration inputs as follows:

cps	Input (g or DA)
5 - 15	.3"DA
15 - 100	3.0g
100 - 500	5.0g
500 - 2000	10.0g

The sweep rate shall be 9 degrees/minute. Resonant frequencies will be recorded.

TEST RESULTS:

The test specimens were subjected to the resonant search as outlined above.

The following resonances were observed:

1. Pin Type Unit

Resonant Frequencies
1050 cps
1500 cps

2. Sine Wave Type Unit

Resonant Frequencies
740 cps
1050 cps
1500 cps

APPENDIX IV
ACOUSTIC TEST REPORT

Contrails

Service To: SOLAR AIRCRAFT COMPANY 2200 PACIFIC HIGHWAY SAN DIEGO, CALIFORNIA	Report No. _____ 4446
	Purchase Order No. _____ 6571-58845-XJE
	Contract No. _____ A133(616)8497
	Date _____ APRIL 2, 1963

**CERTIFIED
TEST REPORT**

ACOUSTIC TESTING

OF

NOSE CAP

rototest laboratories
 2803 Los Flores Boulevard
 Lynwood, California
 NEvada 6-9238

COUNTY OF LOS ANGELES)
 STATE OF CALIFORNIA) SS

VERN L. SANDBERG, LABORATORY SUPERVISOR
 being duly sworn, deposes and says: That the information contained in this report is the result of complete and carefully conducted tests and is to the best of his knowledge true and correct in all respects.

Vern L. Sandberg
 SUBSCRIBED and sworn to before me this _____
 2 day of APRIL, 19 63

William Brown
 Notary Public in and for the County of Los Angeles,
 State of California.
 My commission expires MAY 18, 19 66

Tests Conducted By:
 JACK H. MOODY

Certified By: *A. McKendry*
 Quality Control Engineer

Form QC-11
1/1/59

rototest laboratories, inc.
2803 Los Flores Boulevard
Lynwood, California
NEvada 6-9238

Page No _____ 0.0
Report No _____ 4446

ADMINISTRATIVE DATA

DATE: APRIL 2, 1963

NAME OF PART: NOSE CAP

PURPOSE OF TEST: ACOUSTIC TESTING

MANUFACTURER: SOLAR

MANUFACTURER'S TYPE OR PART NO. : --

DRAWING, SPECIFICATION OR EXHIBIT: SOLAR DEBIT MEMO 54532

QUANTITY OF ITEMS TESTED: ONE (1) SAMPLE

SECURITY CLASSIFICATION OF ITEMS: UNCLASSIFIED

DATE TEST COMPLETED: 3/29/63

TEST CONDUCTED BY: ROTOTEST LABORATORIES, INC.

DISPOSITION OF SPECIMENS: THE SAMPLES WERE RETURNED TO SOLAR AIRCRAFT COMPANY.

SIGNATURES:


VERN L. SANDBERG
LABORATORY SUPERVISOR

ABSTRACT:

rototest laboratories, inc.
2803 Los Flores Boulevard
Lynwood, California
NEvada 6-9238

Page No _____ 1.0

Report No _____ 4446

1. ACOUSTIC NOISE

REFERENCE: SOLAR DEBIT MEMO 54532

REQUIREMENT: VENDOR TO SONIC TEST. 4 1/4" OF SPECIMEN TO OVERALL DB LEVEL OF 153⁺⁰₋₂ DB FOR FREQUENCY RANGE OF 37 TO 9600 CPS. PHOTOGRAPH OF TEST SETUP REQUIRED. CERTIFICATE OF MATERIAL CONFORMANCE REQUIRED.

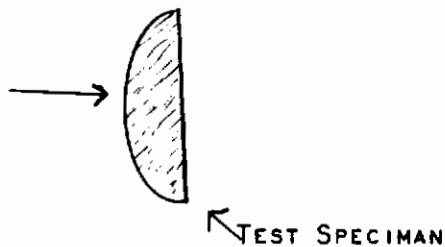
PROCEDURE: THE TEST SPECIMEN WAS PLACED WITHIN THE RTL ACOUSTIC NOISE FACILITY AND SUBJECTED TO A 5 MINUTE ACOUSTIC NOISE EXPOSURE AT A SOUND PRESSURE LEVEL OF 151 DB, OVERALL. THE FREQUENCY SPECTRUM COVERED THE RANGE FROM 37.5 TO 9,600 CPS. THE OCTAVE BAND SOUND PRESSURE LEVELS WERE ADJUSTED "FLAT".

TO ENSURE A NON-RESONANT AND MECHANICALLY ISOLATED MOUNTING MEANS THE SAMPLE WAS SUSPENDED IN THE ACOUSTIC TEST CHAMBER BY MEANS OF BUNGEE CORD WHICH WAS ATTACHED TO THE BACK OF THE TEST SPECIMEN.

FOLLOWING THE TEST EXPOSURE THE TEST SPECIMEN WAS VISUALLY INSPECTED FOR EVIDENCE OF PHYSICAL DAMAGE RESULTING FROM THE NOISE ENVIRONMENT.

ALL TESTING WAS WITNESSED BY MR. ROBERT RAEDEKER OF SOLAR.

AXIS OF EXPOSURE



rototest laboratories, inc.
 2803 Los Flores Boulevard
 Lynwood, California
 NEvada 6-9238

Page No _____ 1.1

Report No _____ 4446

2. ACOUSTIC NOISE - CONTINUED

EQUIPMENT:

<u>TO MEASURE</u>	<u>SYMBOL</u>	<u>UNIT</u>	<u>APPARATUS</u>	<u>CALIBRATION DATE</u>
AMBIENT TEMPERATURE	TA	°C	MERCURY THERMOMETER, 0/200 x 1°C	LAST 2/27/63 DUE 4/27/63
OCTAVE BANDS (FREQ)	--	CPS	SPECIFIED REQUIREMENT, ROTOTEST LABORATORY ACOUSTIC NOISE FACILITY AND CONTROL CONSOLE, F-7049 (WITH OCTAVE BAND FILTERING AND LEVEL CONTROL)	BEFORE USE
OCTAVE BAND SOUND LEVEL	OBL	DB	GENERAL RADIO OCTAVE BAND NOISE ANALYZER, TYPE 1550A, S.N. 611.	LAST 1/7/63 DUE 7/7/63
OVERALL SOUND PRESSURE LEVEL	SPL	DB	GENERAL RADIO SOUND LEVEL METER, TYPE 1551A, S.N. 2087; GENERAL RADIO RANDOM NOISE GENERATOR, TYPE 1390A, S.N. 872; GENERAL RADIO SOUND LEVEL CALIBRATOR, TYPE 1552B, S.N. E-3303 ALTEC LANSING HIGH INTENSITY MICROPHONE, 180-BR-20, M-14, 50/180 ± 1 DB	SAME SAME SAME BEFORE USE
DURATION OF EXPOSURE	M	MINUTE	STANDARD ELECTRIC LAB- ORATORY CLOCK, 0/60 SEC- ONDS - 0/60 MINUTES	

rototest laboratories, inc.
2803 Los Flores Boulevard
Lynwood, California
NEvada 6-9238

Page No 1.2
Report No 4446

1. ACOUSTIC NOISE - CONTINUED

RESULTS:

DATE: 3/29/63;

TIME: 12:05PM;

TA: 22°C

OCTAVE BANDS FREQ CPS	OBL DB	SPL DB	AXIS OF EXPOSURE	M MINUTE	COMMENTS
<u>37.5-9600</u>		<u>153⁺⁰₋₂</u>	<u>NOTED</u>	<u>5.0</u>	<u>SPECIFIED</u>
37.5-75	142	151	SEE		ACOUSTIC NOISE CONDITIONS MET. SAMPLE SUSPENDED WITHIN TEST CHAMBER. STARTED 5 MINUTE NOISE EXPOSURE AT 151 DB SOUND PRESSURE LEVEL.
75-150	142		PROCEDURE	0	
150-300	142				
300-600	142				
600-1200	142				
1200-2400	142				
2400-4800	142				
4800-9600	142				
SAME	SAME	SAME	--	5.0	COMPLETED 5 MINUTE NOISE EXPOSURE. TEST SPECIMEN REMOVED FROM TEST CHAMBER AND VISUALLY INSPECTED FOR EVIDENCE OF DAMAGE.

VISUAL EXAMINATION:

THE TEST SPECIMEN SHOWED NO VISIBLE EVIDENCE OF DAMAGE AS A RESULT OF THE NOISE ENVIRONMENT.

CONCLUSIONS: THE SAMPLE WAS NOT VISIBLY DAMAGED DURING EXPOSURE AND WAS RETURNED TO SOLAR FOR EVALUATION.

JACK H. MOODY

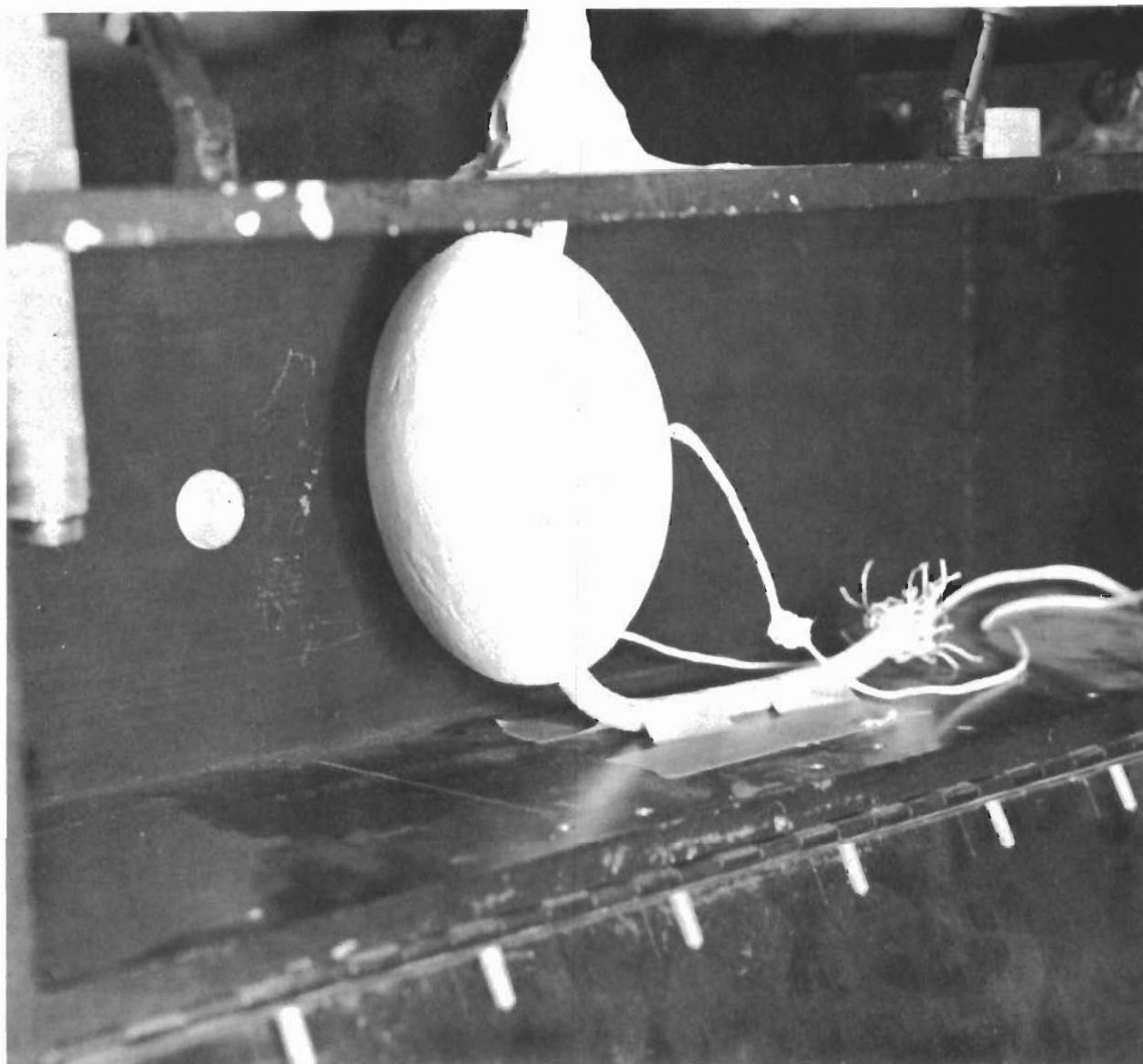
4/2/63
VS

rototest laboratories, inc.
2803 Los Flores Boulevard
Lynwood, California
NEvada 6-9238

Page No _____ 1.3

Report No _____ 4446

1. ACOUSTIC NOISE - CONTINUED



TEST SET-UP

APPENDIX V

VIBRATION AND ACOUSTIC NOISE TEST REPORT

Contrails



Contrails
TEST REPORT

REPORT NO. 14288
OUR JOB NO. D2474
YOUR P. O. NO. 8171-62663-XLF
CONTRACT _____

WYLE LABORATORIES, E. Superior, California, Eastgate 2 1763, Oregon 8 4251, TWX Et. SEG 4236

SOLAR AIRCRAFT
DIVISION OF INTERNATIONAL HARVESTER
2200 PACIFIC HIGHWAY
SAN DIEGO 12, CALIFORNIA

8-PAGE REPORT

DATE JUNE 25, 1963

VIBRATION AND ACOUSTIC NOISE TEST
ON
ASSET NOSE CONE
FOR
SOLAR AIRCRAFT
DIVISION OF INTERNATIONAL HARVESTER COMPANY

1.0 REFERENCES

- 1.1 VERBAL INSTRUCTIONS FROM MR. R. RAEDEKER, CUSTOMER REPRESENTATIVE OF SOLAR AIRCRAFT.
- 1.2 SOLAR AIRCRAFT PURCHASE ORDER NUMBER 8171-62663-XLF.

2.0 PROCEDURES AND RESULTS

2.1 VIBRATION TEST

- 2.1.1 THE VIBRATION TEST ON THE ASSET NOSE CONE WAS CONDUCTED IN ONE AXIS ONLY. THE RESULTS OF VIBRATION TEST WERE NOTED ON DATA SHEETS WHICH ARE PRESENTED IN APPENDIX A.
- 2.1.2 PHOTOGRAPH NUMBER 1 ILLUSTRATES THE VIBRATION TEST SETUP AND ACCELEROMETER LOCATION.

2.2 ACOUSTIC NOISE TEST

- 2.2.1 THE ACOUSTIC NOISE TEST WAS CONDUCTED BY NORTHROP CORPORATION, NORAIR DIVISION. THE TEST REPORT FROM NORTHROP CORPORATION IS PRESENTED IN EXHIBIT I.
- 2.2.2 PHOTOGRAPH NUMBER 2 ILLUSTRATES THE ACOUSTIC NOISE TEST SETUP.

STATE OF CALIFORNIA
COUNTY OF LOS ANGELES

JOHN R. HERRING

do hereby certify that the information contained in this report is the result of complete and careful analysis and tests and to the best of his knowledge true and correct in all respects.

SEAL

SUBSCRIBED and sworn to before me this 25 day of JUNE, 1963
John R. Herring
Paul G. Schmidt

Notary Public in and for the County of Los Angeles, State of California

My Commission expires MARCH 16, 1964

TEST BY DYNAMICS-INSTRUMENTATION DEPT.

Ray E. Myrick

TEST WITNESS _____



WYLE LABORATORIES

APPENDIX A
DATA SHEET

Customer: Solar A/C Job. No. D 2474
 Report No. _____
 Part No. MC6010612 Date 6-7-63
 Spec. Cust Inst Amb. Temp. Room
 Para. _____ Photo Yes
 S/N _____ Test Med. _____
 Specimen Temp. Amb.

Specimen Asset. Nose Cap

- Test Equipment. 1. C-25H Vib. Exciter # 51192. B&K oscillator # 31041
 3. Columbia Amp. # 3779 4. MB Vib. Meter # 3061 5. Evidenco Accel. # RCA 27
 6. CEC Disp. Pickup # 5234 7. Standard Timer # 5586 8. _____
 9. _____ 10. _____ 11. _____
 12. _____ 13. _____ 14. _____
 15. _____ 16. _____ 17. _____
 18. _____ 19. _____ 20. _____

Test Title: Sinusoidal Vibration

Description of Test: One sweep in the longitudinal axis at
the following freq & levels in 7 1/2 minutes.
5-15 cps. .3" RH.
15-100 cps 3 G
100-500 cps 5 G
500-2000 cps 10 G.

Specimen Failed _____
 Specimen Passed _____
 NOD Written _____
 WFLA _____

Tested By A. Hammond Date: 6-7-63
 Witness _____ Date: _____
 Sheet No. _____ of _____
 Approved _____



WYLE LABORATORIES

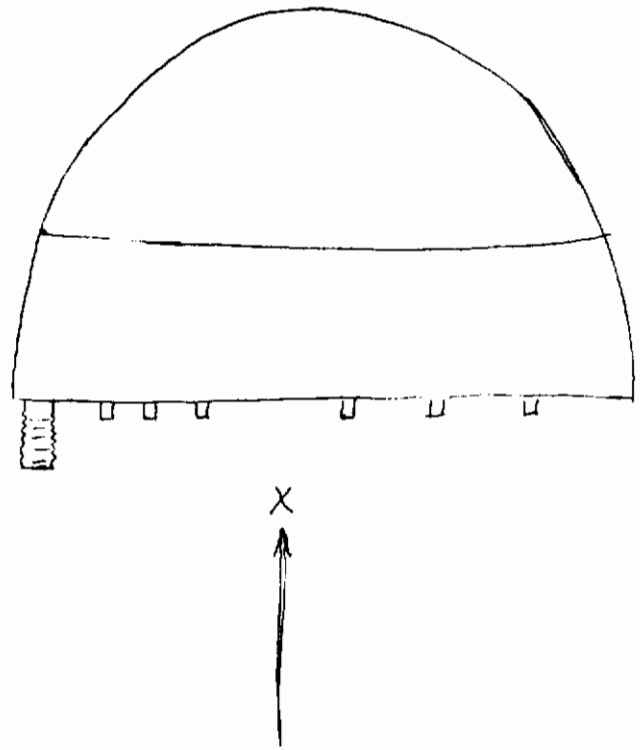
DATA SHEET

Specimen *Asset Nose Cap*
Part No. *AC 6010612*
S/N

Job No. *D2474*
Report No.
Date *6-7-63*
2 of 3

Test Title *Seal, Sine*

Drawing of:



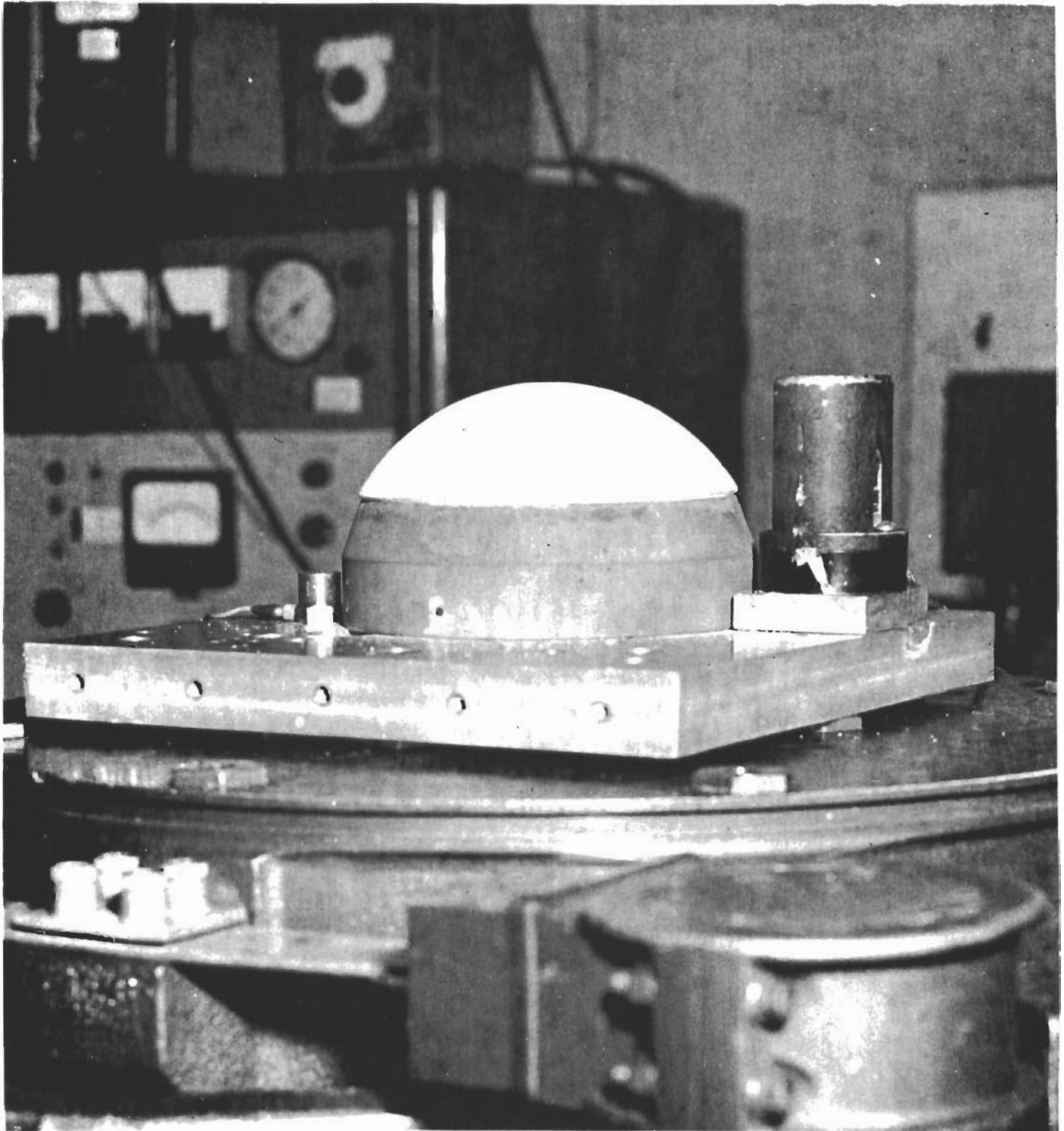
JOB No. 21247
 SHEET 1 OF 3
 I.D. No. _____

DYNAMICS SECTION
 VIBRATION TEST DATA SHEET
 Sinusoidal Vibration



DATE	TIME	AXIS	TEMP (°F)	SINUSOIDAL FREQ (CPS)	DISP (MIL)	ACC (±G)	TEST TIME (MIN)	COMMENTS	NAME
		X	Room	5-2Kc			7.5	TEST REQUIREMENT	
				5-15	.3				
	1530	X	Room	15-100		3			
				100-500		5			
				500-2Kc		10			
6-7	1530	X	Room	5-2Kc	↑	↑	7.5	Resonance noted. Interval specimen raise from 110-205 cps peak @ 140cps; 290-380cps peak @ 340cps; 500-900 cps, peak @ 775cps; 1300-1500 cps, peak @ 1400 cps. All harmonics	
	1538								

SIGNED: _____



VIBRATION TEST SETUP
AND
ACCELEROMETER LOCATION

EXHIBIT I

18 June 1963

Wyle Laboratories
128 Maryland Street
El Segundo, California

Attention: Mr. D. Perkins, Purchasing

Reference: a) Wyle Purchase Order 221797
b) Northrop Norair Test Work Order 95104

Enclosures: 1) Norair Photograph T-3396-063

Gentlemen:

Subject: Acoustic Test of Nose Cap and Simulated Skirt Section

In accordance with the referenced purchase authority, one (1) Nose Cap and Simulated Skirt Section was subjected to a reverberant acoustic test. The test was performed in the Engineering Laboratories of Northrop Corporation, Norair Division, Hawthorne, California on 7 June 1963.

The specimen was suspended by a spring mount system within the Norair 150 Cubic Foot Reverberant Chamber as shown in Norair Photograph T-3396-063. The microphone shown in the photograph was used to monitor the sound field. A Noraircoustic Generator Mk V was used to provide the random sound energy directed at the specimen for a total exposure of 5 minutes.

The test was witnessed by Mr. R. Raedeker of Solar Aircraft, Inc.

A sound spectrum of the service type sound field typical of the run is tabulated below:

<u>Octave Band</u> (cps)	Sound Pressure Level
	(db re .0002 dynes/cm ²)
37 - 75	139
75 - 150	146
150 - 300	148
300 - 600	150
600 - 1200	146
1200 - 2400	141
2400 - 4800	140
Overall	155

To: Wyle Laboratories

3930:411

RBJ:DLB:jf

Attention: Mr. D. Perkins, Purchasing

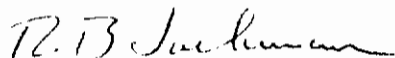
The following test equipment was used to provide and monitor the acoustic environment.

- 1 Noraircoustic Generator, Mk V.
- 1 Altec 21BR200 Microphone.
- 1 B & K Type 2409 Electronic Voltmeter.
- 1 B & K Type 2111 Audio Frequency Spectrometer.
- 1 B & K Type 2305C Level Recorder.
- 1 Special Test Setup within the Norair Reverberant Chamber.

All equipment is currently within a cycle inspection period with the next cycle due September 1963.

Northrop Norair is pleased to have performed this testing service for you. If we can be of any further assistance please contact our organization and your requirements will receive prompt attention.

Very truly yours,



R. B. Jackman
Chief of Engineering Laboratories

Enclosures: (1)

